Myocardial Tissue Characterisation and Functional Assessment by Magnetic Resonance Imaging in ST Elevation Myocardial Infarction

Ananth Kidambi

Submitted in accordance with the requirements for the degree of
Doctor of Philosophy

The University of Leeds

School of Medicine
Leeds Institute of Cardiovascular and Metabolic Medicine

September 2014

Intellectual Property and Publication Statements

The candidate confirms that the work submitted is his own, except where work which has formed part of jointly-authored publications has been included. The contribution of the candidate and the other authors to this work has been explicitly indicated below. The candidate confirms that appropriate credit has been given within the thesis where reference has been made to the work of others.

Chapter 3

Publication: Kidambi A, Mather AN, Swoboda P, Motwani M, Fairbairn TA, Greenwood JP, Plein S. 2013. Relationship between myocardial edema and regional myocardial function after reperfused acute myocardial infarction: an MR imaging study. *Radiology*. **267**(3), pp.701-8.

Authorship: Individual contributions comprise the following:

AK- conception and design, analysis and interpretation of data, drafting and revision of manuscript; **ANM**- data collection, revision of manuscript; **PS**- interpretation of data; **MM**- revision of manuscript; **TAF**- revision of manuscript; **JPG**- interpretation of data, revision of manuscript; **SP**- conception and design, interpretation of data, drafting of manuscript.

Chapter 4

Publication: Kidambi A, Mather AN, Motwani M, Swoboda P, Uddin A, Greenwood JP, Plein S. 2013. The effect of microvascular obstruction and intramyocardial hemorrhage on contractile recovery in reperfused myocardial infarction: insights from cardiovascular magnetic resonance. *J Cardiovasc Magn Reson*. **15**(1), p58.

Authorship: Individual contributions comprise the following:

AK- conception and design, analysis and interpretation of data, drafting and revision of manuscript; **ANM**- data collection, revision of manuscript; **MM**- revision of manuscript; **PS**- interpretation of data; **AU**- revision of manuscript;

JPG- interpretation of data, revision of manuscript; **SP**- conception and design, interpretation of data, drafting of manuscript.

Chapter 5

Publication: Kidambi A, Biglands JD, Zaman A, Higgins DM, Ripley DP, Broadbent DA, McDiarmid AK, Swoboda P, Musa TA, Erhayiem B, Greenwood JP, Plein S. Susceptibility-Weighted Cardiovascular Magnetic Resonance in Comparison to T2 and T2 Star Imaging for Detection of Intramyocardial Hemorrhage Following Acute Myocardial Infarction at 3 Tesla. *Submitted, awaiting publication.*

Authorship: Individual contributions comprise the following:

AK- conception and design, collection, analysis and interpretation of data, drafting and revision of manuscript; **JDB**- analysis methods, revision of manuscript; **AZ**- data collection; **DMH**- data collection, revision of manuscript; **DPR**- revision of manuscript; **DAB**- revision of manuscript; **AKM**- revision of manuscript; **PS**- revision of manuscript; **TAM**- revision of manuscript; **JPG**- revision of manuscript; **SP**- conception and design, interpretation of data, revision of manuscript.

Chapter 6

Publication: Kidambi A, Motwani M, Uddin A, Ripley DP, McDiarmid AK, Swoboda P, Broadbent DA, Musa TA, Erhayiem B, Leader J, Croisille P, Clarysse P, Greenwood JP, Plein S. Myocardial extracellular volume estimation by cardiovascular magnetic resonance predicts functional recovery following acute myocardial infarction. *Submitted, awaiting publication.*

Authorship: Individual contributions comprise the following:

AK- conception and design, collection, analysis and interpretation of data, drafting and revision of manuscript; **MM**- revision of manuscript; **AU**- revision of manuscript; **DPR**- revision of manuscript; **AKM**- revision of manuscript; **PS**- revision of manuscript; **DAB**- analysis of data, revision of manuscript; **TAM**- revision of manuscript; **BE**- revision of manuscript; **JL**- analysis of data, revision of manuscript; **PCr**- analysis methods; **PCl**- analysis methods; **JPG**-

interpretation of data, revision of manuscript; **SP**- conception and design, interpretation of data, revision of manuscript.

Assertion of moral rights:

Acknowledgements

In a field as complex and rapidly evolving as cardiovascular imaging, this work would not have been possible without the support of others. I would like to express my gratitude to Professor Sven Plein and Professor John Greenwood for providing me with their invaluable guidance and support, and for ensuring that my needs as both a researcher and a student were always met.

I would also like to extend my thanks to the CMR research department. I thank Gavin, Petra, Margaret, Caroline, Lisa, Anne, Debbie and Fiona for their advice, assistance and hard work. I am grateful to my colleagues Mani, Akki, Bernhard, David, Adam, Peter, Tarique, Bara and Laura for their support and creativity. I also thank John, David, Arshad and David for their expert assistance with MR physics.

I am also incredibly grateful to all the patients who were integral to this research. Their capacity to show such generosity, concern and kind spirit in a time of serious illness remains a source of inspiration to me.

Finally, I would like to thank my family. To Arpita for her understanding and patience, and to my parents and in-laws for their continual support and encouragement.

List of Abbreviations

AMI	Acute myocardial infarction
ANOVA	Analysis of variance
AUC	Area under the curve
BMI	Body-mass index
BOLD	Blood oxygen level dependent
BSA	Body surface area
CABG	Coronary artery bypass grafting
CK	Creatine kinase
CMR	Cardiovascular magnetic resonance
CSPAMM	Complementary spatial modulation of magnetisation
ECV	Extracellular volume
EDV	End diastolic volume
EF	Ejection fraction
ESV	End systolic volume
FA	Flip angle
HLA	Horizontal long axis
IMH	Intramyocardial haemorrhage
IQR	Interquartile range
LGE	Late gadolinium enhancement
LV	Left ventricle
MACE	Major adverse cardiovascular events
MBF	Myocardial blood flow
MO	Microvascular obstruction
MOLLI	Modified Look-Locker inversion
MPR	Myocardial perfusion reserve
MR	Magnetic resonance
NS	Non-significant

PCI	Percutaneous coronary intervention
PET	Positron emission tomography
RF	Radiofrequency
ROC	Receiver operating characteristic
rSNR	Relative signal to noise
RWMA	Regional wall motion abnormality
SAX	Short axis
SD	Standard deviation
SENSE	Sensitivity encoding
shMOLLI	Shortened MOLLI
SPAMM	Spatial modulation of magnetisation
SSFP	Steady state free precession
STIR	Short tau inversion recovery
SW	Susceptibility weighted
SWIp	Susceptibility-Weighted Imaging with Phase enhancement
T2w	T2-weighted
TE	Echo time
TR	Repetition time
VCG	Vectorcardiogram
VLA	Vertical long axis

Abstract

Objectives

To evaluate myocardial tissue characterisation by cardiovascular magnetic resonance (CMR) to predict functional recovery in reperfused acute myocardial infarction (AMI).

Background

Prognosis following AMI is closely related to recovery of myocardial contractile function. Accurate early prediction of functional recovery may allow for additional therapies in high risk patients, and avoid over-treatment of lower risk patients. Clinical prognostication commonly relies on echocardiographic evaluation of function, which may be misleading acutely. CMR offers a number of ways to refine prediction of functional recovery by characterising myocardial tissue, but these have not been extensively evaluated.

Methods

Patients following reperfusion for first-presentation ST-elevation AMI were scanned by CMR acutely, subacutely and in convalescence. Tissue pathologies visible on acute CMR were evaluated for their ability to predict recovery of contractile function. Oedema in the peri-infarct zone, microvascular obstruction (MO) and intramyocardial haemorrhage (IMH) in the infarct zone, and extracellular volume (ECV) of the infarct zone were evaluated. In addition, susceptibility-weighted MR imaging (SW-MRI) was evaluated against the reference standards of T2-weighted and T2* imaging to detect the known prognostic marker of IMH.

Results

Acutely oedematous myocardium demonstrated recovery of function over time ($p<0.05$), whereas non-oedematous peri-infarct myocardium did not ($p>0.05$). Recovery of function closely mirrored resolution of oedema. Infarct contractile recovery was attenuated in infarcts that demonstrated MO acutely as compared to those without ($p<0.01$), and attenuated further in those that demonstrated IMH acutely ($p<0.01$). SW-MRI had sensitivity 93% and specificity 86% as compared to T2-weighted imaging, with excellent inter-observer reliability and shorter breath-hold times (4 seconds vs. 16 seconds). Infarct ECV had higher accuracy to predict improved wall motion than late gadolinium enhancement imaging (c-statistic 0.80 vs. 0.70, $p=0.04$).

Conclusion

Tissue characterisation by CMR offers a variety of ways to predict functional outcome following AMI, using both established and novel imaging techniques.

Table of Contents

List of Tables

List of Figures

List of Equations

Publications Arising From This Work

Papers

1. Kidambi A, Mather AN, Swoboda P, Motwani M, Fairbairn T, Greenwood JP, Plein S. 2013. Relationship between myocardial edema and regional myocardial function after reperfused acute myocardial infarction: an MR imaging study. *Radiology.* **267**(3), pp.701-8.
2. Kidambi A, Mather AN, Motwani M, Swoboda P, Uddin A, Greenwood JP, Plein S. 2013. The effect of microvascular obstruction and intramyocardial hemorrhage on contractile recovery in reperfused myocardial infarction: insights from cardiovascular magnetic resonance. *J Cardiovasc Magn Reson.* **15**(1), p58.
3. Kidambi A, Mather AN, Swoboda P, Motwani M, Fairbairn TA, Greenwood JP, Plein S. 2013. Reciprocal ECG change in reperfused ST-elevation myocardial infarction is associated with myocardial salvage and area at risk assessed by cardiovascular magnetic resonance. *Heart.* **99**(22), pp.1658-62.

Abstracts

1. Kidambi A, Uddin A, Ripley DP, McDiarmid AK, Swoboda P, Musa TA, Erhayiem B, Bainbridge G, Greenwood JP, Plein S. 2014. Overestimation of infarct size following acute myocardial infarction is related to extent of myocardial edema. *J Cardiovasc Magn Reson.***16**(S1):O21.
2. Kidambi A, Ripley DR, Uddin A, McDiarmid AK, Swoboda P, Musa TA, Bainbridge G, Greenwood JP, Plein S. 2014. Early vs. persistent microvascular obstruction following primary PCI- two pathologies or one? A cardiovascular magnetic resonance study. *J Cardiovasc Magn Reson.* **16**(S1):P192.
3. Kidambi A, Mather AN, Motwani M, Swoboda P, Uddin A, Greenwood JP, Plein S. 2013. Contractile recovery of infarct zone in reperfused acute myocardial infarction is influenced by microvascular obstruction and intramyocardial haemorrhage. *European Heart Journal*. **34**: 359-360.
4. Kidambi A, Mather AN, Uddin A, Motwani M, Ripley DP, Herzog BA, Gunn J, Plein S, Greenwood JP. 2013. Reciprocal ECG change in ST-elevation myocardial infarction is associated with area at risk and myocardial salvage following revascularization. *J Cardiovasc Magn Reson*:**15**(S1):P172.

5. Kidambi A, Mather AN, Motwani M, Swoboda P, Uddin A, Greenwood JP, Plein S. 2013. Microvascular obstruction and intramyocardial haemorrhage influences infarct zone contractile recovery in reperfused acute myocardial infarction. *Heart*;**99**:A57–A58.
6. Kidambi A, Mather AN, Uddin A, Motwani M, Ripley DP, Herzog BA, Gunn J, Plein S, Greenwood JP. 2013. Reciprocal ECG change in ST-elevation myocardial infarction is associated with area at risk and myocardial salvage following revascularization. *Heart*;**99**:A58–A58.
7. Kidambi A, Mather A, Swoboda P, Motwani M, Fairbairn T, Greenwood J, Plein S. 2012. Recovery of regional myocardial function and myocardial oedema following reperfused acute myocardial infarction. *J Cardiovasc Magn Reson.***14**:O64.
8. Kidambi A, Mather A, Swoboda P, Motwani M, Fairbairn T, Greenwood J, Plein S. 2012. Regression of myocardial oedema is related to improvement in myocardial contractility following reperfused acute myocardial infarction. *Heart*. **98**:A51-A52.

1. Chapter 1
General Introduction

1.1. Introduction

Noninvasive imaging of acute myocardial infarction (AMI) has developed rapidly over recent years. From initial fluoroscopic imaging of the heart in the nineteenth century (Williams, 1896), scanning techniques have evolved to enable us to probe myocardial infarction to a cellular level, *in vivo*. Variations in infarct pathophysiology can result in markedly different clinical outcomes for patients suffering from reperfused AMI. The ability to accurately predict prognosis following reperfused infarction closely relates to identifying these variations, which in turn relies on an understanding of variations in infarct pathophysiology and how they relate to imaging. Conversely, some of the most rapid developments in elucidating infarct pathophysiology in a clinical setting have been via clinical imaging techniques, in particular cardiovascular magnetic resonance (CMR). The unique ability of CMR to probe proton molecular environments to high resolution, coupled with a safe and robust extracellular contrast agent, allow for clinically-applicable tissue characterisation to an unprecedented level of detail. In addition to the high resolution and tissue characterisation abilities of CMR, advances in quantitative tissue mapping may allow further pathophysiological mechanisms to be understood. Multiple CMR parameters have been described to characterise infarcts, together with the ability to risk stratify patients to a greater level than simple measures of myocardial contractility. However, it is not clear whether these parameters are independent predictors or linked. In this chapter, we review the pathophysiology of AMI and link imaging parameters to pathology. We also explore which CMR measurements can be used to further stratify patients and where potential therapeutic targets may be, which can then be monitored by CMR.

1.2. Pathophysiology of acute infarction

Infarction denotes local cell death resulting from inadequate blood supply. Chronic coronary insufficiency may lead to cardiac ischaemia or infarction. The clinical consequences and imaging targets of chronic coronary insufficiency have been well categorised (Crossman, 2004) (Figure 1.1). AMI results from

blockage or severe stenosis of an epicardial coronary artery, usually due to coronary atherosclerotic rupture with superimposed thrombosis. There are a number of unique factors associated with acute MI and its evolution which may be used as imaging targets to predict functional outcome.

Overall, injury due to infarction may be divided into three main zones: the peri-infarct zone or 'area at risk', the central area of infarction which expands into the area at risk as infarction progresses, and remote myocardium.

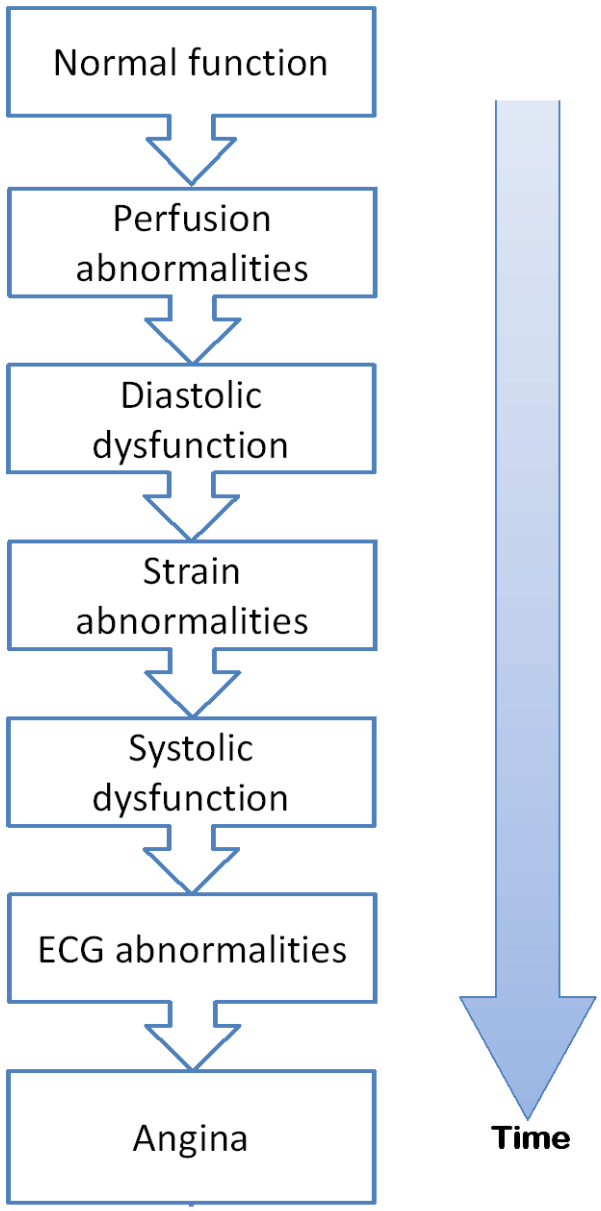

Figure 1.1. Established imaging targets for chronic coronary artery disease.

1.2.1. Peri-infarct pathophysiology

1.2.1.1. Myocardial oedema

Oedema is an early marker of infarction, and may occur within 15 minutes of ischaemia, prior to significant infarction (Jennings et al., 1985). Very early after the onset of acute ischaemia, lactic acidosis results in the disassociation of water from a protein-bound state to the 'free' state (Kuntz et al., 1969) leading to an increase in free intracellular water throughout acutely ischaemic myocardium. With ongoing ischaemia, increased intracellular osmolarity due to metabolite accumulation and failure of active Na^+ efflux leads to additional interstitial oedema (Eitel and Friedrich, 2011). Oedema may be indirectly detected by measurements of LV wall thickness and mass by echocardiography (Gaasch and Bernard, 1977; Turschner et al., 2004). A nonspecific decrease in metabolic activity can be detected by positron emission tomography (PET) within oedematous myocardium (Lee et al., 2012). The T2 changes caused by accumulation of free water can be detected directly by CMR. Accurate detection of oedema by T2 sensitive MRI techniques has been shown to correlate to the 'area at risk' (Aletras et al., 2006; Friedrich et al., 2008; Verhaert et al., 2011), and may be detectable as quickly as 1 hour after coronary interruption (Schulz-Menger et al., 2003). However, T2-weighted imaging has been comparatively slow to enter the clinical arena, in part due to long breath-hold times and sensitivity to motion artefacts, but also in part due to doubts regarding the utility of the technique (Croisille et al., 2012). The preclinical validation of T2-weighted imaging has been performed in animal models, which differ significantly in their propensity to develop myocardial oedema. In particular, canine models appear to develop less oedema than pig models (Karolle et al., 1991; Garcia-Dorado et al., 1992; Tranum-Jensen et al., 1981), and it is unclear which is a more accurate representation of the acutely ischaemic human heart. This, coupled with the inability of T2-weighted imaging to clearly differentiate viable from infarcted myocardium (Choi et al., 2000), may lead to difficulties in interpreting T2-weighted imaging. In a research setting, contrast enhanced echocardiography (Iliceto et al., 1996) and Tc^{99m} SPECT (prior to reperfusion) (Sinusas et al., 1990) have been used to denote the area at risk. Some advances have been made to detect oedema with CT (Mahnken et al., 2009), though this has not yet been developed for clinical use. The development of CMR T1 and T2 mapping techniques may help more accurately differentiate oedematous from infarcted myocardium (Ugander et al., 2012; Verhaert et al., 2011). Oedema is important not only for differentiating acute from chronic infarction; it has functional implications in itself. Oedema increases the stiffness of the left

ventricle (Pogatsa et al., 1976; Dongaonkar et al., 2010), and may cause contractile dysfunction by steric hindrance of the contractile apparatus (Bragadeesh et al., 2008), a factor contributing to stunning of viable myocardium acutely. Oedema is also associated with arrhythmic events (Yeatman et al., 1988; Garcia-Dorado and Oliveras, 1993).

In contrast to the adverse prognostic factors associated with oedema, the presence of oedema may also be considered a positive prognostic factor following reperfusion. Myocardial salvage, the difference between actual and potential infarct size, may either be measured by single-photon emission tomography (SPECT) (Verani et al., 1988) or MRI based techniques (Verani et al., 1988). CMR T2w imaging delineates the 'area-at-risk' prior to reperfusion, and by measuring infarct size by LGE, the amount of myocardial salvage can be estimated (Arai, 2011b). By either method, a higher ratio of oedematous at-risk myocardium to infarcted myocardium (i.e. higher salvage) is associated with improved prognosis (Verani et al., 1988; Eitel et al., 2010). The role of intracellular vs. interstitial oedema in humans has not been established (Reimer et al., 1981; Steenbergen et al., 1985; Tranum-Jensen et al., 1981), and may be modulated in ischaemia by abnormal cell membrane ion transport. Recent advances in the modelling of first-pass contrast enhancement may be able to provide further insights into these mechanisms (Broadbent et al., 2013), by providing estimates of contrast uptake in different tissue compartments. In addition, the duration of oedema persistence after ischaemia has not been established. The area of T2-weighted hyperintensity in man appears relatively constant within the first 7 days (Dall'Armellina et al., 2011), though oedema seems to largely resolve by 5 weeks (Fishbein et al., 1978).

1.2.1.2. Myocardial stunning

Myocardial stunning refers to reversible myocyte dysfunction following a reperfused ischaemic event, which persists after blood flow has returned to normal or near-normal. Initially described in dogs (Heyndrickx et al., 1975), stunning is relevant clinically in man as it may result in significant acute LV dysfunction despite adequate reperfusion (Bolli, 1992). Stunning has been observed in a variety of clinical and experimental settings, including reperfused infarction, and its causes are likely multifactorial. The majority of experimental studies on stunning have been performed in a canine model of viable myocardium, though the interplay of mechanisms underpinning stunning in reperfused infarction are likely to be different in man (Bolli and Marban, 1999).

As discussed below, as the wavefront of infarction is arrested by reperfusion in a canine model, there may be viable subepicardial tissue with infarcted subendocardial tissue. Stunning in this subepicardial portion may last days to weeks (Bush et al., 1983; Ellis et al., 1983; Lavallee et al., 1983; Theroux et al., 1976). The severity and duration of stunning is influenced by the duration of ischaemia (Preuss et al., 1987), suggesting that ischaemia, rather than reperfusion *per se* is a primary determinant of stunning.

The pathophysiology of stunning is complex, and a variety of different mechanisms are likely to contribute. Oxygen-derived free radicals and alterations in cellular response to calcium have been extensively studied in the literature (Bolli and Marban, 1999), but do not currently contribute to clinical imaging of stunning. Oedema imaging, as discussed above, may be related to stunning, but visualisation of oedema is insufficient to categorise myocardium as stunned, and absence of oedema does not exclude stunning.

A technical diagnosis of stunning requires acute and convalescent studies to demonstrate improvement in myocardial function. However, myocardial stunning can be predicted by a variety of imaging modalities. Positron emission tomography can identify stunned myocardium directly, by identifying mismatch between myocardial blood flow and cardiac function in chronic coronary artery disease (Conversano et al., 1996), though there is limited evidence on its use acutely, where coronary flow may be submaximal following intervention. SPECT imaging can infer stunning of myocardium from a discrepancy between LV function and infarct size (Christian et al., 1997). Echocardiography can identify stunned myocardium acutely by visualizing improvement in regional wall motion during administration of low dose dobutamine (Salustri et al., 1994). CMR can similarly use low dose dobutamine to identify contractile improvement in regional wall motion. CMR may also indirectly detect stunned myocardium by identifying areas with wall motion abnormalities on cine imaging or tissue tagging (Kraitchman et al., 2000), but without hyperenhancement on LGE imaging that is typical of scarred, nonviable myocardium. A meta-analysis comparing the dobutamine and LGE methods to evaluate stunning concluded that LGE imaging has higher sensitivity for the detection of stunning post-AMI, whereas low dose dobutamine CMR has higher specificity (Romero et al., 2013). To differentiate stunning from hibernation (where hypokinetic myocardium is viable but hypoperfused) would require establishing preserved myocardial blood flow (MBF) in this region. This can be performed noninvasively using coronary flow reserve estimation by

echocardiography (Caiati et al., 1999), or by visual, semi-quantitative or quantitative analysis of first pass perfusion CMR (Jerosch-Herold, 2010), which should be performed in the presence of a coronary vasodilator as resting measurements have lower sensitivity (Marinho et al., 1996). However, to date, the only reliable and quantitative method of MBF estimation in routine clinical use is with ^{82}Rb, $^{13}NH_3$ or $H_2{}^{15}O$ PET (Kaufmann and Camici, 2005). Clinically in this setting, coronary angiography is recommended to provide a definitive answer to the diagnostic differentiation of ongoing ischaemia and stunning (Underwood et al., 2004).

1.2.2. Infarct pathophysiology

Infarction, which follows on from this process to evolve within the area at risk, is a nontrivial cellular diagnosis, even by histological examination (Myocardial infarction redefined--a consensus document of The Joint European Society of Cardiology/American College of Cardiology Committee for the redefinition of myocardial infarction, 2000). CMR has formed the reference standard *in-vivo* diagnosis of infarction by utilizing the T1 shortening properties of extracellular gadolinium-based contrast agents, which accumulate within the increased extracellular space of infarcted myocardium. Unlike oedema, which appears to be uniformly distributed throughout the area at risk (Reimer and Jennings, 1979a), infarction has been shown to progress from the endocardium towards the epicardium with increasing amounts of time and severity of ischaemia in dogs (Reimer et al., 1977; Reimer and Jennings, 1979b). The transmural extent of infarction has been demonstrated to have an inverse relationship with the likelihood of visual improvement in contractile function, and forms the cornerstone of clinical prognostic evaluation of infarction (Kim et al., 2000). However, there are a number of observed caveats to this straightforward evaluation of infarct extent. The endocardial to epicardial wavefront theory may have limitations in the context of reperfused acute infarction. Dog myocardium, where the wavefront phenomenon has been primarily described, has an extensive network of epicardial collateral circulation (Maxwell et al., 1987), as compared to that in man. Using an ovine model, with less epicardial collateralisation, infarction was not found to be in a ‘wavefront’ distribution, and was more prominent in the mid-myocardium (Leshnower et al., 2007). Nonetheless, the endocardial to epicardial progression of infarction in man can be readily surmised from CMR studies in infarct patients using late gadolinium enhancement (LGE) to accurately depict scar, which characteristically extends from the endocardial to epicardial myocardium (Kim et al., 2000; Ingkanisorn

et al., 2004). The lateral extension of infarction also appears to differ between canine models and man, with relatively little lateral infarct extension in dog experiments (Factor et al., 1981), but evidence of lateral infarct extension by comparing the area at risk with infarcted myocardium by CMR in man (Kidambi et al., 2013b; O'Regan et al., 2009) (Figure 1.2). In man also, there is conflicting evidence for the transmural extent theory following reperfused AMI. When using strain as the marker of contractility in the setting of reperfused AMI, the correlation with infarct transmural extent was relatively weak (Kidambi et al., 2013a; Gerber et al., 2002). Contractile cell types are found within hyperenhanced areas on contrast-enhanced CMR (Gunning et al., 2002), and myocytes are often found within the infarct zone on human autopsy examination (Fishbein et al., 1978). Although patients with larger or more transmural infarction have adverse LV remodelling (Larose et al., 2010) and worse prognosis over the first 2 years (Hombach et al., 2005), extent of myocardial scar may not independently predict adverse outcome after accounting for remodelling and reperfusion injury (Hombach et al., 2005; de Waha et al., 2010). LGE may overestimate scar size by approximately 20-40% in the acute setting, as compared to chronic infarction, in a process that appears to be distinct from the extent of scar remodelling (Dall'Armellina et al., 2011; Engblom et al., 2009; Oshinski et al., 2001). The pharmacokinetics and distribution of gadolinium acutely is still not fully understood, and gadolinium can accumulate in ischaemic but viable myocardium (Pereira et al., 1996). Intracellular distribution of gadolinium acutely has not been ruled out.

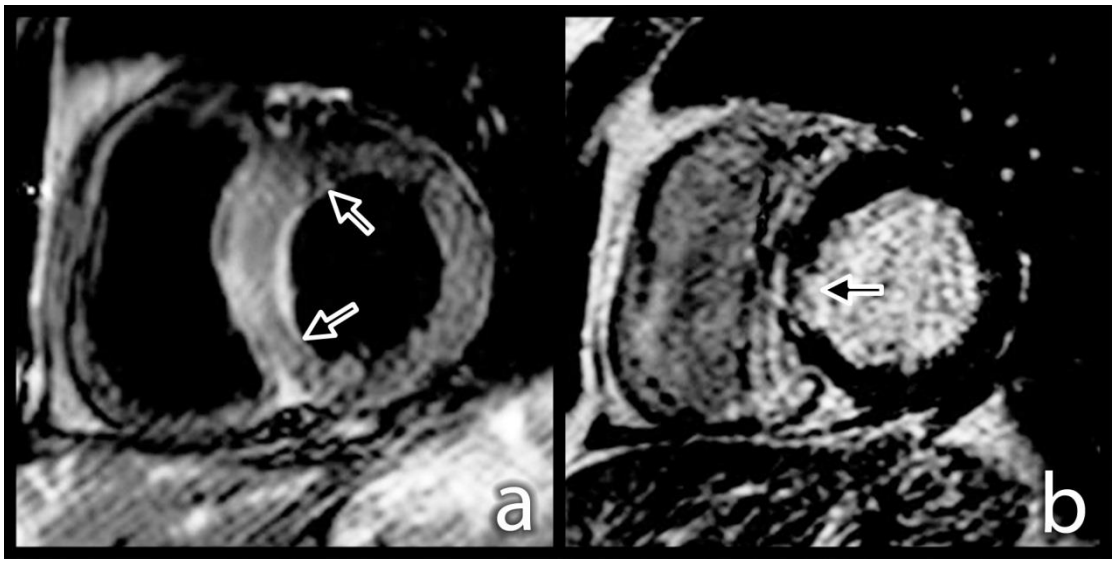

Figure 1.2. T2 and LGE imaging. Comparison of T2-weighted CMR (Panel a) and late gadolinium enhancement CMR (Panel b) in the same patient and slice location 2 days following reperfused AMI. Lateral extension of oedema (Panel a, arrowed) is more extensive than infarct (Panel b, arrowed).

Myocardial dysfunction in AMI is not limited to the infarct related artery. Remote myocardial dysfunction has been observed by CMR tissue tagging (Kramer et al., 1996; Bogaert et al., 2000), which may be due to microvascular change (Homans et al., 1986), tethering to infarcted and/or peri-infarct myocardium or changes in myocardial loading. Remote segment hyperkinesis has been observed in approximately one-third of patients following AMI in echocardiographic studies (Grines et al., 1989; Yoshino et al., 1998; Bodi et al., 1999; Stamm et al., 1983).

1.2.3. Reperfusion injury

In addition to the above processes, reopening the culprit artery may result in further myocardial cell injury, the so-called “double edged sword” of reperfusion (Braunwald and Kloner, 1985). Despite the well-established benefits of timely reperfusion, in animal models, up to 50% of cell death may be associated with reperfusion rather than ischaemic injury (Matsumura et al., 1998; Arai et al., 1996). Reperfusion alters cellular processes in the area at risk, infarction zone and remote myocardium.

Within the area at risk, reperfusion results in “explosive swelling” with concomitant cellular architectural disruption in the dog model (Jennings et al.,

1960). Necrotic myocardium is thought to contribute to the development of oedema, though the distribution of oedema appears to be homogenous throughout the area at risk in both animal models and CMR estimates in man (Garcia-Dorado and Oliveras, 1993).

Within the infarct zone, reperfusion may increase cellular necrosis, in part due to increased oxygen-derived free radicals (Zweier, 1988) and intracellular calcium changes (Brooks et al., 1995). Free-radical mediated lipid peroxidation results in loss of cell membrane integrity, leading to cell death (Kim et al., 1994). Neutrophil activation may lead to oxidative stress and production of reactive oxygen species, associated with further endothelial disruption (Erbel and Heusch, 2000). Microembolisation of thrombus or atherosclerotic debris may trigger the above cascades clinically (Kawano et al., 2005). Microvascular obstruction (MO) may be found in approximately 40% of reperfused patients with acute infarction (Mather et al., 2009). MO is caused by a combination of endothelial dysfunction (Kloner et al., 1974), oedema and endothelial protrusion, facilitating microembolisation of platelets, neutrophils or thrombus (Heusch et al., 2009) (Figure 1.3). In both the rabbit and canine model, MO largely develops in the 1-2 hours after reperfusion (Reffelmann and Kloner, 2002; Galiuto et al., 1998).

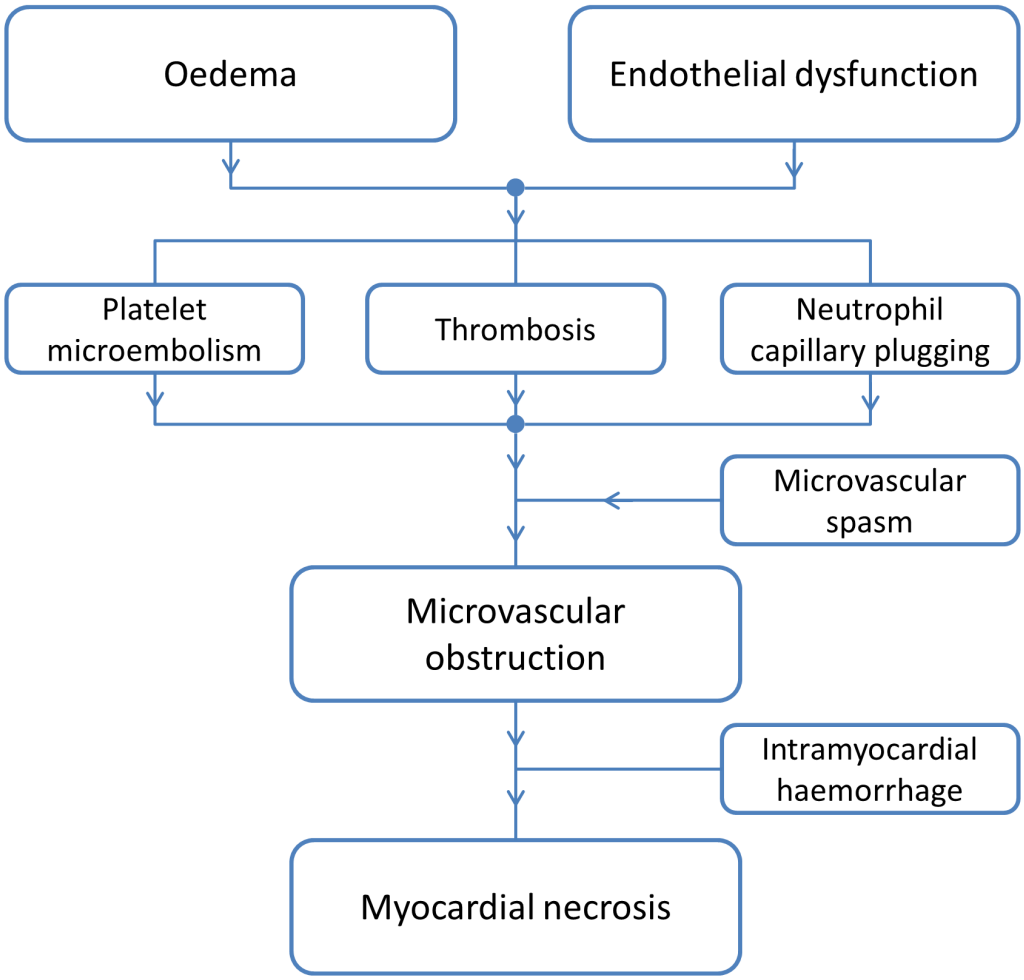

Figure 1.3. Relationship of microvascular obstruction, intramyocardial haemorrhage and myocardial necrosis.

MO is the primary factor leading to the “no-reflow” phenomenon, where restoration of epicardial arterial flow does not lead to complete downstream tissue perfusion. The extent of MO is not strongly correlated with total infarct size(de Waha et al., 2012), and is more prevalent in males (Rezkalla et al., 2010; Iwakura et al., 2003), patients with diabetes mellitus, advanced age (Jaffe et al., 2008) and renal dysfunction (Ndrepepa et al., 2010). It may be related to the morphology of the culprit plaque (Ozaki et al., 2011). In both animal models and in man, it appears to progress in a wavefront fashion, from endocardium to epicardium (Krug et al., 1966; Kloner et al., 1974; Kloner et al., 1980). MO is an important pathology to identify, as it is associated with adverse prognosis and adverse left ventricular remodelling independent of the infarct size alone (Ito et al., 1996; Sutton and Sharpe, 2000; Morishima et al., 2000). In particular, strategies to prevent reperfusion injury are focused on reducing the development of MO (Moens et al., 2005). The effects of MO on functional recovery and prognosis appear to be mediated via the infarct zone itself, rather than remote myocardial change (Gerber et al., 2000; Kidambi et al., 2013a). The exact mechanisms by which pathology within already non-viable infarct tissue can affect prognosis are yet to be determined.

A variety of imaging modalities can detect MO, such as TIMI flow and myocardial blush grade on coronary angiography (Rezkalla et al., 2010; Sorajja et al., 2005), coronary flow wires (Iwakura et al., 1996), or echocardiography with myocardial contrast (Iwakura et al., 1996; Galiuto et al., 2003; Iwakura et al., 2003; Iwakura et al., 2006). ST-resolution on ECG also relates to the presence of MO, albeit with relatively low sensitivity (Santoro et al., 1998). CMR offers visualisation of myocardial tissue at higher resolution than these modalities, and is more sensitive at detection of MO than contrast echocardiography (Wu et al., 1998b). MO may be seen readily on CMR as a hypoenhanced core after administration of contrast, either on first-pass perfusion imaging, early or late gadolinium enhancement imaging, as the contrast is slow to enter the hypoperfused area of MO (Figure 1.4). High resolution first-pass perfusion and early contrast enhancement appears to be more sensitive for MO (Mather et al., 2009), whereas the detection of MO on late contrast enhancement has evidence of its prognostic value (de Waha et al., 2010; Wu et al., 1998a; Hombach et al., 2005). Whether these differences are due to imaging parameters, simply due to timing after contrast administration or reflect additional late mechanisms has yet to be determined. Similarly it is unclear if different patient groups are predisposed to early or persistent

hypoenhancement, though in one comparative study, risk factor distribution appeared to be similar (de Waha et al., 2010). For the present time, it would seem prudent to use both early and late gadolinium enhancement techniques when assessing for MO by CMR.

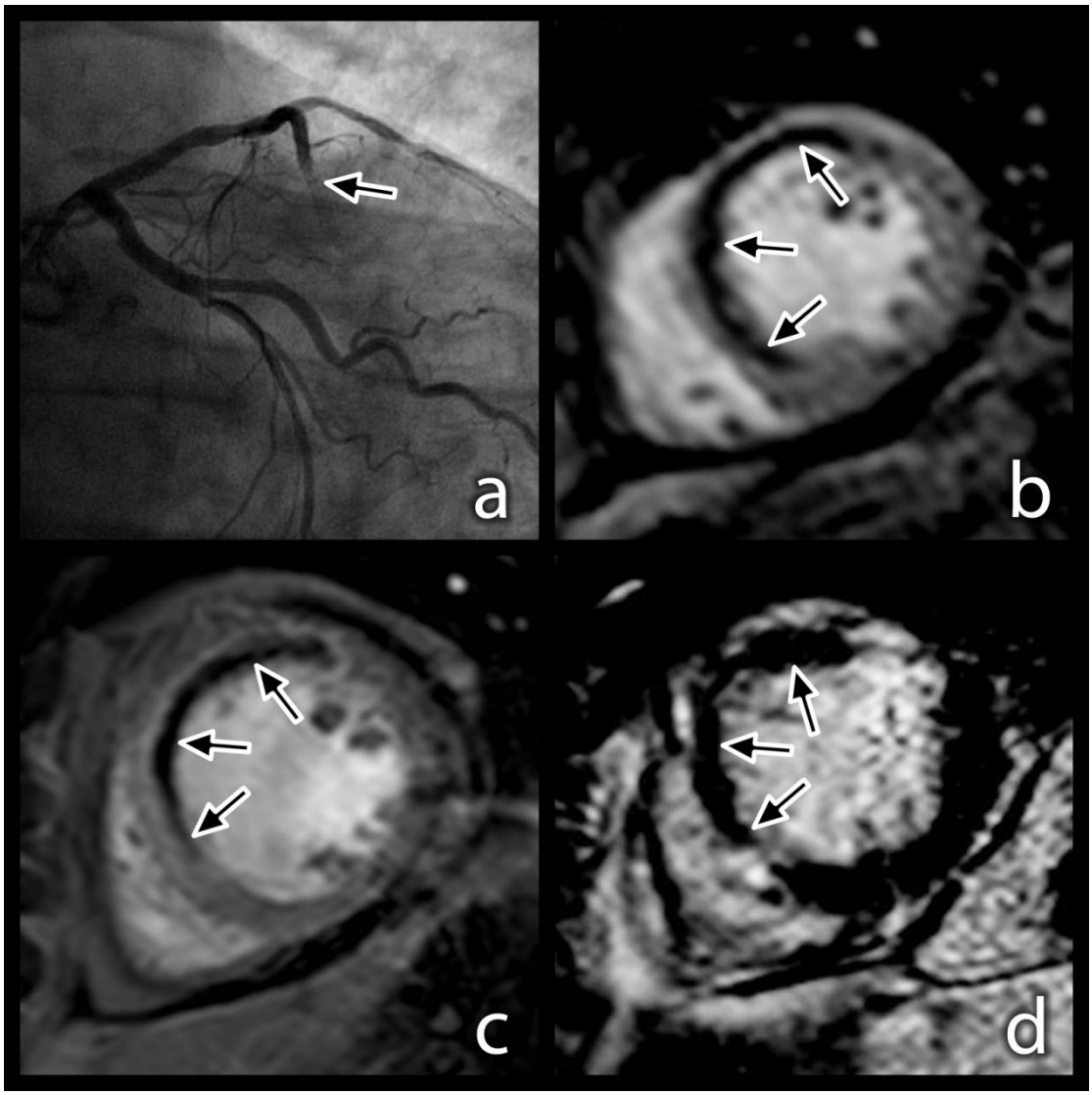

Figure 1.4. Microvascular obstruction following reperfusion to the left anterior descending coronary artery. No-reflow following revascularisation is seen on X-ray coronary angiography (Panel a). Corresponding anterior territory hypoperfusion is seen on first pass perfusion CMR (Panel b), and a hypointense infarct core is seen on early gadolinium enhancement (Panel c) and late gadolinium enhancement (Panel d).

There is increasing evidence for the clinical value of a further subtype of infarct pathophysiology within MO, that of intramyocardial haemorrhage (IMH). Reperfusion in both canine and pig models revealed leakage of red cells into the interstitium within the core of the infarct during the reflow period (Fishbein et al., 1980; Kloner et al., 1983; Higginson et al., 1982; Capone and Most, 1978), but IMH was not observed in a nonreperfused canine model (Pislaru et al., 1997). IMH appears to be independent of lytic therapy, with no difference in amount of IMH observed in mechanically-reperfused canine infarcts with or without a thrombolytic agent present (Kloner et al., 1989; Kloner and Alker, 1984). CMR has the ability to distinguish IMH *in-vivo*, by combining the properties of hypoenhancement on contrast imaging, characteristic of MO, with the short T2 of blood and the magnetic field irregularities induced by iron leading to a shortened T2* in IMH. Within the infarct zone, a dark core on both T2 (Lotan et al., 1992; Basso et al., 2007) and T2* (Cochet et al., 2010; Kramer et al., 1993) imaging have been shown to correspond to IMH. Whilst T2 imaging for IMH has human histological validation (Basso et al., 2007), infarction without IMH may also exhibit a hypointense core on T2 weighted imaging (Jackowski et al., 2006; Mikami et al., 2009), and the hyperenhancing effects of oedema may mask the presence of IMH. IMH may also be demonstrated using direct T1 quantification (Pedersen et al., 2012), but the ability to differentiate from infarct and MO in individual patients has not been fully established. Interestingly, IMH is most pronounced in the mid-section of myocardium in a pig model, rather than the endocardial to epicardial progression which is observed for infarction (Garcia-Dorado et al., 1990). Whether this is also true in man has not been histologically identified. IMH is exclusively found within zones of MO. In a dog model, IMH develops in areas of severe vascular injury, suggesting that it may be a late consequence of MO (Fishbein et al., 1980). On the other hand, pig hearts injected with intracoronary collagenase to produce IMH consistently develop MO in this area (Ghugre et al., 2012). Local oedema and extravasation of red cells may also produce MO by local compression of microvasculature. It remains unclear whether MO is a prerequisite for haemorrhage, or whether IMH engenders local MO, or a combination of both. The presence of IMH confers adverse prognosis over that of MO alone (Eitel et al., 2011), and is associated with impaired LV remodelling (Beek et al., 2010; Ganame et al., 2009) and attenuated contractility within the infarct zone, but not remote myocardium (Kidambi et al., 2013a). It is also associated with late arrhythmic risk (Mather et al., 2011). The presence of IMH is associated with age, but other patient or treatment factors are yet to be discovered, in part due to the strong association of IMH with MO size and LV function (Eitel et al.,

2011). Unlike MO, which may be reversible, IMH may lead to chronic intramyocardial iron deposition, as validated in human subjects by T2* CMR, and histologically in a canine model of reperfused infarction (Kali et al., 2013a). However, in a porcine model, IMH resolved by 4 weeks (Ghugre et al., 2011). The precise mechanisms by which IMH confers adverse prognosis remain unknown.

Both MO and IMH are, at best, weakly associated with infarct size itself (de Waha et al., 2012; Eitel et al., 2011), and a large infarct does not necessarily lead to MO or IMH. However, prognostic data on infarct subtypes must account for the confounder of infarct size, which is strongly associated with adverse prognosis. Regression analysis has been used to differentiate these factors, though the utility of regression analysis in comparatively small studies may be debated. Nonetheless, the data to date suggests that patients with MO have poorer prognosis than those without, and patients with IMH have poorer prognosis still, regardless of infarct size. The extent of MO has been shown to be more predictive of MACE than infarct size, and interestingly a larger relative amount of MO compared to total infarct size is a stronger predictor still (de Waha et al., 2012). With current CMR methods, IMH is more difficult to accurately quantify, and no definite relationship between size of IMH and prognosis has been reported to date.

1.2.4. Ventricular remodelling

LV remodelling is clinically defined as the 'molecular, cellular and interstitial changes manifested as changes in size, shape and function of the heart resulting from cardiac load or injury' (Cohn et al., 2000). Early identification of adverse remodelling is a key function of imaging techniques, for a number of reasons: firstly, as clinical signs and symptoms are a poor indicator of LV remodelling; secondly, LV remodelling is closely associated with adverse prognosis; and thirdly, a number of therapeutic interventions are thought to improve prognosis post-AMI by limiting this process. Traditionally, pathological remodelling following AMI was divided into early (<72 hours) and late (>72 hours). However, this distinction is less commonly used, as the time course varies depending on the severity of infarction, and development of recent imaging techniques can demonstrate features of early remodelling such as oedema to 10 days or more (Dall'Armellina et al., 2011).

The key measure of LV remodelling continues to be ejection fraction (EF), which has been repeatedly shown to be a strong marker of prognosis following infarction (Burns et al., 2002). However, acutely following AMI, EF may be misleadingly lowered due to stunning (Braunwald and Kloner, 1982) or hibernation (Rahimtoola, 1989). Echocardiography can identify LV geometry change, and measure EF quickly and cheaply, though CMR is demonstrated to have improved accuracy and reproducibility (Semelka et al., 1990). End systolic volume may also be used as a measure of remodelling, and correlates with prognosis following AMI (White et al., 1987). Wall thickening is another feature of adverse remodelling, and may be quantified by comparing diastolic and systolic LV wall thickness on echocardiography (Nieminen et al., 1982), gated nuclear imaging (Sharir et al., 2001) or cine CMR (Peshock et al., 1989). Increased wall thickness early after AMI, has been shown to confer adverse prognosis and is associated with increased LV volumes (Verma et al., 2008) and persistent segmental dysfunction (Kramer et al., 1993). Interestingly, it is thought that the main contributor to increased wall thickness is myocardial oedema (Turschner et al., 2004), which opposes the above notion that oedema, as a marker of salvage, is a favourable marker after reperfusion. Early wall thickening is in contrast to late remodelling, where oedema has subsided, and thinning in the infarct zone is associated with adverse prognosis (Eaton et al., 1979). LV dilatation as a marker of adverse remodelling may also be seen by echocardiography, nuclear imaging, CT or MRI. Compensatory hyperkinesis of remote segments may also be seen by echocardiography, cine or tissue tagging CMR (Jaarsma et al., 1986; Marcus et al., 1997).

1.2.4.1. Remodelling and strain

Myocardial strain is an index of motion relative to the original or unstressed dimension and measures lengthening/ expansion (denoted as positive strain) and shortening/ compression (negative strain). Strain is estimated as per Equation 1.1.

$$(L-L_0)/L_0$$

Equation 1.1. Tissue strain.
L0 is the maximum length and L is the instantaneous length at a given point in time.

Lagrangian strain is technically given where L0 is the length at zero stress, but as this is rarely possible to measure *in vivo*, it is commonly taken as the maximal length, namely the end diastolic length. Strain may be measured by monitoring the motion of myocardium over the cardiac cycle, and may be measured by tissue Doppler echocardiography (Urheim et al., 2000) or tissue tagging CMR (Ibrahim el, 2011). More recently, speckle tracking echocardiography and feature tracking CMR have been developed to enable strain measurements without the need for acquisition of separate images (Schuster et al., 2013; Gorcsan and Tanaka, 2011). Myocardial strain offers improved sensitivity and increased reproducibility over quantitative LV volumetric analysis by echocardiography (Thavendiranathan et al., 2013), and can discriminate functional from dysfunctional myocardium more accurately than wall thickness by CMR (Gotte et al., 2001). It can also be measured in precisely-defined areas of myocardium, allowing for assessment of motion within different infarct pathologies. It may also be measured in any direction, allowing for comparison of radial, circumferential and longitudinal motion, and may be used to analyse diastolic, as well as systolic function.

Strain analysis following AMI has revealed a number of insights into the remodelling process. Attenuated longitudinal strain by echo is associated with increased ventricular arrhythmic events (Haugaa et al., 2013), and may be more sensitive than EF to predict adverse events (Ersboll et al., 2013b). Impaired early diastolic strain rate is associated with adverse outcomes following ST elevation AMI (Ersboll et al., 2013a). Strain as measured by CMR can distinguish impaired, normal and hyperkinetic function post AMI (Marcus et al., 1997). Strain within regions affected by MO is attenuated acutely and subacutely as compared to infarcts without MO (Gerber et al., 2000; Kidambi et al., 2013a). Within the border zone between infarction and remote myocardium there is intermediate strain (Inoue et al., 2010), and improvement of strain in the peri-infarct zone appears to be closely associated with both the presence and the time-course of resolution of oedema (Kidambi et al., 2013b).

As described above, a number of imaging factors have shown association with adverse remodelling, such as infarct size and transmural extent, presence of MO, presence of IMH and reduced myocardial salvage. Adverse remodelling is also related to the presence of arrhythmias following AMI. In addition to infarct size and ejection fraction (Izquierdo et al., 2013), the amount of heterogeneous myocardium adjacent to the infarct, the ‘grey zone’, is associated with the

likelihood of ventricular arrhythmias (Robbers et al., 2013). In light of studies that have failed to show an advantage for routine early ICD implantation in post-AMI patients with impaired EF (Steinbeck et al., 2009; Hohnloser et al., 2004), infarct characterisation by CMR may provide a role in evaluating which patients are most likely to benefit from device therapy.

1.2.5. Resolution of microvascular obstruction and intramyocardial haemorrhage

Whilst there are a number of studies that focus on the development of MO and IMH, very few studies detail the nature of its resolution. One reason for this may be the lack of accurate noninvasive characterisation of these processes prior to the recent development of CMR-based methods. The extent of MO in a canine model appears unchanged up to 9 days post-infarct (Wu et al., 1998b), though the exact duration of MO, or factors influencing this is uncertain. Monocyte recruitment occurs as part of the healing process in MO, and this has been visualised in the research setting by monocyte-labelled ^{19}Fluorine/^{1}Hydrogen CMR scanning (Ye et al., 2013). The healing of IMH also has a paucity of research, though T2* CMR imaging has revealed persistent T2* shortening in areas of IMH in both humans and a canine model, suggesting that persistent iron deposition occurs within haemorrhagic regions (Kali et al., 2013a).

1.2.5.1. Resolution of oedema

Clinically, myocardial oedema appears to be maximal and constant for the first 7 days following infarction (Dall'Armellina et al., 2011), with persistence of oedema on CMR up to 12 days after infarction (Friedrich et al., 2008) and resolution at 6 months (Monmeneu et al., 2009). Noninfarcted oedematous myocardium develops normalisation of wall thickness and improves contractility as the oedema regresses, both in canines and man (Aletras et al., 2006; Kidambi et al., 2013b). However, the factors associated with regression and time course of myocardial oedema have not been established.

A summary of the current understanding of evolution and resolution of infarct pathophysiology is presented in Figure 1.5.

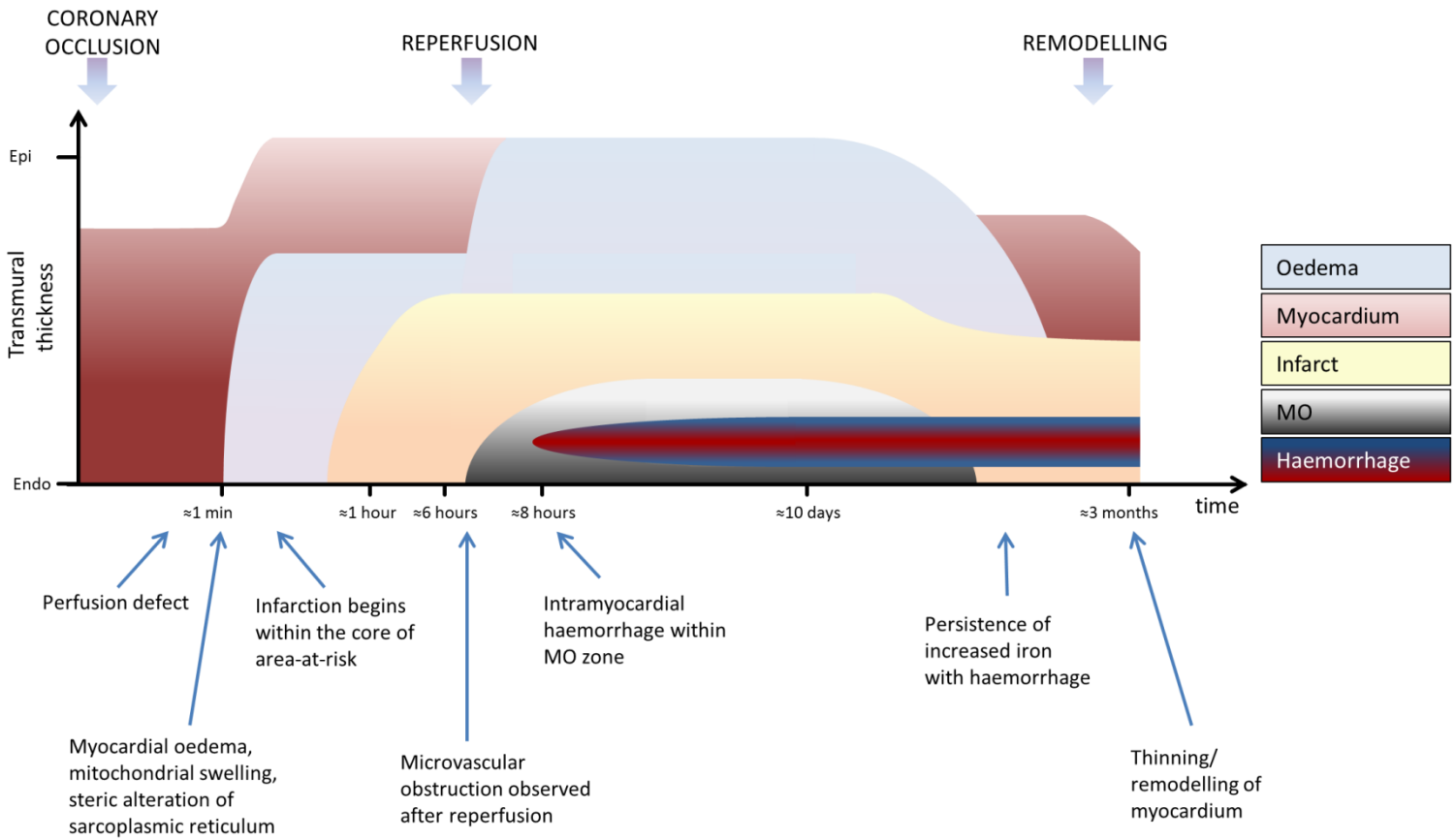

Figure 1.5. Summary of infarct evolution and remodelling as visualised by CMR. The diagram depicts the effect of pathologies on the endocardial to epicardial layers of the myocardium over time. Swelling and oedema precedes infarction and is exacerbated by reperfusion. Microvascular obstruction (MO) and intramyocardial haemorrhage (IMH) may appear following reperfusion. MO is usually no longer visible by 3 months, whereas IMH may leave persistent T2* changes. Contraction of the scar, and the infarct segment as a whole, is visible after approximately 1 month.

1.2.6. Post-infarction arrhythmias

Following the acute post-MI period, a major cause of death is due to infarct-related ventricular tachyarrhythmias. Although some ventricular arrhythmias may originate from the infarct core in canines (Kramer et al., 1985), the peri-infarct zone has been shown to have abnormal fibre arrangements which have been associated with development of ventricular tachycardia (de Bakker et al., 1990). CMR may be able to detect heterogeneous myocardium around the infarct as a 'grey zone' of intermediate hyperenhancement on LGE imaging (Yan et al., 2006). The amount of grey zone has been shown to correlate with both prognosis and susceptibility to ventricular arrhythmias (Schmidt et al., 2007). The interaction between infarction, oedema, remote myocardium and reperfusion injury in this grey zone is complex and incompletely characterised (Manning and Hearse, 1984).

1.3. CMR biomarkers of prognosis

The imaging studies described above have furthered our understanding of the pathophysiology of myocardial infarction. However, a number of steps need to be fulfilled in order to establish the clinical utility of an imaging biomarker. In addition to a valid theoretical basis, a fully validated imaging biomarker would require the following (Sado et al., 2011):

- Direct comparison (animal models followed by human autopsy material).
- Detection of changes in established disease compared with normal subjects.
- Correlation with known cardiac imaging biomarkers.
- Correlation with known biomarkers.
- Demonstration of the test in more than one clinical scenario.
- Demonstration of test sensitivity (early disease or with age).
- Demonstration of the ability to track change (with time, after treatment).
- Demonstration of predictive or prognostic value of the test.
- Standardisation of the test (reproducibility, different equipment, in non-research settings, quality control, limitations of test).
- Development of robust age/ethnic normal reference ranges.
- Changes in biomarker remain tied to the disease after treatment.
- Demonstration of the test as a surrogate trial endpoint.
- Clinical use and regulatory approval of the test.
- Proof test use improves clinical outcome.

Very few imaging biomarkers fulfil all these requirements. However, establishing an imaging biomarker as a surrogate marker of prognosis or outcome has clinical utility in itself. There are no agreed criteria to validate an imaging biomarker as a predictor of prognosis. A systematic meta-analysis of prognostic CMR biomarkers following AMI defined the highest level of evidence as 3 or more studies with a summed total of more than 1000 patients, with more than 50% of studied patients belonging to a study that demonstrated significant prognostic association on multivariate analysis (El Aidi et al., 2014). Using these criteria for a systematic review, there were no CMR biomarkers that were established to predict hard events alone, whilst LV ejection fraction was established to predict MACE. Table 1.1 lists other CMR biomarkers with some prognostic evidence.

	Hard events		*MACE*	
Biomarker	**Number of studies**	**Patients evaluated**	**Number of studies**	**Patients evaluated**
LVEF	2 (Eitel et al., 2010; de Waha et al., 2012)	624	12 (Amabile et al., 2012; Lonborg et al., 2013; Husser et al., 2010; Grothoff et al., 2012; Prunier et al., 2008; Wu et al., 2008; Miszalski-Jamka et al., 2010; Cochet et al., 2010; Bruder et al., 2008; Klug et al., 2012; de Waha et al., 2012; Eitel et al., 2010)	2467
MO	2 (Eitel et al., 2010; de	624	9 (Amabile et al., 2012; Bruder et	1822

	Hard events		*MACE*	
Biomarker	**Number of studies**	**Patients evaluated**	**Number of studies**	**Patients evaluated**
	Waha et al., 2012)		al., 2008; Cochet et al., 2010; de Waha et al., 2012; Grothoff et al., 2012; Husser et al., 2010; Klug et al., 2012; Miszalski-Jamka et al., 2010; Wu et al., 1998a; Cochet et al., 2009)	
Infarct size	1 (de Waha et al., 2012)	422	16 (Ahn et al., 2013; Bello et al., 2011; Bodi et al., 2010; Bodi et al., 2009; Bruder et al., 2008; Cochet et al., 2010; Cochet et al., 2009; de Waha et al., 2012; Eitel et al., 2010; Husser et al., 2010; Husser et al., 2013; Klug et al., 2012; Larose et al., 2010; Miszalski-Jamka et al., 2010; Wu et al., 2008; Wu et al., 1998a)	2598
Oedema	1 (Eitel et al.,	202	3 (Husser et al., 2013; Raman et	600

	Hard events		*MACE*	
Biomarker	**Number of studies**	**Patients evaluated**	**Number of studies**	**Patients evaluated**
	2010)		al., 2010; Eitel et al., 2010)	
IMH	-	-	2 (Amabile et al., 2012; Eitel et al., 2011)	445

Table 1.1. CMR imaging biomarkers associated with prognosis following AMI. Adapted from (El Aidi et al., 2014).

1.4. CMR imaging protocol

Taking the above established biomarkers, it is possible to construct a CMR imaging protocol for patients acutely following AMI. Such a protocol would need to include established biomarkers that would reflect prognosis and influence clinical decision making, and conducted in as short a time span as possible, both for logistic scanning reasons and to minimise patient discomfort so soon after a major cardiac event. The optimal time point would be whilst myocardial oedema is detectable, to allow derivation of myocardial salvage. Oedema measurement by T2-weighted remains approximately constant for the first 7 days following reperfused AMI (Dall'Armellina et al., 2011).

Figure 1.6 shows one example of such a protocol.

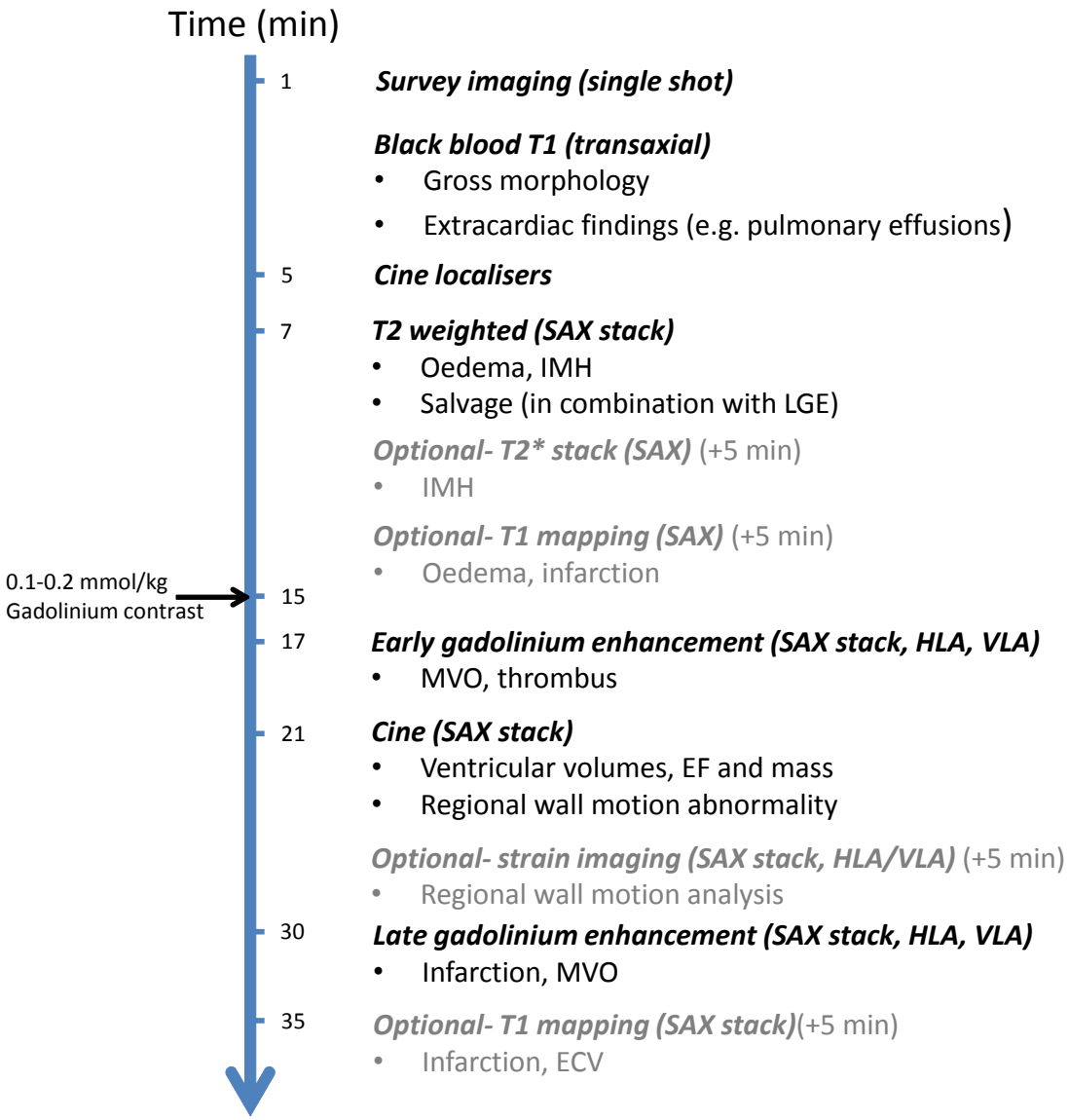

Figure 1.6. Example CMR imaging protocol acutely following AMI.

1.5. Novel imaging targets

Whilst conventional CMR biomarkers are gaining evidence to be evaluated for their clinical utility, novel CMR techniques may also prove to be useful following AMI.

1.5.1. Parametric acquisition (tissue 'mapping')

Quantitative or parametric 'mapping' techniques are rapidly gaining popularity in cardiovascular research. Rather than utilising differences in T1 between

tissues to generate contrast, T1 mapping sequences aim to quantify the underlying T1 values of tissue itself. Techniques such as the Modified Look-Locker Inversion (MOLLI) acquisition sequence allow an accurate and reproducible estimate of T1 to be performed in a single breath hold (Messroghli et al., 2007a). Modifications of the technique, such as the shortened MOLLI (shMOLLI) allow for even shorter breath hold times, an important factor when imaging patients acutely following infarction. Images from these sequences can be reconstructed to form a pixelwise map of tissue T1 (Figure 1.7).

T1 mapping may allow for identification of infarcted and oedematous myocardium without administration of contrast (Dall'Armellina et al., 2012), and may also detect intramyocardial haemorrhage (Pedersen et al., 2012). When combined with contrast administration, either by infusion (Flett et al., 2010) or bolus dose (White et al., 2013) followed by a delay of 12+ minutes, pre and post-contrast T1 levels can be used to derive the volume of distribution of gadolinium. By factoring away the proportion of this volume that is red cells (estimated by measuring serum haematocrit), the extracellular volume [ECV] of a tissue may be estimated. CMR derivation of ECV has been shown to agree with histological collagen volume fraction (Flett et al., 2010). Equation 1.2 shows the most clinically validated method of calculation (Jerosch-Herold et al., 2008).

$$ECV = (1 - haematocrit) \times \frac{R1_{myo\ post} - R1_{myo\ pre}}{R1_{blood\ post} - R1_{blood\ pre}}$$

Equation 1.2. CMR derivation of ECV. R1 denotes the reciprocal of T1.

ECV may be calculated on a pixel-wise basis, producing an ECV map (Kellman et al., 2012) (Figure 1.7).

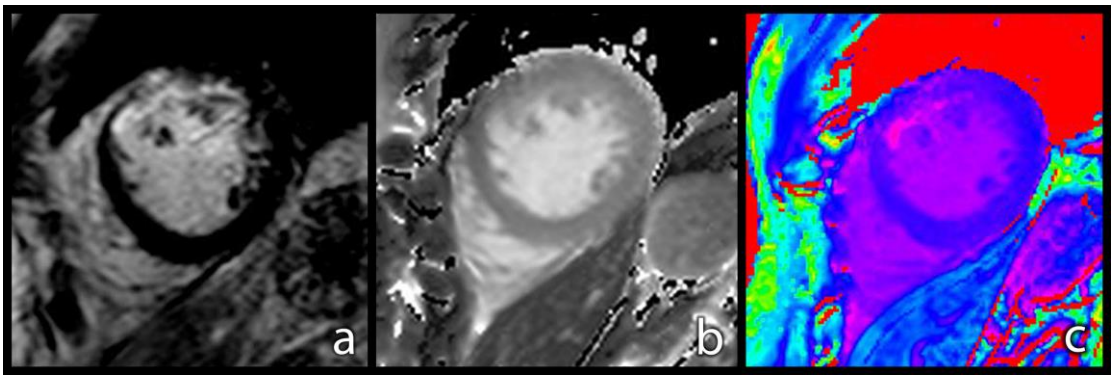

Figure 1.7. Weighted and parametric T1 acquisition in acute myocardial infarction. Identical patient and slice position shown for comparison. T1-weighted LGE imaging (Panel a), pre-contrast parametric T1 map (Panel b) and an ECV map (Panel c), generated from pre-and post-contrast T1 parametric acquisitions are shown.

Analogous to T1 mapping, absolute T2 values in tissue may also be quantified. T2 mapping has been shown to accurately delineate the area at risk as measured by microspheres in canines (Ugander et al., 2012), and to identify oedematous myocardium in man (Verhaert et al., 2011). Absolute values for both T2 and T2* are lower in areas of IMH in canines and man (Kali et al., 2013b).

1.5.2. Blood-level oxygen dependent (BOLD) imaging

Deoxyhaemoglobin is more strongly paramagnetic than oxyhaemoglobin (Atalay et al., 1995), leading to relative shortening of T2* times dues to local magnetic field inhomogeneity. T2* shortening correlates with a relative increase in the amount of tissue deoxyhaemoglobin, which forms the basis of BOLD imaging. Rest and dipyridamole stress BOLD MRI can differentiate scarred from hibernating myocardium in chronic infarction (Egred et al., 2003), but applications in AMI thus far have been limited.

1.5.3. Magnetic resonance spectroscopy

Magnetic resonance spectroscopy allows for analysis of metabolic pathways in cardiac muscle in vivo, without the need for an external tracer. Spectroscopy can detect signal from protons in addition to other nuclei with nuclear spin such as ^{23}sodium (Na), ^{13}carbon (C), and ^{31}phosphorus (P). The majority of

clinical studies to date have focussed on ^{31}P spectroscopy, which can be used to estimate the phosphocreatine to adenosine triphosphate ratio, which provides information on the energetic state of myocardium (Hudsmith and Neubauer, 2009). Measuring creatine content using ^{1}H-spectroscopy has been applied to canines and patients with myocardial infarction, revealing that creatine concentrations were significantly lower in the infarct zone (Bottomley and Weiss, 1998).

1.6. Future directions

The future of infarct characterisation will likely come in a number of directions. Existing biomarkers need further validation, both for widespread use and applicability, and for their influence on prognosis. Both existing and novel imaging targets will likely see improvements in their execution, with reduced scan times, more robust and standardised imaging sequences, and hardware improvements. For CMR, improvements may well be alongside the drive for higher magnetic field strengths, as these are approaching the limit where artefacts generated by the magnetic field are more likely to degrade cardiac images than the potential gain in signal. Optimisation of image collection and processing is rapidly becoming the limiting factor for CMR image quality. Novel techniques, such as hyperpolarisation (Schroeder et al., 2011) may allow for CMR targeting of specific biomarkers to a greater degree than CMR or spectroscopy can currently achieve. Alongside all these improvements, there is a wider need to establish the use of diagnostic cardiac imaging to influence and change management, either by specifically targeting at-risk patients or potentially scaling back treatments for those with favourable prognosis.

1.7. Conclusions

The goal of any diagnostic imaging technique is to provide insights into disease processes that have prognostic implications, and that can be changed by intervention. This review has highlighted a number of techniques, from those that are well established to those in their infancy. CMR is becoming a powerful technique to image acute myocardial infarction, and can provide a variety of meaningful observations that influence prognosis. CMR is increasingly being used as a surrogate endpoint in trials for management strategy, and the breadth of pathophysiology that can be identified should ensure that CMR

continues to develop into a leading technique to categorise cell injury and predict recovery following AMI.

2. Chapter 2
Aims and Standard Methods

2.1. Aims

As discussed in Chapter 1, predicting functional outcome following reperfused ST-elevation AMI remains a highly relevant clinical question. The most widespread imaging modality for this purpose, transthoracic echocardiography, does not provide detailed insights into infarct pathophysiology, a factor which has profound effects on functional outcome. CMR is established in the detection of oedema, scar, microvascular obstruction and intramyocardial haemorrhage, but the relationship of these to functional recovery post AMI has not been well studied. In addition, there are a number of promising novel CMR imaging sequences, which remain relatively under-evaluated in the AMI population.

With this background, the aims of this thesis were:

- To investigate the role of myocardial oedema in predicting regional recovery of contractile function following reperfused ST-elevation AMI
- To evaluate the influence of microvascular obstruction and intramyocardial haemorrhage on recovery of contractile function
- To examine the clinical utility of novel CMR sequences to investigate infarct pathophysiology. The experiments concentrate on two CMR sequences in particular: susceptibility-weighted imaging and extracellular volume estimation by T1 mapping.

2.2. Standard methods

Individual methods pertaining to each experiment will be detailed in the appropriate chapter. However, there are a number of general methods applicable to all experiments, which are summarised in each chapter and provided in more detail below.

2.2.1. Ethical approval

Written informed consent was obtained from all patients prior to recruitment (Appendix 9.3). Ethical approval was obtained from the regional ethics committee for all experiments (Appendix 9.1). For the experiments focussing

on established pulse sequences (Chapters 3 and 4), ethical approval was granted by the National Research Ethics Service (NRES), Leeds (West) Research Ethics Committee, reference number 08/H1307/8. For the experiments evaluating novel sequences (Chapters 5 and 6), ethical approval was again granted by Leeds (West) Research Ethics Committee, reference number 12/YH/0169. All experiments were performed in accordance with the Declaration of Helsinki.

2.2.2. Study population

The experiments in Chapters 3 and 4 were performed on the same study population. 57 hospitalised patients with first presentation ST-elevation AMI were recruited from our institution between August 2008 and December 2009. The experiments in Chapters 5 and 6 were from a different cohort, 54 patients hospitalised at our institution with first presentation ST-elevation AMI between February 2012 and August 2013. For chapter 5, all 54 patients were studied. For chapter 6, the first 37 patients that were recruited were analysed, once a sample size that met the power calculation was included.

Inclusion criteria were first presentation ST-elevation AMI, diagnosed using contemporaneous guidelines (Thygesen et al., 2007; Thygesen et al., 2012) and treated using primary percutaneous coronary intervention within 12 hours of symptom onset. Exclusion criteria were: patients with a history of previous coronary revascularisation (percutaneous or surgical bypass grafting), previous myocardial infarction, renal failure (estimated glomerular filtration rate <30ml/min/1.73m^2) or contraindication to CMR examination (such as MR unsafe device implantation). Numbers of patients that did not undergo testing is described in each chapter. Some patients tolerated a shortened scan with limited imaging sequences, resulting in an examination that could be utilised for some experiments but not others.

For all patients, clinical management (including anticoagulation, use of aspiration catheters, drug-eluting stents and antiplatelet regimen) was performed blind to the CMR results and at the discretion of the responsible clinician, reflecting contemporary practice and guidelines.

2.2.3. Data collection

All imaging data acquisition was planned prospectively, using standard analysis methods where these have been established. The rationale for specific analyses is presented in individual chapters.

2.2.4. CMR hardware

Experiments at 1.5 Tesla (Chapters 3 and 4) were performed using a 1.5 Tesla Philips Gyroscan Intera MR imaging system (Philips Healthcare, Best, The Netherlands), equipped with "Master" gradients. Maximum gradient strength and slew rate were 30mT/m and 150mT/sec respectively. A five-element cardiac phased-array synergy coil was used for signal reception. Vectorcardiographic (VCG) heart rate monitoring was performed to allow for cardiac-gated image acquisition.

Experiments at 3.0 Tesla (Chapters 5 and 6) were performed using a 3.0 Tesla Philips Achieva TX MR imaging system (Philips Healthcare, Best, The Netherlands), equipped with a Quasar Dual gradient system (maximum gradient strength and slew rate were 40 mT/m and 200 T/m/s respectively), and RF shimming with dual-source RF transmission. A dedicated 32-channel cardiac phased array receiver coil was used, together with VCG cardiac gating.

2.2.5. Scanner protocol

Due to differing scanner capabilities, protocols were different on 1.5T and 3T scanners. Results presented used only one scanner and one protocol for each experiment.

Figure 2.1 and Figure 2.2 summarise the CMR protocols used in the 1.5T and 3T experiments respectively. Details of individual sequences used are presented in the respective chapters. Note the addition of T1 mapping at 3T.

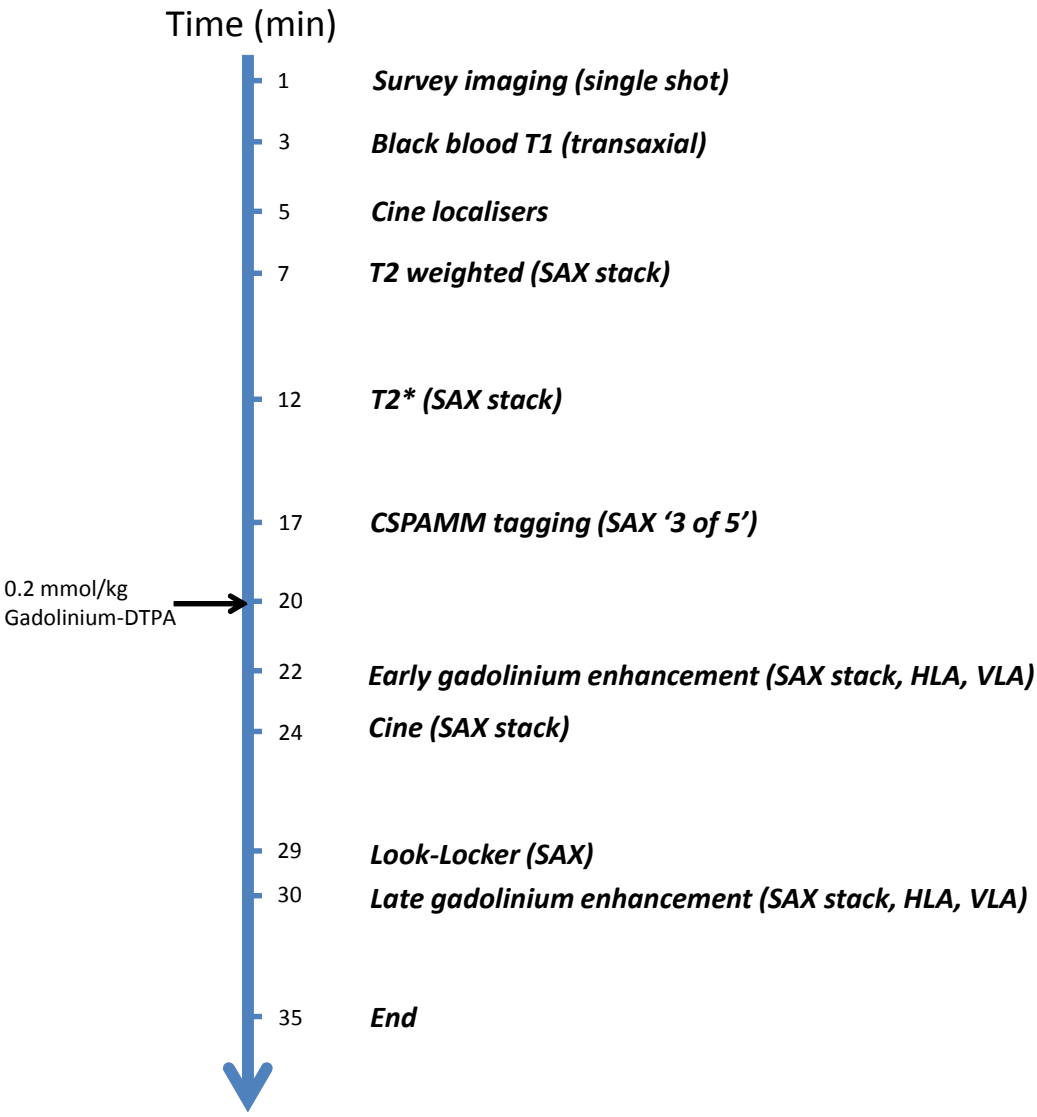

Figure 2.1. Imaging protocol for 1.5T experiments.

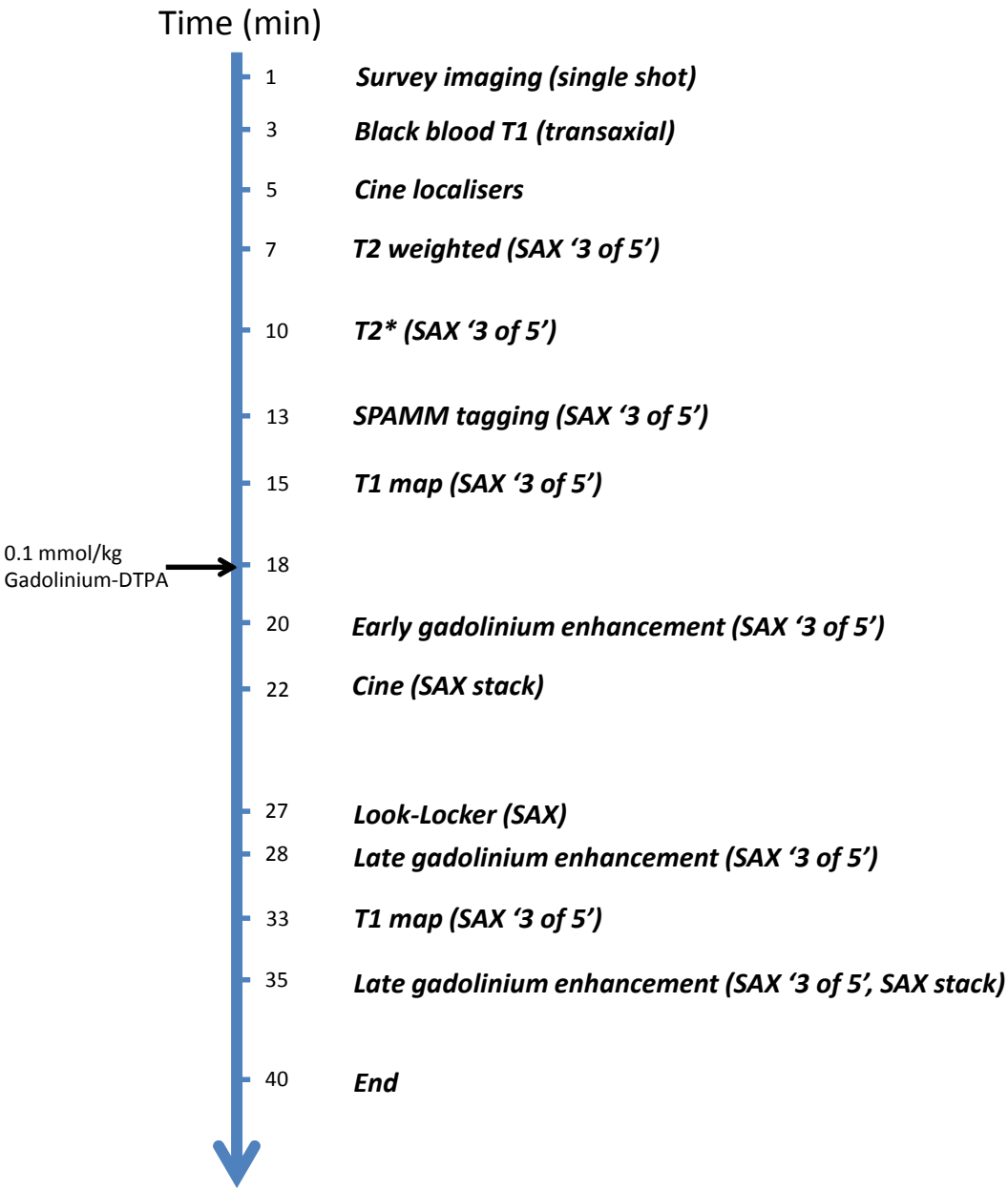

Figure 2.2. Imaging protocol for 3T experiments.

2.2.6. Contrast agents and delivery

All contrast-enhanced sequences were performed following an intravenous bolus dose of Gd-DTPA (dimeglumine gadopentetate, Magnevist, Bayer, Berlin, Germany) administered at a rate of 5 ml/s by a power injector (Medrad Spectris Solaris, Medrad, PA, USA). Experiments at 1.5 Tesla used a dose of 0.2 mmol/kg, and experiments at 3 Tesla administered at dose of 0.1 mmol/kg.

2.2.7. Analysis

Imaging analysis was primarily performed using commercially available analysis software wherever feasible. For the studies at 1.5 Tesla (Chapters 3 and 4), analysis was performed using MASS (versions 6.2.1-7.2, Medis, Leiden, The Netherlands). Studies at 3.0 Tesla were analysed using cvi42 (version 4.1, Circle Cardiovascular Imaging Inc., Calgary, Canada). Statistical analysis was performed using IBM SPSS® Statistics (versions 19.0-21.0, IBM Corporation, NY, USA).

3. Chapter 3
Peri-infarct Oedema and Contractile Recovery

3.1. Abstract

3.1.1. Objectives

To compare the relationship of myocardial oedema and corresponding contractile function over time in patients with reperfused acute myocardial infarction (AMI).

3.1.2. Background

Myocardial oedema is found following reperfused AMI, and contributes to stunning of peri-infarct myocardium. Regression of oedema on T2 weighted (T2w) cardiovascular magnetic resonance (CMR) imaging relates to improved myocardial contractility post AMI in animal models, but has not been demonstrated in humans.

3.1.3. Methods

Thirty-nine patients (34 men; mean age 57 years, range 35-73) underwent T2-weighted (T2w), tagging and late gadolinium enhancement magnetic resonance imaging at three time-points following primary percutaneous coronary intervention for ST-elevation AMI. We measured circumferential strain, T2w signal intensity and volume of infarct and peri-infarct zones, and remote myocardium. Patients were stratified by presence or absence of peri-infarct oedema defined as areas with T2w signal intensity ≥2 SD above remote myocardium. Statistical analysis used repeated measures ANOVA with *post-hoc* Bonferroni correction.

3.1.4. Results

Oedematous peri-infarct myocardium had attenuated strain compared to remote at day 2 (-0.137 vs. -0.226, $p<0.001$), day 30 (-0.188 vs. -0.240, $p<0.01$) and day 90 (-0.207 vs. -0.241, $p=0.01$). Non-oedematous peri-infarct myocardium had similar ($p>0.05$) strain to remote at all time points. Strain improved in oedematous peri-infarct myocardium at day 30 ($p=0.02$) and 90 ($p<0.01$), closely mirroring resolution of intensity and volume of oedema. Decreased strain correlated with oedema volume ($r=0.30$; $p=0.01$) and normalised oedema signal intensity ($r=0.28$; $p<0.01$). In 8 patients with fully transmural infarction, infarct zone strain improved between day 2 and 90 ($p=0.02$).

3.1.5. Conclusion

The improvement of strain in peri-infarct myocardium closely follows regression of myocardial oedema. Volume of oedema and intensity of signal on T2w imaging relate to functional recovery following reperfused AMI.

3.2. Objectives

To compare the relationship of myocardial oedema and corresponding contractile function over time in patients with reperfused acute myocardial infarction (AMI).

3.3. Background

Reperfusion of acute myocardial infarction (AMI) is associated with post-ischaemic dysfunction ("stunning") of viable myocardium (Bijnens et al., 2007). In animal models a dominant mechanism contributing to stunning is myocardial oedema due to the ischaemic insult (Bragadeesh et al., 2008). Cardiovascular magnetic resonance (CMR) imaging offers a number of techniques to determine the effects of AMI *in vivo*. The area of infarction may be delineated with late gadolinium enhancement (LGE) imaging (Kim et al., 2000). T2-weighted (T2w) imaging can be used to detect myocardial oedema, and when combined with LGE, can differentiate viable peri-infarct myocardium from non-viable tissue. The cellular processes that increase signal in peri-infarct myocardium on T2w imaging are currently debated (Friedrich et al., 2011), and the pathophysiological relevance of hyperintensity on T2w imaging is not fully understood. In particular, studies relating oedema on T2w CMR to quantitative evaluation of myocardial function are lacking. MR tagging is able to accurately measure regional myocardial strain (Swoboda et al., 2014). In a porcine model, peri-infarct myocardium had relatively preserved mechanical function post reperfusion, and the size of myocardial oedema as defined by T2w imaging correlated with strain in this area (Ruzsics et al., 2009). Whether a similar relationship between myocardial oedema and regional myocardial function exists in man has not been established.

In this experiment, patients were prospectively studied by serial CMR after primary percutaneous coronary intervention (PCI). The hypothesis was that strain is attenuated in oedematous myocardium, and that resolution of tissue

oedema correlates with recovery of contractile function in these regions. In order to test this hypothesis, the contractile function of oedematous and non-edematous myocardium was examined over time in patients with reperfused AMI.

3.4. Methods

Fifty-seven consecutive patients that fulfilled study criteria were enrolled, each of whom had first-presentation ST segment elevation AMI, treated with primary PCI within 12 hours of symptom onset. Patients with previous coronary revascularisation (PCI or coronary artery bypass surgery), previous myocardial infarction, renal failure (glomerular filtration rate <30 ml/min/1.73m^2) or contraindication to CMR were excluded. Serial CMR early after AMI is both feasible and safe (Greenwood et al., 2007). The study was approved by the regional research ethics committee. Written informed consent was obtained from all patients.

3.4.1. Image acquisition

Patients were scanned on a 1.5T MR system (Intera CV, Philips Healthcare, Best, The Netherlands) at median 2, 30 and 90 days post-AMI. An identical MR protocol was used for each visit. Cine, T2w, tagging and LGE images were performed in short axis slices with full left ventricular (LV) coverage and identical slice geometry. Cine imaging used a steady state free precession (SSFP) pulse sequence (echo time (TE) 1.4 ms; repetition time (TR) 2.8 ms; flip angle 55 degrees, spatial resolution 2 x 2 x 10 mm, sensitivity encoding (SENSE) factor 1.5, ≥18 phases per cardiac cycle). T2w imaging used a dark-blood T2w short tau inversion-recovery (STIR) fast spin echo sequence (TE 100 ms, TR two R-R intervals, flip angle 90 degrees, spatial resolution 1.43 x 1.43 x 10 mm). A 5-element phased-array surface coil was used with constant level appearance (CLEAR) homogeneity correction. Tagged images were acquired with a complementary spatial modulation of magnetisation (CSPAMM) sequence (spatial resolution 1.67 x 1.67 x 10 mm, typical TR/TE/flip angle 30ms/6ms/20 degrees, no slice gap, tag separation 8 mm, 18 phases). 10 minutes after an injection of 0.2 mmol/kg gadolinium-DTPA (dimeglumine gadopentetate; Magnevist, Bayer, Berlin, Germany), a short-axis stack of LGE images was acquired (inversion recovery-prepared T1-weighted gradient echo, TR/TE/flip angle 4.9 ms, 1.9 ms, 15 degrees, TI adjusted according to a Look-Locker scout, spatial resolution 1.35 x 1.35 x 10 mm). For follow-up scans, care

was taken to ensure similar slice positioning as the index scan, by aligning the proximal border of the most basal slice of the short axis stack to the mitral valve annulus in end-diastole.

3.4.2. Analysis

Images were analysed offline using standard software (MASS 6.2.1; Medis, Leiden, The Netherlands). In addition to alignment of slices during image acquisition, we ensured accurate registration between serial scans by selecting slices with similar myocardial features, such as ventricular shape and the presence and shape of papillary muscles. Left ventricular volumes and wall thicknesses were analysed from SSFP cine-images. Analysis was divided into two regions of interest around the infarction: the infarct zone, localised on LGE images, and the peri-infarct myocardium (salvaged myocardium), localised on T2w images. LGE imaging early after AMI may overestimate infarct size (Ibrahim et al., 2010; Ingkanisorn et al., 2004); conversely, T2w imaging for oedema delineates the area at risk acutely. To accurately differentiate non-viable infarct myocardium from viable peri-infarct myocardium, the infarct zone was therefore delineated on the 90-day scan, and the peri-infarct zone was defined on the acute scan. These areas were then cross-referenced to the other time points (Figure 3.1). The peri-infarct zone was defined as myocardium with hyperintensity on T2w imaging that surrounded, but was not within, infarcted myocardium (Figure 3.2).

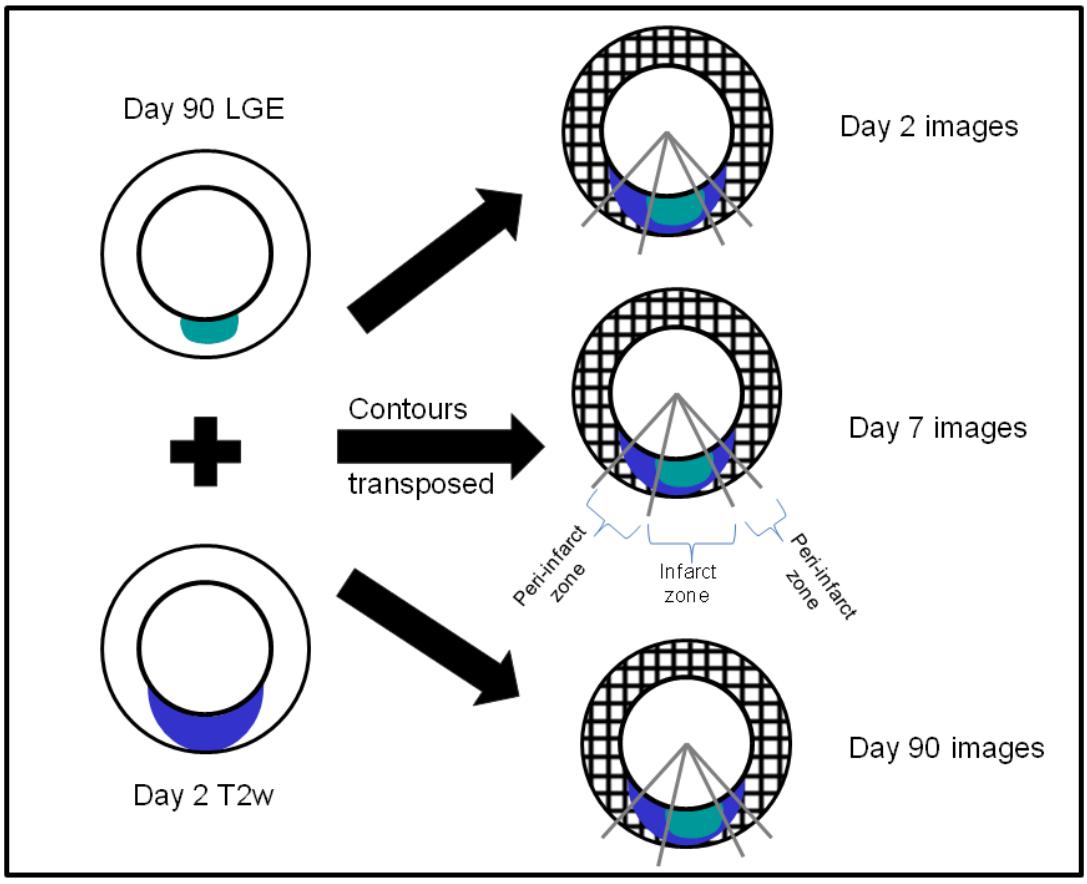

Figure 3.1. Delineation of infarct and peri-infarct zones.

The area of established infarction was taken from day 90 LGE images. The extent of peri-infarct oedema was taken from the day 2 T2w images. These contours were transposed to all time points for calculation of T2w signal intensity and strain.

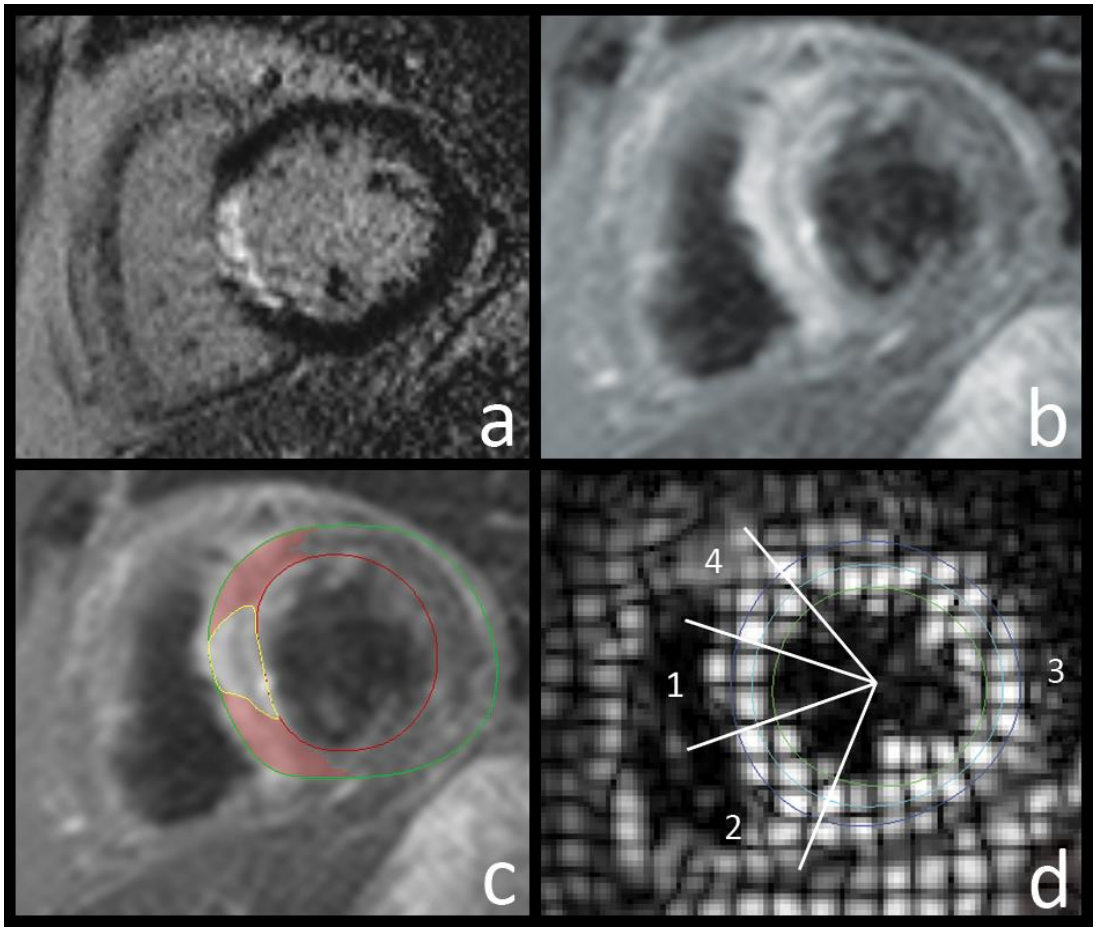

Figure 3.2. Case example delineating infarct and peri-infarct zones.

a) Infarction zone and transmural extent was defined on the 90-day short axis LGE image that showed maximum infarction. b) and c) The peri-infarct zone was determined from the corresponding acute T2w image. d) Strain analysis was performed on the corresponding CSPAMM image in the infarct (1) and peri-infarct (2 and 4) zones, and remote myocardium (3).

Areas of interest were manually transferred between images using in-house tracing software ('Tracer', Microsoft C#, .NET 4.0). The outline of the area of interest was manually traced on to the Tracer software, and was then manually traced back on to the target area of interest. Patients with respiratory artefact or motion artefact compromising the myocardium on T2w imaging at any time point were excluded. LV contours were drawn, with care taken to exclude endocardial high signal from slow-flowing blood. A reference region of interest was placed in normal remote myocardium. Myocardial hyperintensity for both T2w and LGE images were both defined using a similar thresholding technique to avoid bias; as areas with signal intensity ≥2 SD above the mean signal intensity of remote myocardium (Dall'Armellina et al., 2011). Volume of hyperintensity, and signal intensity of hyperintense and remote myocardium were calculated for T2w and LGE images, including any hypointense core. To allow for comparison of myocardial signal intensity between patients and studies, the ratio of peri-infarct to remote myocardial T2w signal intensity was calculated for each study. Data were also calculated using skeletal muscle as a reference point to T2w signal in oedematous myocardium (Abdel-Aty et al., 2005).

CSPAMM analysis was performed blinded to T2w and LGE (Tagtrack 1.8; Biomedical engineering, ETH Zurich, Switzerland), independently by two reviewers. Patients in whom the software was unable to match or propagate contours accurately were excluded. To maximise differentiation of peri-infarct and infarct zones, we performed strain analysis on the single short axis slice which demonstrated maximal infarction on the 90-day scan for each patient. As with T2w and LGE images, the position of this slice was tracked and cross-referenced for analysis at all three time points. Peak mid-myocardial circumferential Lagrangian strain was measured through infarct, peri-infarct and remote zones using the Tagtrack software (Figure 3.2d). For peri-infarct measurements, strain was evaluated in peri-infarct myocardium that was circumferentially adjacent to the infarcted myocardium. For comparison, patients without visible peri-infarct myocardium had strain measurements in the infarct and remote zones, and separately in a 12-degree sector circumferentially adjacent to either side of the infarct. This angle represented the mean extent of the peri-infarct zone in patients with T2w hyperintensity. To further investigate strain within the infarct zone, patients with fully transmural infarcts on the 3-month LGE images were analysed, and strain measured at all three visits in myocardium that demonstrated completely transmural infarction in the selected short axis slice *and* both neighbouring

slices (‘core infarct zone’).

3.4.3. Statistical analysis

Data are expressed as means ± SD. Differences in patient characteristics were evaluated with an independent samples t-test. Correlation between T2w and strain data were derived using Spearman’s rank test; differences in strain, size and intensity measurements over time were evaluated using repeated measures ANOVA; post-hoc testing with the Bonferroni correction. Differences between infarct locations were evaluated using one-way ANOVA; post-hoc testing performed with Tukey’s test. P values <0.05 were considered significant. Error bars denote standard error.

3.5. Results

3.5.1. Patient characteristics

57 patients were included. 9 did not attend all follow up scans, 6 had suboptimal tagging data (unsuitable for contour analysis) on one or more visits, and 3 had suboptimal T2w images for quantification on one or more visits, leaving 39 patients with data at all three time points available for analysis (Figure 3.3). 9 patients had no peri-infarct oedema. There were no significant differences in patient characteristics between patients with peri-infarct oedema and those without (Table 3.1, $p>0.05$ for all). Mean age was 57 years (range 35-73). There was no significant difference in age between males (57 (35-73) years) and females (60 (58-63) years) ($p=0.2$). All patients received dual antiplatelet therapy, angiotensin converting enzyme inhibition and beta blockade. No patient had an acute coronary event or revascularisation between baseline and the 90 day scan.

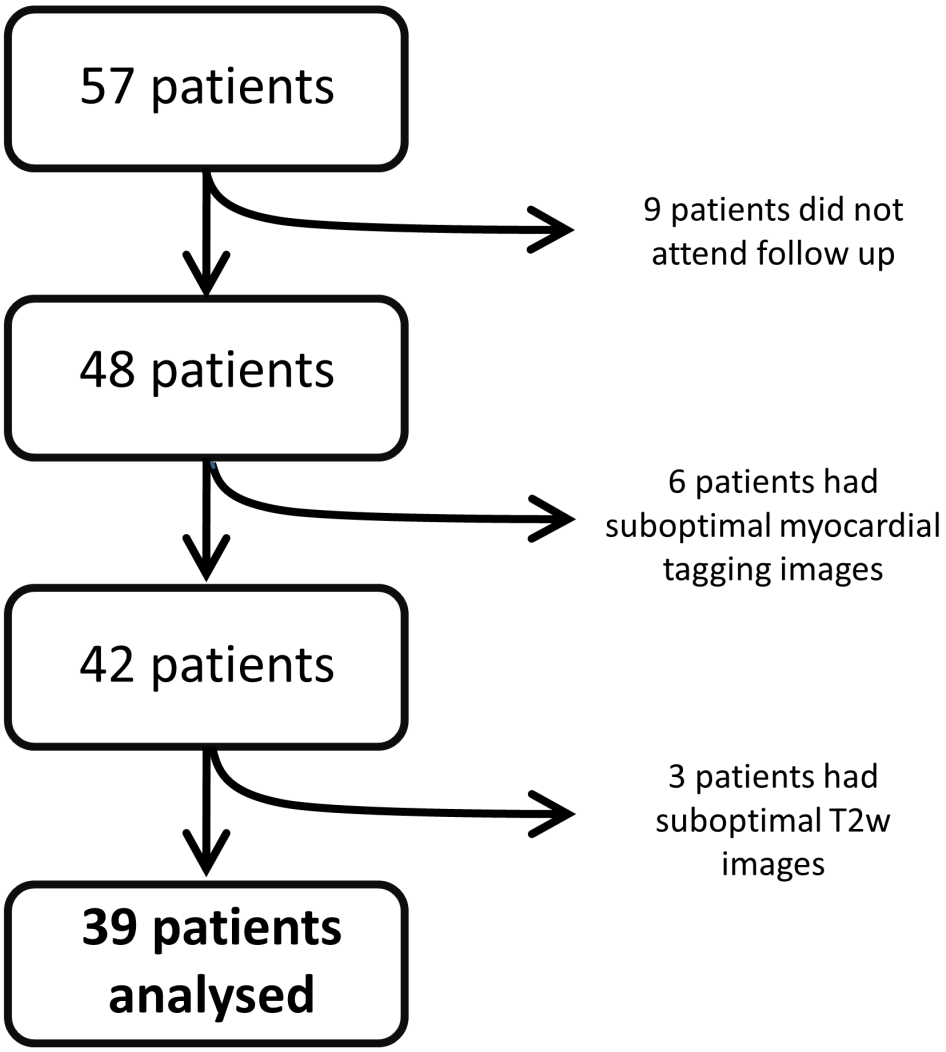

Figure 3.3. Recruitment flowchart.

Table 3.1. Patient characteristics

	Peri-infarct oedema present	**No peri-infarct oedema**
N	30	9
Mean age, years (range)	56 (35-69)	63 (49-73)
Male	27 (90%)	7 (78%)
Hypertensive	8 (27%)	4 (44%)
Diabetic	2 (7%)	0 (0%)
>50% transmural infarction	23 (76%)	9 (100%)
Anterior infarction	14 (47%)	2 (22%)
Median creatine kinase, U/l	1336	1527
Median door to balloon time (IQR), mins	68 (48-86)	65 (54-106)
Median pain to balloon time (IQR), mins	194 (157-238)	205 (147-345)
Infarct mass/LV mass, %	17 ± 15	23 ± 14
Oedema mass/LV mass, %	41 ± 22	17 ± 12
Indexed left ventricular end-diastolic volume, ml/m^2	88 ± 13	83 ± 16
Indexed left ventricular end-systolic volume, ml/m^2	49 ± 13	50 ± 14
Ejection fraction, acute, %	45 ± 9	41 ± 8
Ejection fraction, 90 days, %	51 ± 8	46 ± 6

Data are expressed as numbers with percentages in parentheses, or means ± standard deviation unless otherwise indicated. Masses and volumes are for entire LV stack, taken from acute images. Oedema mass refers to a combination of peri-infarct and infarct T2w signal hyperintensity.

Mean left ventricular end diastolic wall thickness in the infarct, peri-infarct and remote zones was 9±2mm, 9±2mm and 8±1mm respectively on day 2, and 8±2mm, 8±1mm and 7±1mm on day 90. There was no significant difference in LV wall thickness between acute and 90-day scans in the remote zone ($p=0.19$), and significantly lower wall thickness at 90 days in infarct ($p=0.01$) and peri-infarct ($p=0.011$) zones.

3.5.2. Oedema and infarct volume versus strain in patients with peri-infarct oedema

There was a significant decrease in normalised peri-infarct T2w signal intensity with time (mean 2.09 at 2 days, 1.26 at 30 days, 1.10 at 90 days; $F=6.21$; $p=0.014$), between 2 and 30 days ($p=0.04$), and between 2 and 90 days ($p=0.01$). A significant decrease in peri-infarct oedema volume was observed over time (means 39.3ml vs. 19.0ml vs. 4.6ml; $F=83.3$; $p<0.0001$), between 2 and 30 days ($p<0.01$), and between 2 and 90 days ($p<0.01$). Table 3.2 shows mean strain values in infarct, peri-infarct and remote zones. Significant improvement of oedematous peri-infarct strain was observed with time. This improvement in strain closely mirrored resolution of peri-infarct T2w signal intensity, and oedema volume (Figure 3.4).

Decreased circumferential strain correlated with oedema volume ($r=0.30$; $p=0.01$, Figure 3.5) and normalised T2w signal intensity ($r=0.28$; $p<0.01$, Figure 3.6). Over time, the infarct zone demonstrated significantly attenuated strain compared to the peri-infarct zone; both had attenuated strain compared to remote myocardium ($p<0.01$). Improvement in strain was observed in peri-infarct ($F=6.03$, $p<0.01$) and infarct zones ($F=20.34$, $p<0.01$) (Figure 3.7, Table 3.2), but not in remote myocardium ($F=1.44$, $p=0.24$).

Using a myocardial: skeletal ratio in the analysis did not affect the overall findings of the present study (e.g. T2w myocardial: skeletal ratio vs. strain, $r=0.41$, $p<0.001$).

Table 3.2. Circumferential strain by myocardial location and time in patients with peri-infarct oedema.

	2 days	**30 days**	**90 days**	**2 days – 30 days**	**2 days – 90 days**	**30 days – 90 days**
Infarct zone	-0.102	-0.160	-0.186	(<0.001)	(<0.001)	(0.04)
Peri-infarct zone	-0.137	-0.188	-0.207	(0.01)	(0.002)	(0.14)
Remote zone	-0.226	-0.240	-0.241	(0.10)	(0.17)	(1.00)
Infarct – peri-infarct zone comparison	(0.01)	(0.03)	(0.08)			
Infarct – remote zone comparison	(<0.001)	(<0.001)	(<0.001)			
Peri-infarct – remote zone comparison	(<0.001)	(0.003)	(0.01)			

n=30. Data are expressed as means; P values are shown in parentheses

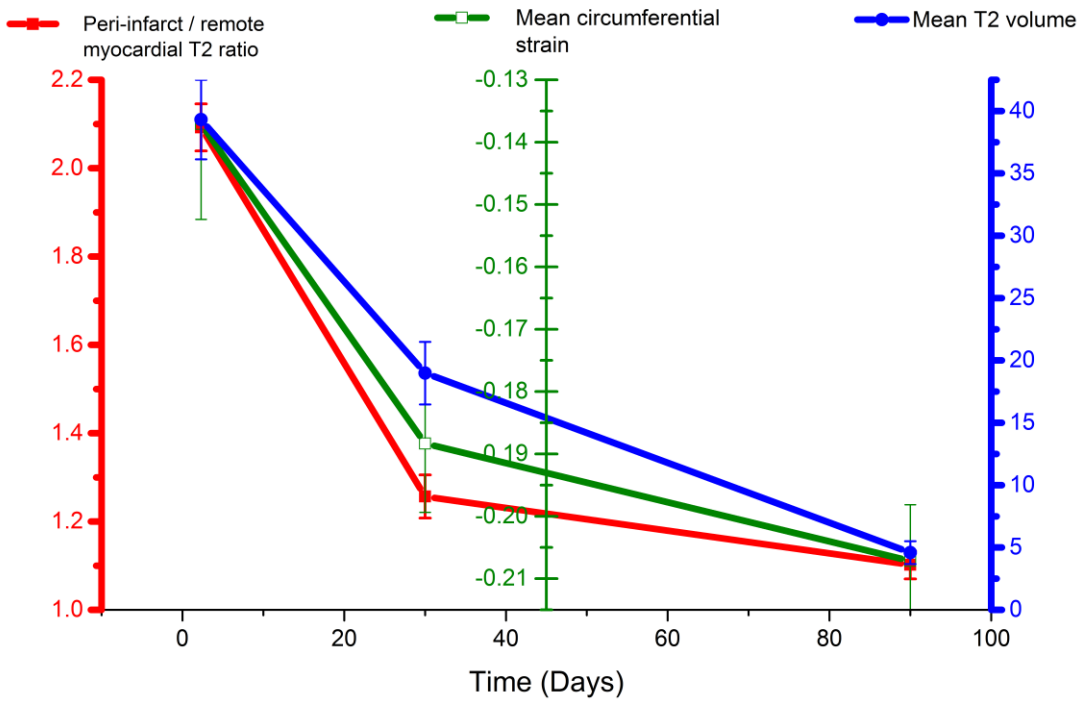

Figure 3.4. Change in strain, T2w signal intensity, and peri-infarct myocardial oedema volume (area at risk) in the peri-infarct zone. T2 volume in millilitres (ml).

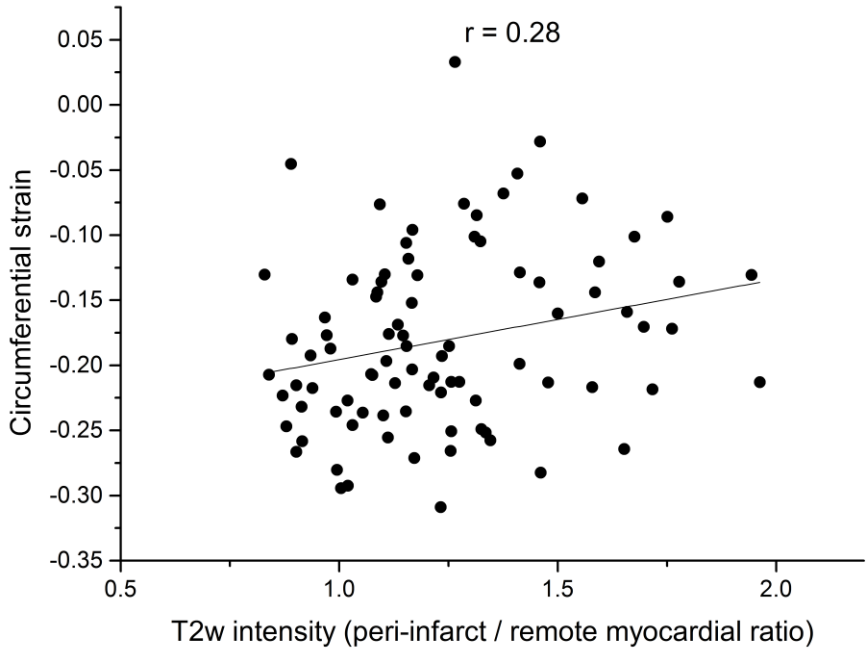

Figure 3.5. Volume of hyperintense myocardium on T2w images (oedema volume) vs. circumferential strain in the peri-infarct zone.

n=90 (30 patients at 3 time points).

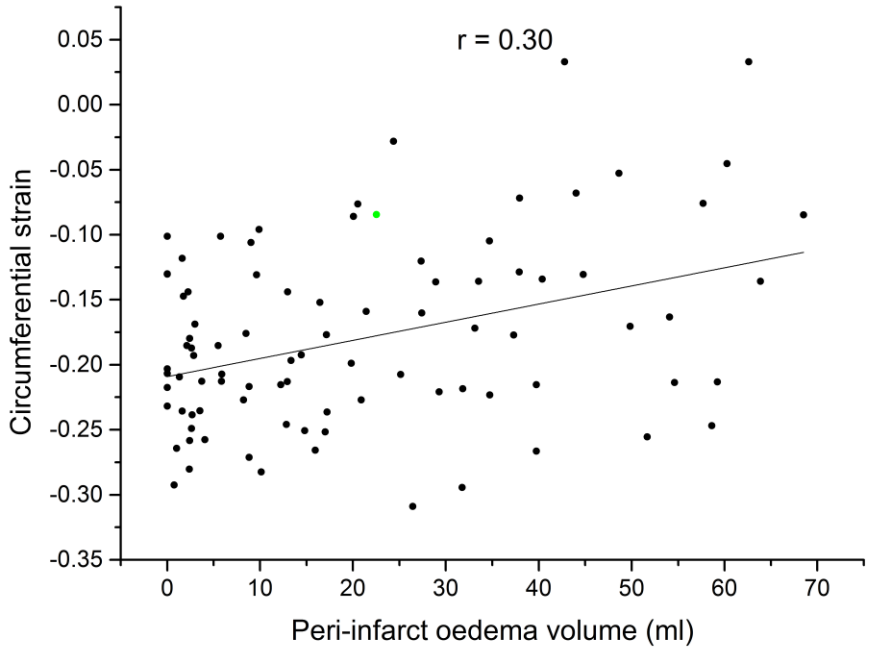

Figure 3.6. Strain in the peri-infarct zone vs. peri-infarct T2w signal intensity when normalised to remote myocardial intensity.

n=90 (30 patients at 3 time points).

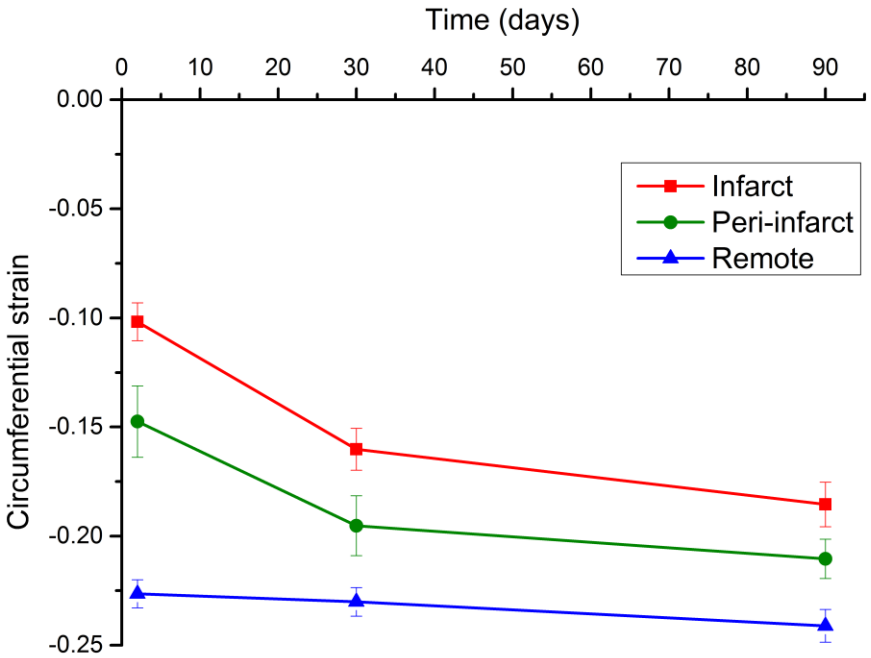

Figure 3.7. Strain according to proximity to infarct zone in patients with peri-infarct oedema.

n=30.

3.5.3. Strain in patients without peri-infarct oedema

For comparison, we measured strain in a similar area adjacent to the infarct zone in the 9 patients without visible peri-infarct oedema. Infarcted myocardium showed significant improvement in strain over time (means --0.087 (day 2), -0.127 (day 30), -0.177 (day 90), $F=19.1$, $p<0.01$). There was no significant difference in strain over time in the peri-infarct zone (means −0.229; −0.210; −0.216; $F=0.39$, $p=0.69$) and remote zone (means −0.218; −0.195; −0.203; $F=0.52$, $p=0.60$). There was no significant difference between peri-infarct strain and remote strain at 2 days, 30 days or 90 days ($p=0.69$, $p=0.38$, $p=0.34$ respectively).

3.5.4. Infarct location and transmural extent

Differing infarct locations had similar strain, normalised T2w signal intensity and T2w oedema volume (Table 3.3). Changes in infarct zone strain were similar in the <50% and >50% transmural infarction groups ($p=0.63$; $p=0.88$; $p=0.41$ at day 2, 30 and 90 respectively, Figure 3.8). Dividing infarct transmural extent into quartiles showed recovery of strain in each quartile, with most contractility in the 0-24% quartile (Figure 3.9).

Eight patients had 100% infarct transmural extent on at least 3 contiguous short axis LGE slices at day 90 (all had peri-infarct oedema). Strain in the core infarct zone improved at each time point (mean strains −0.103; −0.148; −0.194 at day 2, 30 and 90 respectively, $p=0.04$ for trend; $p=0.83$ for day 2 vs. 30, $p=0.02$ for day 2 vs. 90).

Table 3.3. Characteristics by infarct location in patients with peri-infarct oedema.

	Anterior	**Inferior**	**Posterior**	**Lateral**	**P**
n	14	12	3	1	
Mean infarct strain	-0.104	-0.107	-0.085	-0.067	0.80
Mean peri-infarct strain	-0.136	-0.180	-0.105	-0.045	0.29
Mean remote strain	-0.228	-0.235	-0.199	-0.188	0.29
Mean normalised T2w intensity	1.59	1.47	1.22	0.89	0.72
Mean T2w volume (ml)	44.6	29.3	47.9	60.3	0.051
Infarct volume (ml)	18.7	12.6	22.3	13.4	0.57

n=30.

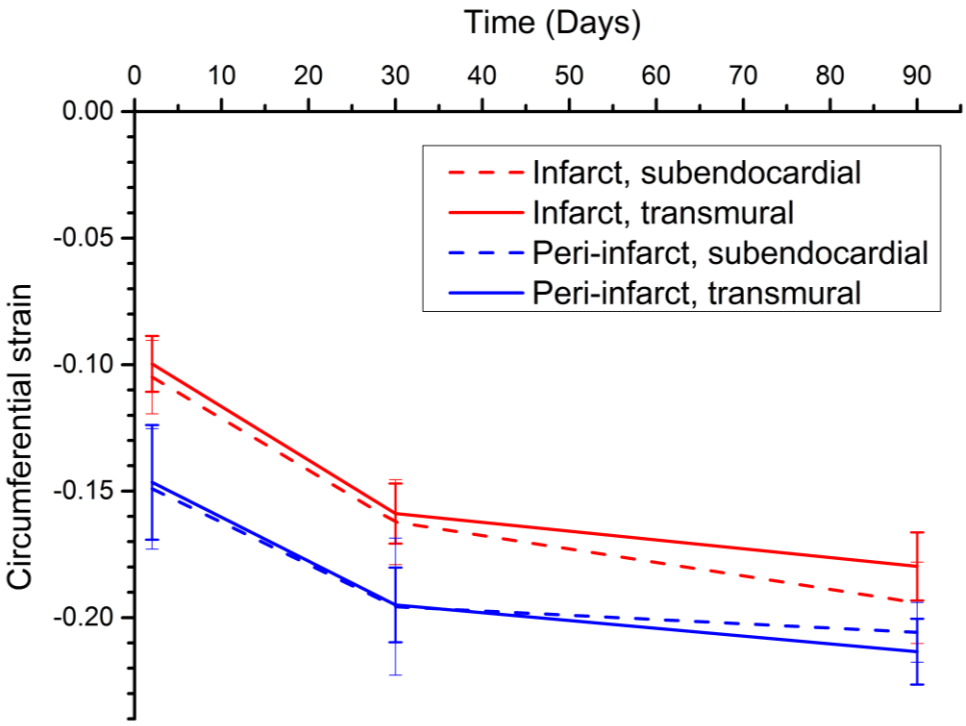

Figure 3.8. Infarct and peri-infarct zone circumferential strain according to infarct transmurality.

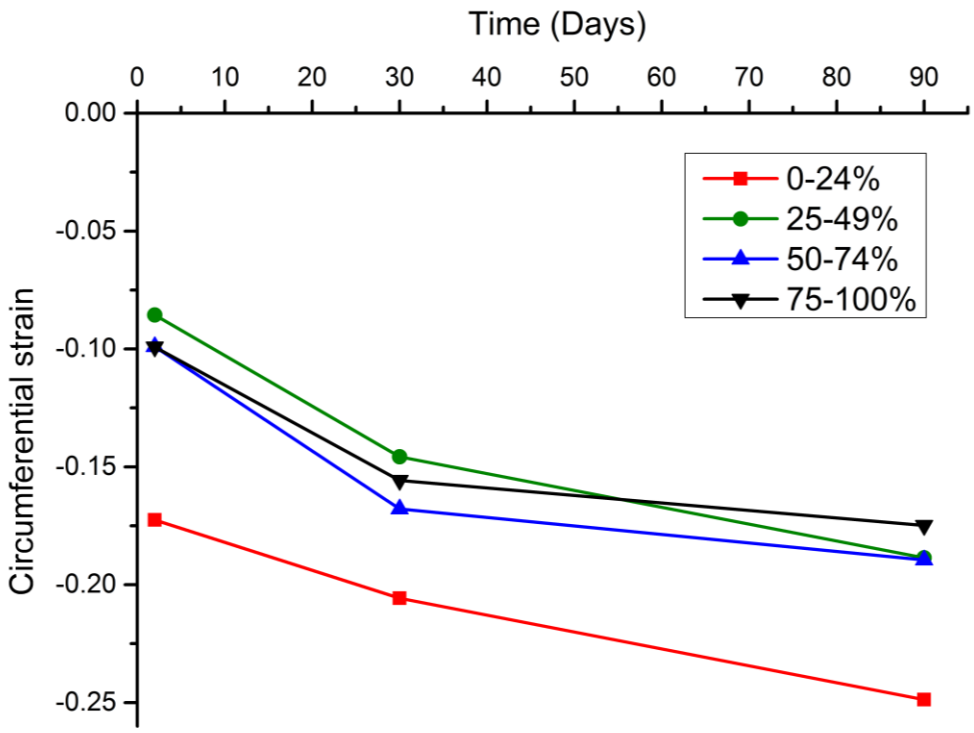

Figure 3.9. Infarct zone strain according to infarct transmural extent.

Transmural extent expressed as the percentage of LV myocardial thickness that demonstrated LGE hyperenhancement. n=2, n=5, n=7 and n=16 from lowest to highest quartile respectively.

3.6. Discussion

This study has found that early after AMI, the peri-infarct zone as delineated by T2w CMR demonstrates significantly impaired strain compared to remote myocardium and recovery of regional function in the peri-infarct zone follows the normalisation of T2w signal intensity. This effect is not seen in patients without peri-infarct T2w hyperintensity. Both transmural and subendocardial infarcts show evidence of functional recovery after AMI.

Myocardial salvage is the goal of reperfusion therapy, and is an important surrogate endpoint to assess the success of reperfusion techniques (Pennell, 2006). T2w CMR accurately depicts the area at risk in canine (Aletras et al., 2006) and murine (Beyers et al., 2012) models. The cellular processes that lead to hyperintensity on T2w imaging are poorly understood, and the utility of T2w imaging in the acute setting remains the subject of debate (Friedrich et al., 2011). This study helps confirm the functional relevance of T2w imaging, namely that salvaged myocardium, as measured by T2w, has significant contractile impairment early after AMI, and shows functional improvement in comparison to peri-infarct myocardium without hyperintensity up to 90 days following AMI. Patient management may be improved via enhanced functional stratification, as well as giving further insights into the mechanisms behind the prognostic value of myocardial salvage imaging.

The mechanisms of myocardial stunning are multifactorial, including tissue oedema (Bolli, 1990). Many of the other proposed processes leading to stunning are difficult to study *in vivo*. The functional effects of myocardial oedema have been observed in animal studies with findings similar to our study. In a porcine model, an inverse relationship between myocardial oedema and circumferential myocardial strain was demonstrated, with resolution of myocardial oedema mirroring improvement in strain up to 5 days following reperfusion (Bragadeesh et al., 2008). Additionally, strain in the infarct zone was more attenuated than the peri-infarct zone, which in turn had depressed strain as compared to remote myocardium (Ruzsics et al., 2009). The authors suggested that myocardial oedema reduces contractility by increasing the distance between actin and myosin filaments.

Human studies have largely estimated myocardial oedema via indirect measures such as myocardial wall thickness by echocardiography. Echocardiography studies have looked at strain in the peri-infarct region (Becker et al., 2009) and noted recovery of strain with time (Ingul et al., 2005),

but have not been able to relate the region of recovery to myocardial oedema. T2w CMR has been shown to directly visualise ischaemia-related oedema, and reflects the ischaemic zone rather than infarction (Johnston et al., 1988). Dall'Armellina *et al*. found a visual improvement in wall motion with regression of T2w hyperintensity (Dall'Armellina et al., 2011), but prior to the current report no human study has demonstrated the association of regression of myocardial oedema on T2w with improvement in regional contractile function by strain analysis.

We observed a correlation of both the oedema volume and of increased signal intensity of oedematous myocardium with impairment of circumferential strain. Myocardial strain is affected by a variety of factors, such as presence of diabetes (Fang et al., 2004), hypertension (de Simone et al., 1997), preload or left ventricular cavity size (Sutherland et al., 2004). These factors may help account for the relatively wide variance around the trend when examining absolute strain values and could not be corrected for in the current study due to sample size limitations. Our data are observational and the conclusion that LGE and T2 predict strain cannot be reliably made. Nonetheless, patients with more peri-infarct T2w hyperintensity have comparatively attenuated contractile function acutely within that zone, and that patients with larger volumes of oedematous myocardium may have potential for increased functional recovery with time.

Recovery of function within the infarct zone was observed regardless of infarct transmural extent. The core infarct zone in patients with complete transmural LGE hyperenhancement showed significant improvement in strain over time, together with a significant, but small, decrease in mean wall thickness in the infarct zone for all patients. These findings question the conventionally upheld belief that hyperenhanced tissue on LGE imaging is completely non-viable and that functional recovery cannot be expected in segments showing transmural hyperenhancement (Choi et al., 2001; Kim et al., 2000). The findings in our study are supported by a number of previous observations. Histopathologically, sections of myocardial infarct scars demonstrate foci of normal myocardial fibre architecture within the areas of necrosis (Fishbein et al., 1978). In one report the mean myocyte fraction from sections of scar tissue defined by LGE imaging was 62% (Gunning et al., 2002). Recovery of regional function with time has been previously reported following reperfused transmural AMI (Bogaert et al., 1999; Rogers et al., 1999). Gerber *et al.* (Gerber et al., 2002) found approximately 1.5-fold improvement in circumferential strain in infarcted segments between 4 days and 7 months. There are several potential

reasons for the apparent discrepancy in the literature. The original MR viability studies used qualitative, visual scoring of regional function. LGE early after AMI may overestimate infarct size (Ibrahim et al., 2010; Ingkanisorn et al., 2004); this study defined infarct extent on the 90 day scan. Measurement overlap or tethering of the infarct segment to viable peri-infarct tissue may give rise to an apparent measurement of strain. The spatial resolution of myocardial tagging is unlikely to have generated substantial error. Harmonic phase (HARP) analysis tracks motion between tag intersections, and the displacement map is accurate to <1mm (Osman et al., 1999). At least 60 tagging points per contour were used, giving an approximate resolution of 2.9mm. Additionally, our finding of *higher* peri-infarct contractile impairment with larger T2w volumes is contrary to the suggestion that partial volume affects may have substantially influenced the results. Additionally, remote myocardial hypertrophy and hyperkinesis have been reported post-AMI (Anversa et al., 1985a). Studies in man (Grines et al., 1989; Yoshino et al., 1998) have shown compensatory hyperkinesis in less than one third of patients. The absence of LV wall thickening in infarct and peri-infarct zones over time, and the lack of remote myocardial strain changes with time suggest that these are not dominant effects in this cohort.

3.6.1. Limitations

The study has limitations. Nine of 57 patients eligible for the study had T2w or tagging series of insufficient quality for analysis. Myocardial T2 signal is affected by water content but also by general patient characteristics and inhomogeneity in MR coil sensitivities. The coil sensitivity correction methods used correct for some of these issues. Using remote myocardium to normalise T2w signal intensity may not account for global myocardial water content change; however, no change of this type has been observed in animal models (Bragadeesh et al., 2008). All patients received standardised interventional and medical treatment in accord with contemporary practice, but given the limited sample size of this study, we were not able to control for any variations in this treatment. Alternative T2w sequences (Aletras et al., 2008; Payne et al., 2011) may offer increased tissue contrast or reproducibility, however T2-STIR is suited to detecting myocardial oedema in the acute setting (DO et al., 2012), and remains the reference standard with pathological validation (Aletras et al., 2006). This study has not examined the role of peri-infarct myocardium epicardially to the infarct zone. Such a study would have to control for infarct transmural extent, LV wall thickness and the decreased reproducibility of epicardial strain measurements (Swoboda et al., 2014). Whilst a number of

steps were used to ensure corresponding slice positioning between different imaging modalities and time points, different areas of myocardium may have been sampled due to patient factors or change in heart geometry. Defining the infarct zone on the 3-month LGE study may not account for infarct size remodelling between the acute and follow up scans. This remodelling predominantly occurs in an endocardial-epicardial direction, rather than circumferentially. The authors felt this effect to be smaller than the potential error introduced by inferring the infarct zone from the contemporaneous LGE scan, which has been shown to overestimate the true infarct size by up to 50% in the acute phase (Ibrahim et al., 2010), or by using a segmental analysis, which offers no method to control for heterogeneity of tissue within a segment.

3.7. Conclusions

This study provides direct evidence of oedematous, stunned myocardium demonstrating contractile recovery as oedema regresses. The volume and intensity of hyperenhanced myocardium on T2w imaging, as surrogates of myocardial oedema, correlated with CMR measurements of myocardial strain. Larger regions of stunned myocardium have decreased contractile function compared to smaller regions, suggesting that reperfused hearts with large volumes of T2w hyperintensity may be subject to greater recovery of function with time.

4. Chapter 4
Infarct Characterisation and Contractile Recovery

4.1. Abstract

4.1.1. Objectives

To investigate the role of microvascular obstruction (MO) and intramyocardial haemorrhage (IMH) in contractile recovery within infarcted and remote myocardium following reperfused acute myocardial infarction (AMI).

4.1.2. Background

Following AMI, MO and IMH adversely affect left ventricular remodelling and prognosis independently of infarct size. Whether this is due to infarct zone remodelling, changes in remote myocardium or other factors is unknown. We investigated the role of MO and IMH in recovery of contractility in infarct and remote myocardium.

4.1.3. Methods

Thirty-nine patients underwent cardiovascular magnetic resonance (CMR) with T2-weighted and T2* imaging, late gadolinium enhancement (LGE) and myocardial tagging at 2, 7, 30 and 90 days following primary percutaneous coronary intervention for AMI. Circumferential strain in infarct and remote zones was stratified by presence of MO and IMH.

4.1.4. Results

Overall, infarct zone strain recovered with time ($p<0.001$). In the presence of MO with IMH and without IMH, epicardial strain recovered ($p=0.03$, $p<0.01$ respectively), but mid-myocardial or endocardial strain did not (mid-myocardium: $p=0.05$, $p=0.12$; endocardium: $p=0.27$, $p=0.05$, respectively). By day 90, infarcts with MO had more attenuated strain in all myocardial layers compared to infarcts without MO ($p<0.01$); those with IMH were attenuated further ($p<0.01$). Remote myocardial strain was similar across groups at all time-points ($p>0.2$). Infarct transmural extent did not correlate with strain ($p>0.05$ at each time point). In multivariable logistic regression, MO and IMH were the only significant independent predictors of attenuated 90-day infarct zone strain ($p=0.004$, $p=0.011$, respectively).

4.1.5. Conclusions

Strain improves within the infarct zone overall following reperfusion with or without MO or IMH. Mid-myocardial and endocardial infarct contractility is diminished in the presence of MO, and further in the presence of IMH. MO and IMH are greater independent predictors of infarct zone contractile recovery than infarct volume or transmural extent.

4.2. Objectives

To investigate the role of microvascular obstruction (MO) and intramyocardial haemorrhage (IMH) in recovery of contractility in infarcted and remote myocardium following reperfused acute myocardial infarction (AMI).

4.3. Background

Following reperfused AMI, the left ventricle (LV) undergoes structural alterations both within and outside of the area of infarction, referred to as LV remodelling. The pathophysiology of this process is complex, with multiple ultrastructural, metabolic and neurally mediated processes occurring in infarcted and remote myocardium (Sutton and Sharpe, 2000). In up to 30% of patients, coronary reperfusion is associated with MO (Moens et al., 2005), seen angiographically as 'no-reflow' (Kloner et al., 1974). MO has been associated with adverse prognosis, adverse LV remodelling and diminished recovery of LV function, independently of infarct size (Morishima et al., 2000; Wu et al., 1998a). Reperfusion may also lead to IMH in the infarct core (Roberts et al., 1983) via extravasation of blood through damaged endothelium (Basso and Thiene, 2006). Like MO, IMH is associated with adverse LV remodelling and adverse prognosis, independently of infarct size (Mather et al., 2011). The mechanisms by which MO and IMH affect LV remodelling are poorly understood. Specifically, it is not known how they affect local remodelling and recovery in the infarct zone compared with remote myocardium.

Cardiac magnetic resonance (CMR) imaging can non-invasively evaluate myocardial infarction, MO and IMH. Hyperenhanced myocardium on late gadolinium enhancement (LGE) imaging correlates with infarction histologically (Kim et al., 2000), whilst a hypoenhanced infarct core on LGE corresponds to MO (Rochitte et al., 1998). IMH has been assessed by T2-weighted (T2w) and T2* CMR (Basso et al., 2007; Ganame et al., 2009; Mather et al., 2011; O'Regan et al., 2010). In chronic infarction, increasing transmural extent of infarction with LGE imaging correlates with impaired recovery of contractile function after revascularisation (Kim et al., 2000). However, in AMI, LGE can overestimate infarct size (Ingkanisorn et al., 2004). Within hyperenhanced myocardium on LGE, contractile activity has been demonstrated both by measures of strain at rest (Rogers et al., 1999), and as contractile reserve with dobutamine (Dendale et al., 1998). Contractile function

can also be measured by CMR, using myocardial tissue tagging, allowing a direct comparison of contractility and infarct characteristics from CMR data. We sought to investigate how MO and IMH affect contractile function as measured by tissue tagging CMR in infarcted and remote myocardium acutely and late following AMI.

4.4. Methods

Patients with first AMI, revascularised by primary percutaneous coronary intervention (PCI) within 12 hours of onset of pain were included. Myocardial infarction was defined by symptoms consistent with acute myocardial ischaemia, with electrocardiographic ST-segment elevation or new onset left bundle branch block associated with a rise and/or fall in cardiac enzyme concentration. Exclusion criteria were previous MI or coronary revascularisation, estimated glomerular filtration rate <30ml/min/1.73m^2, cardiomyopathy, or contraindications to CMR. Patients with maximal circumferential extent of myocardial scar <4mm, without scar on adjacent slices were deemed too small for accurate tagging analysis and excluded from the analysis. Clinical management (including use of aspiration catheters and glycoprotein IIb/IIIa receptor inhibitors) was at the discretion of the responsible physician, with the intention to reflect contemporary practice and guidelines. CMR results were not revealed to the clinical team. All patients were considered for beta-blockade, angiotensin converting enzyme inhibitors, statins, dual antiplatelet therapy, and cardiac rehabilitation.

4.4.1. Image acquisition

All patients underwent CMR scanning on a 1.5T system (Intera CV, Philips Healthcare, Best, The Netherlands) within 3 days of their index presentation and at 7-10, 30 and 90 days post-AMI. The same CMR protocol was used for each of the visits. A stack of images covering the whole LV, with the same slice geometry, position and slice thickness were used for all sequences. Cine imaging used a steady state free precession (SSFP) pulse sequence (echo time (TE) 1.4ms; repetition time (TR) 2.8ms; flip angle 55°, spatial resolution 2 x 2 x 10 mm, ≥18 phases per cardiac cycle), covering the whole heart in parallel short axis slices. To minimise differing volume effects between image types, 10mm slice thickness was used for all sequences. Tagged CMR used a complementary spatial modulation of magnetisation (CSPAMM) pulse sequence

(spatial resolution 1.67 x 1.67 x 10 mm, no gap, tag separation 8mm, ≥18 phases, typical TR/TE/flip angle 30ms/6ms/20°). T2w CMR used a dark-blood T2w short tau inversion-recovery fast spin echo sequence (TE 100 ms, TR 2x R-R interval, flip angle 90°, spatial resolution 1.43 x 1.43 x 10 mm). T2* images were obtained with a dual echo T2* gradient echo sequence (TE 4.6/9.2ms, TR 12.3ms, flip angle 30°, spatial resolution 1.43 x 1.43 x 10 mm). A dose of 0.2 mmol/kg of gadolinium-DTPA (dimeglumine gadopentetate; Magnevist, Bayer, Berlin, Germany) was then administered using a power injector (Spectris, Solaris, PA). A short-axis LGE stack was acquired after 10 minutes (inversion recovery-prepared T1 weighted gradient echo, inversion time according to a Look-Locker scout, TR/TE 4.9/1.9ms, flip angle 15°, spatial resolution 1.35 x 1.35 x 10 mm). For follow-up, care was taken to ensure similar slice positioning, by aligning the proximal border of the most basal slice of the short axis stack to the mitral valve annulus in end-diastole and comparing slice position to the index scan.

4.4.2. Image analysis

Images were analysed offline using commercial software (MASS 7.2; Medis, Leiden, The Netherlands and Tagtrack 1.8; Biomedical engineering, ETH Zurich, Switzerland). Infarct location was determined by CMR, according to standard guidelines (Cerqueira et al., 2002). In addition to the alignment of slices during image acquisition, we verified accurate alignment of serial scans by comparing features such as the presence and shape of papillary muscles. Left ventricular volumes and wall thicknesses were analysed from SSFP cine-imaging. Infarcts and MO were measured from LGE images. Infarct was defined as an area of gadolinium hyperenhancement ≥2 standard deviations (SD) above remote myocardium, and infarct volume estimation included any hypointense core. MO was defined visually as the hypointense core within the infarcted zone and planimetered manually. Volumes of infarct and MO were calculated from planimetered areas across the whole LV stack by the modified Simpson's method. The presence and extent of myocardial haemorrhage was assessed by combined analysis of T2w and T2* sequences (Mather et al., 2011). On T2w images, areas with mean signal intensity more than 2 SD below the periphery of the area at risk (AAR) were considered to be haemorrhage (Basso et al., 2007; Ganame et al., 2009). On the T2* images, the presence of a dark core within the infarcted area by visual inspection of the images was used as confirmation of myocardial haemorrhage. Only when T2w and T2* images showed concordant findings was an area considered to represent haemorrhage.

For CSPAMM analysis, endocardial and epicardial borders were drawn by a semi-automated process, and a midline calculated automatically. To minimise partial volume effects, strain was measured in the single short axis slice which demonstrated maximal infarction on LGE imaging. One short axis slice per patient at each time point was analysed for strain. In all cases, this slice was in the same position along the long axis for each of the time points in a given patient, and every slice had LGE hyperenhanced myocardium on the adjacent slices. Circumferential Lagrangian strain was measured at endocardial, mid-myocardial and epicardial layers through the infarct and remote zones (Figure 4.1). Remote strain measurement was taken in a 30 degree arc of myocardium diametrically opposite to the infarct zone. No patient had LGE in remote myocardium. To minimise the effects of passive post-systolic shortening (Kukulski et al., 2003), strain was measured at end systole, taken as the phase at the time of end-systole on the corresponding SSFP cine slice.

Transmural extent of infarction was graded into quartiles at each time point from anonymised LGE images at the same position as the selected CSPAMM slice by consensus of two observers (AK and SP), blinded to the results of other sequences.

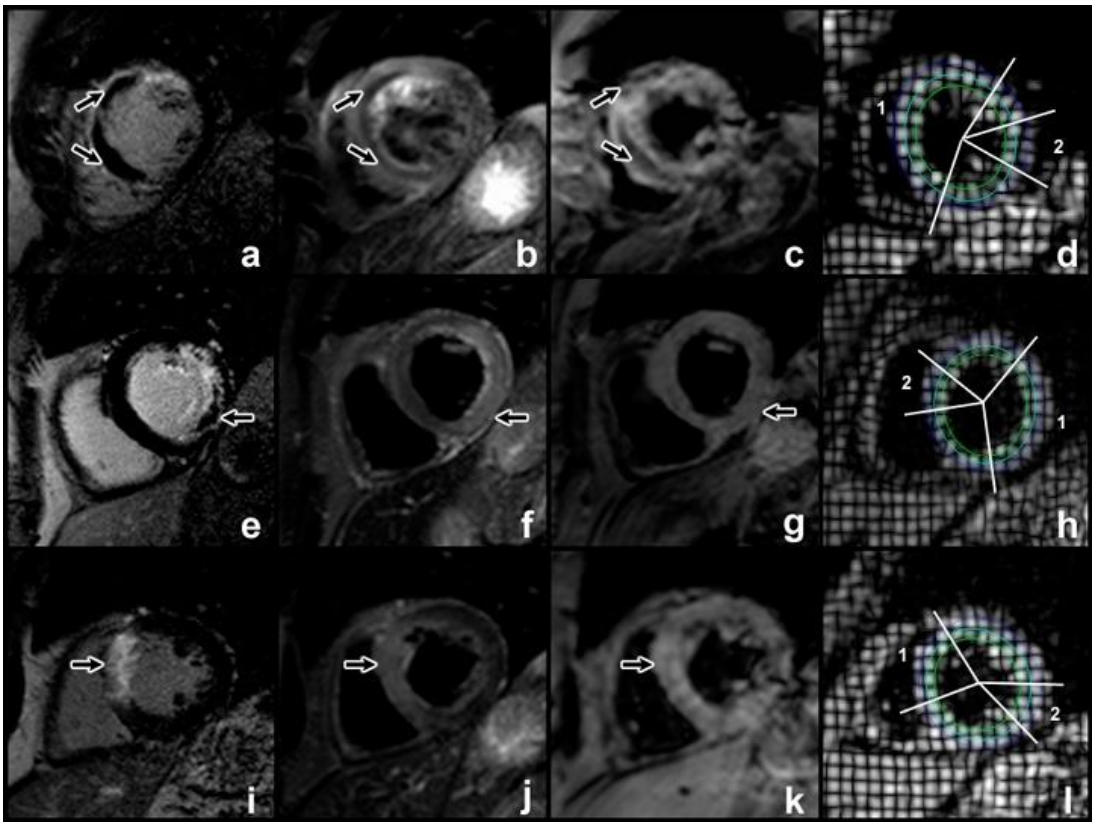

Figure 4.1. Infarct characterisation by CMR.

Patient with MO and IMH (a-d). LGE image demonstrates anterior and septal hyperenhancement, corresponding to scar. The central hypoenhanced core corresponds to MO (a, arrowed). T2w (b) and T2* (c) imaging show central hypoenhancement (arrowed), indicative of IMH. Strain measurements in epicardial, mid-myocardial and endocardial tracks are measured (d) for infarcted (1) and remote (2) zones. A similar arrangement of images for infarction with MO but no IMH is shown (e-h). Note absence of central hypoenhancement in T2w and T2* sequences (arrowed). A patient without MO is shown (i-l).

4.4.3. Statistical analysis

Statistical analysis was performed using IBM SPSS® Statistics 19.0. Continuous variables were expressed as means ± SD. Correlation between T2w and strain data were derived using Spearman's rank test; differences in strain and size measurements over time were evaluated using repeated measures analysis of variance (ANOVA); post-hoc testing was performed with the Bonferroni correction. Differences in transmural quartiles over time were evaluated with the Friedman test. Normality for strain data was established using the Kolmogorov-Smirnov test. Differences in infarct pathophysiology at a single time point were evaluated using one-way ANOVA; post-hoc testing was performed with Tukey's test. Univariable analyses were performed to identify predictors of reduced strain at 90 days. Variables with a probability value <0.1 in the univariable analysis were included in a multivariable analysis, which was based on a logistic regression model with a repeated measures variable (to adjust for non-independence of strain data). All statistical tests were 2-tailed; P values <0.05 were considered significant. Error bars for mean values denote standard error.

4.5. Results

4.5.1. Demographics

50 patients met the inclusion criteria. Two patients were excluded due to claustrophobia, 2 refused follow-up and 1 died before completing follow-up. In 6 other patients the tagging software failed to accurately track the tagged images due to artefact. Therefore 39 patients completed baseline and follow up scans and were included in the statistical analysis. Of these, 10 patients had tagging and T2w imaging at either day 2 or day 7, with 29 having these images at both these time points. All 39 had imaging at day 30 and day 90.

4.5.2. Infarct characteristics

Patient data were divided into three groups for analysis; patients without MO or IMH, patients with MO but no IMH, and patients with both MO and IMH. No patient had IMH without MO. Patient characteristics were similar between the three groups (Table 4.1). Infarct characteristics are shown in Table 4.2.

Table 4.1. Patient characteristics.

	No MO or IMH (n=17)	**MO only (n=8)**	**MO and IMH (n=14)**	**p value**
Age, years	58 ± 10	55 ± 9	59 ± 8	0.70
Male	16 (94%)	8 (100%)	10 (71%)	0.12
Current smoker	9 (53%)	4 (50%)	7 (50%)	1.00
Hypertension	7 (41%)	3 (38%)	1 (7%)	0.08
Hypercholesterolemia	11 (65%)	3 (38%)	8 (57%)	0.50
Family history of premature heart disease	6 (35%)	3 (38%)	6 (43%)	0.91
Diabetes mellitus	0 (0%)	1 (13%)	1 (7%)	0.31
Pain to balloon time, mins (median (IQR*))	205 (126)	194 (77)	210 (200)	0.93
Infarct territory				
Anterior	5	4	6	
Inferior	11	3	6	0.69
Lateral	1	1	1	
GP† IIb/IIIa inhibitor used	3 (18%)	3 (38%)	4 (29%)	0.64
TIMI flow pre-PCI ≥ 2	4 (24%)	0 (0%)	1 (7%)	0.25
TIMI flow post PCI				
Grade 2	1 (6%)	1 (11%)	0 (0%)	0.69
Grade 3	16 (94%)	8 (89%)	14 (100%)	
Peak CK‡ (U/l)	1234 ± 976	1711 ± 1442	2640 ± 1997	0.051

Data as mean ± SD or n (%). *IQR = interquartile range, †GP = Glycoprotein, ‡CK = creatine kinase

Table 4.2. Infarct characteristics.

Days post AMI		No MO or IMH	MO only	MO and IMH	p value between groups
2	Ejection fraction, %	45 ± 10*	42 ± 5*	38 ± 9*	0.10
	LV EDVi†, ml/m^2	85 ± 14	96 ± 15*	93 ± 22	0.27
	LV ESVi‡, ml/m^2	47 ± 14*	56 ± 14*	58 ± 20	0.16
	LV end-diastolic wall thickness, infarct zone, mm	8 ± 2*	9 ± 2	8 ± 2	0.72
	LV end-diastolic wall thickness, remote zone, mm	7 ± 1	8 ± 1	7± 1	0.78
	LV mass, g/m^2	58 ± 15*	59 ± 11*	57 ± 19*	0.92
	LGE infarct volume, ml	21 ± 16*	32 ± 17	41 ± 20*	0.02
	Median LGE infarct transmural extent	75-100%	75-100%	75-100%*	0.10
	LGE MO volume, ml	-	3 ± 3*	4 ± 4*	0.41
90	Ejection fraction, %	51 ± 9*	50 ± 5*	42 ± 8*	<0.01
	LV EDVi, ml/m^2	85 ± 19	90 ± 14*	100 ± 27	0.17
	LV ESVi, ml/m^2	42 ± 17*	45 ± 11*	59 ± 23	0.04
	LV end-diastolic wall thickness, infarct zone, mm	7 ± 1*	7 ± 1	6 ± 1	0.13
	LV end-diastolic wall thickness, remote zone, mm	7 ± 2	7 ±1	7 ± 1	0.72
	LV mass, g/m^2	55 ± 15*	56 ± 11*	52 ± 18*	0.82
	LGE infarct volume, ml	14 ± 10*	16 ± 7	29 ± 16*	<0.01
	Median LGE infarct transmural extent	75-100%	75-100%	50-75%*	0.73

Data as mean ± SD or n (%) unless indicated. *Characteristics that are significantly different between day 2 and day 90 are indicated. †LV EDVi = Left ventricular end diastolic volume, indexed to body surface area, ‡LVESVi = Left ventricular end systolic volume, indexed to body surface area

Patients without MO or IMH had similar infarct size to patients with MO, but those with IMH had significantly larger infarcts than patients without IMH both at baseline (mean infarct volume 41±20ml vs. 21±16ml, p=0.02) and 90 days (mean infarct volume 21±16ml vs. 14±10ml, p<0.01). Infarct size decreased significantly over time in all three groups (no MO group, F=7.5, p<0.01; MO with no IMH group, F=9.8, p<0.01; MO and IMH group, F=7.2, p=0.01) (Table 4.2, Figure 4.2). There was also a significant decrease in infarct transmural extent over time in the patients with MO and IMH (p<0.01), but not in patients with MO and no IMH (p=0.1) or without MO or IMH (p=0.6) (Table 4.1). There was no significant difference in infarct transmural extent between the groups at any time point (p>0.05 at each time point).

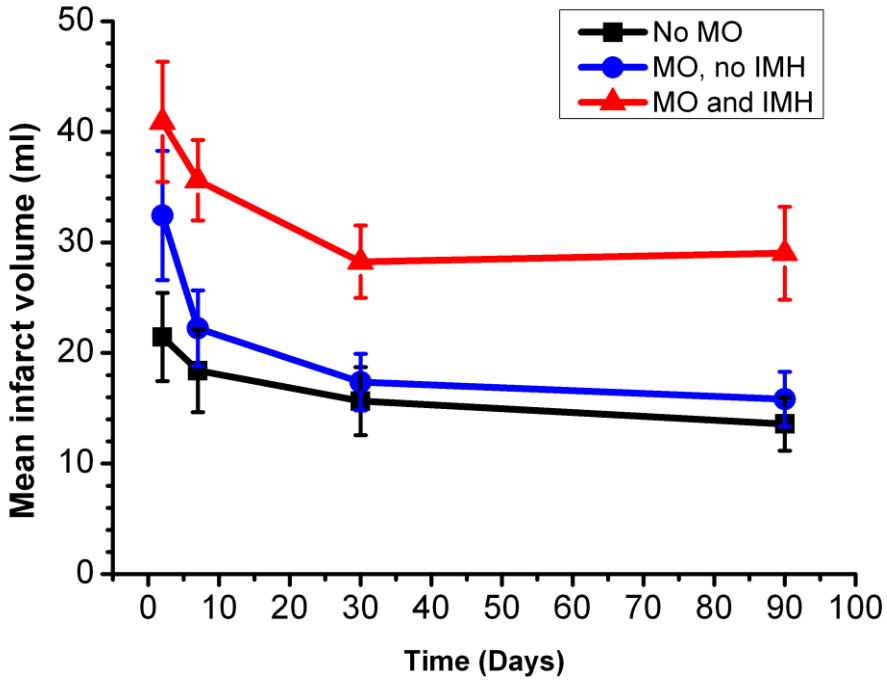

Figure 4.2. Mean infarct zone size at 4 time points post AMI. Stratified by presence of MO and IMH.

Table 4.3. Summary of changes in infarct characteristics between 2 and 90 days.

Variable	**No MO or IMH**	**MO only**	**MO and IMH**
Infarct volume	⇩	⇩	⇩
Ejection fraction	⇧	⇧	⇧
Transmural extent of infarction	⇔	⇔	⇩
Magnitude of infarct endocardial strain	⇧	⇔	⇔
Magnitude of infarct mid myocardial strain	⇧	⇔	⇔
Magnitude of infarct epicardial strain	⇧	⇧	⇧
Magnitude of remote endocardial strain	⇔	⇔	⇔
Magnitude of remote mid myocardial strain	⇔	⇔	⇔
Magnitude of remote epicardial strain	⇔	⇔	⇔

Arrows indicate direction of change. Horizontal arrow denotes no significant change.

4.5.3. Effects of MO, IMH, infarct size and transmural extent on myocardial strain

Within the infarct zone, examining strain across all layers showed overall recovery with time ($F=44$, $p<0.001$). For individual layers, endocardial, mid-myocardial and epicardial strain recovered over the 4 time points ($p\leq0.01$ for each) for patients without MO or IMH. For patients with MO, regardless of the presence of IMH, there was no significant recovery of endocardial ($F=3.1$, $p=0.05$; $F=1.4$, $p=0.3$ in the absence and presence of IMH, respectively) or mid-myocardial strain ($F=2.1$, $p=0.1$; $F=2.9$, $p=0.05$ respectively), but epicardial strain recovered significantly ($F=7.7$, $p<0.01$; $F=3.3$, $p=0.03$ respectively; Figure 4.3).

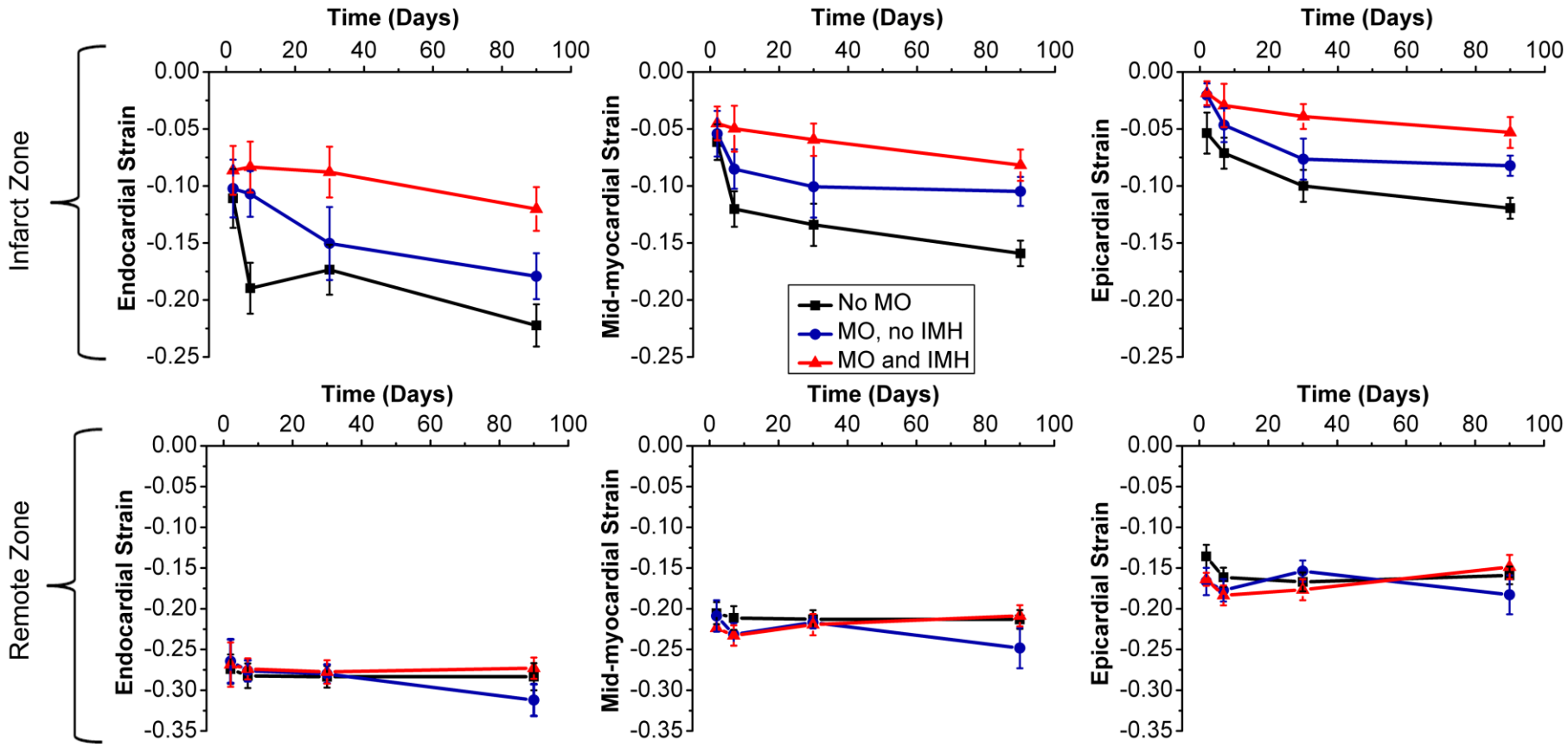

Figure 4.3. Endocardial, mid-myocardial and epicardial circumferential strain at 4 time points post AMI. Infarct zone (top row) and remote zone (bottom row) are shown.

Analysis of individual time points showed differences between infarcts with MO and IMH evolving over time. At day 2, there was no significant difference in infarct strain in endocardial, mid-myocardium or epicardial zones according to the presence of MO or IMH ($F=0.27$, $p=0.8$; $F=0.27$, $p=0.8$; $F=1.9$, $p=0.2$ for endocardial, mid-myocardial and epicardial strain, respectively). By day 7, there was significant difference in endocardial and mid-myocardial strain between the groups, but not epicardial strain ($F=6.9$, $p=0.03$; $F=4.3$, $p=0.02$; $F=1.9$, $p=0.2$ respectively). At day 30 and day 90, there were significant differences in endocardial, mid-myocardial and epicardial strain according to the presence of MO or IMH (day 30: $F=3.7$, $p=0.03$; $F=4.5$, $p=0.02$; $F=5.5$, $p<0.01$; day 90: $F=7.9$, $p<0.01$; $F=11$, $p<0.01$. $F=10$, $p<0.01$ respectively).

Remote myocardial strain was similar over time, and similar at each time point ($p\geq0.2$ for all) regardless of infarct characteristics (Figure 4.3).

At each time point, infarct zone endocardial strain was not associated with infarct transmural extent ($F=1.1$, $p=0.3$; $F=0.3$, $p=0.8$, $F=1.1$, $p=0.3$; $F=2.3$, $p=0.1$ for days 2, 7, 30 and 90 respectively). Endocardial strain was chosen as it was consistently within the infarct zone.

Univariable linear regression analysis (examining the variables in Table 4) showed that presence of MO, presence of haemorrhage and total infarct volume, but not infarct transmurality were significantly associated with decreased strain in the infarct zone at 90 days. Of these, the presence of MO and/or IMH, but not infarct volume, were significantly associated with strain on multivariable logistic regression analysis (Table 4.4).

Table 4.4. Predictors of decreased infarct zone strain in regression analysis

	Univariable	**Multivariable**
Variable	**p value**	**p value**
Age	0.40	...
Sex	0.84	...
Current smoker	0.04	...
Hypertension	0.13	...
Hypercholesterolemia	0.75	...
Family history	0.17	...
Diabetes	0.79	...
Onset to balloon time	0.18	...
Anterior AMI	0.34	...
TIMI flow grade before PCI > 0	0.69	...
TIMI flow grade after PCI < 3	0.46	...
Transmural extent of infarction >50%	0.12	...
Transmural extent of infarction 100%	0.58	...
Infarct volume (at 90 days)	0.001	0.07
Presence of MO only	<0.0001	0.03
Presence of MO + IMH	<0.0001	0.005

4.6. Discussion

This study has found that contractile function as measured with CMR tissue tagging improves within the overall infarct territory following reperfused AMI with or without the presence of MO or IMH. However, this recovery was diminished in the presence of MO and further in the presence of IMH. Remote myocardial contractility did not change over time or with MO or IMH. The presence of MO and/or IMH was a stronger independent predictor of infarct zone contractile recovery than transmural extent of infarction or overall infarct volume.

There are limited existing data on how MO or IMH affect infarct zone contractile recovery. In canines, the extent of MO early post MI relates to reduced deformation and dysfunction of non-infarcted adjacent myocardium (Gerber et al., 2001). In humans, the relationship between infarction, MO and regional function has conflicting evidence. Rogers et al. (Rogers et al., 1999), showed that hyperenhanced myocardium on LGE recovered function with time, but hypoenhanced myocardium did not. Gerber et al. (Gerber et al., 2002), found no significant difference in strain between hypoenhanced and hyperenhanced segments 7 months following AMI. IMH on T2 and T2* imaging post-AMI has been shown to be the strongest predictor of adverse LV remodelling globally (Mather et al., 2011), and strain recovers significantly within hyperenhanced myocardium, even when accounting for scar zone remodelling (Kidambi et al., 2013b).

In this study, patients with IMH had significantly larger infarcts than those without, as previously observed (Beek et al., 2010; Mather et al., 2011). However, even when accounting for infarct size, patients with IMH had poorer infarct zone contractile function from day 7 onwards. The mechanisms by which MO and IMH confer reduced LV contractile function and adverse remodelling remain unclear (Gerber et al., 2000; Wu et al., 1998a), and are not simply explained by infarct expansion. Notably, we found no significant changes in remote strain, suggesting that MO and IMH affect contractility by processes in or around the infarct. Our findings of MO and IMH as the strongest independent predictors of attenuated infarct zone strain support this notion.

One possible interpretation of these findings is that circumferential motion is transmitted from a viable epicardial rim to the endocardium and that myocardial tagging by CMR detects this passive motion rather than active contraction. Epicardial strain recovery was consistently observed in all three groups and would support this interpretation. However, three points do not readily concord with this interpretation: 1) the transmural extent of infarction was similar across the three groups, and so one would expect that the magnitude of circumferential compression should be similar, 2) infarct endocardial strain did not show an association with infarct transmural extent and 3) patients with fully transmural infarction demonstrate strain recovery over time in the core of the infarct zone (Kidambi et al., 2013b).

An alternative interpretation of our findings is that residual viable myocardium remains within the reperfused infarct zone and that the surviving myocytes are responsible for the evolving contractility over time in the infarct zone. The current literature on this issue is inconsistent. Most of the evidence suggests that hyperenhanced zones on LGE imaging are entirely non-viable (reviewed in (Arai, 2011a)). However, it is also known that hyperenhancement on LGE CMR can overestimate infarct size acutely, and that the viable, oedematous border zone can show hyperenhancement (Dall'Armellina et al., 2011). Histologically, preserved islands of viable myocytes have been shown to exist within the infarct zone (Factor et al., 1978). In one study the mean myocyte fraction from sections of scar tissue defined by LGE imaging was as high as 62% (Gunning et al., 2002).

What is less controversial is that the extent of damage within the infarct zone varies. Ultrastructural damage is more pronounced in areas of no-reflow (Kloner et al., 1974; Kloner et al., 1980) and IMH is associated with diminished healing within the infarct core, and altered inflammatory response (Roberts et al., 1983). It is possible therefore that any differences in contractile function and functional recovery between these pathologies reflect the variation in the proportion of residual viable myocytes following reperfusion that may not be apparent on qualitative LGE imaging. Alternatively, these structural differences may lead to differential transmission of epicardial contraction into the infarct zone depending on the presence of MO or IMH.

Patients without MO or IMH showed recovery of strain in the endocardial, mid-myocardial and epicardial infarct borders, but in patients with MO (with or without IMH), there was no significant recovery in endocardial and mid-myocardial areas. Furthermore, when examining the differences between the groups over time, endocardial and mid-myocardial contractile function was significantly different at day 7 whilst this was not apparent in the epicardial border until day 30. These findings accord with the wavefront theory of infarction, and that MO and IMH principally develop in the endocardium and mid-myocardium, with relative sparing of epicardial ischaemia and infarction prior to reperfusion.

Hypoenhancement on LGE produces a conservative estimate of the extent of MO (Mather et al., 2009) compared with early gadolinium enhancement (at 2 min following contrast injection). We chose to define MO by LGE as it is considered to be of higher prognostic value (de Waha et al., 2010). In our study, findings on early and late gadolinium enhancement were similar and only one of the 16 patients with no MO on LGE showed MO on early enhancement imaging. The results and significant findings of the study were not changed by analysing this patient in the MO group.

4.6.1. Limitations

This study has limitations. The number of patients is relatively small, though sufficient to generate significant results and in keeping with other CMR studies in this demographic, where serial imaging including early post AMI is challenging. Five patients did not have strain and T2w imaging at baseline. It is possible that any MO/IMH may have resolved by day 7, although of 22 patients with MO at day 2, all but one had MO at day 7. We used a dual-echo T2* method in this study. Multi-echo techniques permit more reliable quantitative estimates of T2* but were not available to us at the time of this study. For this reason, we only performed a qualitative assessment of IMH size from T2* images. Different cut-offs to define LGE hyperenhanced myocardium have been proposed in the literature; we chose 2SD to ensure consistency with T2 image analysis. Using concurrent LGE images for tagging at each time point may be affected by geometric changes in the LV or infarct zone for follow up scans, and a potential change in the position of myocardium that is sampled. Resolving three circumferential layers in remodelled infarcted myocardium may have been limited by the resolution of CMR, though the harmonic phase analysis software

is able to produce a displacement map between tagging intersections to <1mm (Osman et al., 1999), and the infarct zone did not thin in the vast majority of patients with timely reperfusion. End systolic strain may not account for infarct zone dyssynchrony, though this was not observed visually in any patient.

4.6.2. Clinical context

This study provides two important clinical findings. Firstly, we have shown that following reperfused AMI, infarct zone remodelling comprises recovery of strain as measured by tissue tagging CMR, regardless of the transmural extent of LGE hyperenhancement. Secondly, we have demonstrated that MO and IMH affect this infarct zone remodelling process, but do not affect remote zone contractility. Our data suggest that the prognostic effects of MO and IMH are mostly due to effects within the infarct zone rather than infarct expansion or remote myocardial change. In addition to reducing its occurrence, strategies to mitigate the poor prognosis associated with MO or IMH could target these processes, with strain used as a measure of efficacy.

4.7. Conclusions

The infarct zone following reperfused AMI demonstrates contractile recovery over time as measured by tissue tagging CMR. The presence of hypoenhancement on LGE, suggestive of MO, is associated with reduced functional recovery over time, affecting in particular endocardial and mid-myocardial functional recovery. Hypoenhancement on T2w and T2* imaging, suggestive of IMH, is associated with further reduction in infarct zone functional recovery. Both MO and IMH are independent predictors of impaired contractile recovery in the infarct zone, but neither independently affects remote myocardial contractility.

5. Chapter 5
Susceptibility-Weighted Imaging to Detect Intramyocardial Haemorrhage

5.1. Abstract

5.1.1. Objectives

To compare the image quality and diagnostic ability of susceptibility-weighted magnetic resonance imaging (SW MRI) with T2-weighted and T2* CMR for detection of intramyocardial haemorrhage (IMH) following reperfused acute myocardial infarction (AMI).

5.1.2. Background

IMH is an established prognostic marker following AMI. Detection of IMH by T2-weighted or T2* CMR can be limited by long breath hold times and sensitivity to artefacts, especially at 3T.

5.1.3. Methods

Forty-nine patients (42 males; mean age 58 years) underwent 3T CMR 2 days following reperfused AMI. T2-weighted, T2* and SW MRI images were obtained. Signal and contrast measurements were compared between the three methods and diagnostic accuracy of SW MRI was assessed against T2w images by 2 independent, blinded observers. Image quality was rated on a 4-point scale from 1 (unusable) to 4 (excellent).

5.1.4. Results

Of 49 patients, IMH was detected in 20 (41%) by SW MRI, 21 (43%) by T2-weighted and 17 (34%) by T2* imaging (p=ns). Compared to T2-weighted imaging, SW MRI had sensitivity of 93% and specificity of 86%. SW MRI had similar inter-observer reliability to T2-weighted imaging ($\kappa = 0.90$ and $\kappa = 0.88$ respectively); both had higher reliability than T2* ($\kappa = 0.53$). Breath hold times were shorter for SW MRI (4 seconds vs. 16 seconds) with improved image quality rating (3.8±0.4, 3.3±1.0, 2.8±1.1 respectively; $p<0.01$).

5.1.5. Conclusion

SW MRI is an accurate and reproducible way to detect IMH at 3T. The technique offers considerably shorter breath hold times to T2-weighted and T2* imaging, and higher image quality scores.

5.2. Objectives

To compare a susceptibility-weighted magnetic resonance imaging technique with the established markers of T2-weighted and T2* imaging for the detection of intramyocardial haemorrhage following reperfused acute myocardial infarction at 3T.

5.3. Background

The aim of emergency treatment for ST-elevation acute myocardial infarction (AMI) is coronary reperfusion, optimally via primary percutaneous coronary intervention (PCI). In approximately 40% of patients, reperfusion by primary PCI is associated with detectable reperfusion injury (Mather et al., 2009). Reperfusion injury may manifest as microvascular obstruction (MO), which is associated with adverse functional outcome (Kidambi et al., 2013a) and worse prognosis (de Waha et al., 2012; Wu et al., 1998a). A subset of patients with MO may also have haemorrhage within the infarcted myocardium. Intramyocardial haemorrhage (IMH) is independently associated with adverse prognosis over and above MO alone (Eitel et al., 2011). The most sensitive clinical way of detecting IMH is by CMR imaging (Kumar et al., 2011). The breakdown products of haemoglobin within IMH exert a paramagnetic effect which shortens T2 relaxation times, resulting in the presence of a characteristic hypointense infarct core on T2-weighted (T2w) or T2* imaging (Mather et al., 2011). However, this important prognostic marker has been relatively underused in the clinical setting. One reason for this underuse is the difficulty in obtaining reliable diagnostic quality images, which for dark-blood T2w or T2* commonly require long breath hold times (~16s) with minimal respiratory movement. This may be especially difficult in the context of recent acute myocardial infarction, which commonly causes breathlessness and orthopnoea.

Alternative methods that can detect IMH with shorter breath hold times are therefore desirable. MR imaging is capable of detecting differences in the magnetic susceptibility of tissues. The paramagnetic properties of haemoglobin products within IMH cause local phase shifts relative to surrounding tissue (Weisskoff and Kiihne, 1992). The k-space data acquired for each magnitude image can be also used to derive phase data. With the exception of large vessel flow quantification, clinical CMR largely relies on magnitude data, and phase data are mostly discarded. Phase data can be filtered and combined with

magnitude data to generate susceptibility-weighted MR images (SW MRI) (Haacke et al., 2004). SW MRI has the inherent potential advantage of short acquisition times, without the need for spin refocusing or multiple images. SW MRI effects may be more pronounced at 3T due to increased phase differences between tissues, whereas myocardial T2 and T2* images may be degraded at higher field strengths, in part due to these susceptibility effects (Zaman et al., 2014).

SW MRI has been used clinically in neuroimaging, to visualise venous structures in the brain (Mittal et al., 2009), and has been shown to be highly sensitive for the detection of cerebral haemorrhage in stroke (Akter et al., 2007). We hypothesised that SW MRI could be used to detect haemorrhage following AMI, especially at 3T. We compared the image quality and diagnostic accuracy of SW MRI with T2w and T2* MR imaging at 3T for the detection of IMH following reperfused AMI.

5.4. Methods

5.4.1. Patient selection

Patients with first ST-segment elevation AMI, revascularised by primary PCI within 12 hours of onset of pain were prospectively recruited from a single tertiary centre from February 2012 to August 2013. AMI was defined as per current guidelines (Thygesen et al., 2012). Exclusion criteria were previous AMI or coronary artery bypass grafting, cardiomyopathy, estimated glomerular filtration rate <30 ml/min/1.73 m^2, or contraindications to MR imaging. The study protocol was approved by the institutional research ethics committee and complied with the Declaration of Helsinki; all patients gave written informed consent. Patients with maximal total scar extent (including MO or IMH) less than 2 voxels of the in-plane resolution of LGE (approximately 3-4 mm) were deemed too small for accurate evaluation of the infarct zone and not included in the analysis. Clinical management (including anticoagulation and use of aspiration catheters) was performed blind to the CMR results and at the discretion of the responsible clinician, reflecting contemporary practice and guidelines. All patients were considered for angiotensin converting enzyme inhibitors, beta-blockade, statins, dual antiplatelet therapy and cardiac rehabilitation.

5.4.2. Image acquisition

All patients had CMR imaging at 3.0T within 3 days (median 2 days) of their index presentation (Achieva TX, Philips Healthcare, Best, The Netherlands equipped with a Quasar Dual gradient system (40 mT/m; 200 T/m/s) and radiofrequency (RF) shimming with dual-source RF transmission). A dedicated 32-channel cardiac phased array receiver coil was used. Cine imaging was performed using a contiguous stack of parallel short-axis slices covering the whole left ventricle (LV), with a balanced steady-state free precession pulse sequence (echo time (TE) 1.3 ms; repetition time (TR) 2.6 ms; flip angle 40°, spatial resolution 1.6×2.0×10 mm, 40 phases per cardiac cycle). SW, T2w, T2* and late gadolinium enhancement (LGE) imaging were performed using the '3-of-5' approach by acquiring the central 3 slices of 5 parallel short-axis slices spaced equally from mitral valve annulus to LV apical cap (Messroghli et al., 2005). The same slice geometry, position and a 10mm slice thickness were used for all pulse sequences. The SW sequence used a black-blood inversion recovery turbo gradient echo sequence (sensitivity encoding (SENSE) parallel acceleration factor = 2.3, TR/TE/flip angle 4.1 ms/3.0 ms/20 degrees, spatial resolution 1.8×2.5×10 mm, typical matrix 212 x 146, pre-pulse black blood delay 775 ms). Magnitude and phase images were generated online at the time of scanning. T2w imaging used a dark-blood T2w fast spin echo short tau inversion-recovery (STIR) sequence (TE 90 ms, TR two R-R intervals, flip angle 90 degrees, spatial resolution 1.7×1.7×10 mm, typical matrix 208 x 200) and constant level appearance (CLEAR) homogeneity correction. For T2* imaging, 32 gradient echoes were subdivided into six groups, with a linear k-space order within each group contributing to a separate k-space. The echoes used for the centre of k-space for each image/group had consistent parity. T2* imaging parameters were as follows: SENSE = 2, TFE factor 8, TR/TE1/echo spacing (ms) 15/2.3/2.2, spatial resolution 1.8×2.5×10 mm, typical matrix 176 x 128, pre-pulse black blood delay 420 ms, trigger delay set to image in late diastole. To minimise regional myocardial variation for T2* imaging, image-based shimming was employed (Zaman et al., 2014). 0.1 mmol/kg gadolinium-DTPA (gadopentetate dimeglumine; Magnevist, Bayer, Berlin, Germany) was then administered using a power injector (Spectris, Solaris, PA). LGE imaging was performed at 16-20 minutes following contrast (inversion recovery-prepared T1 weighted gradient echo, inversion time according to Look-Locker scout, TR/TE/flip angle 3.7 ms/2.0 ms/25 degrees, spatial resolution 1.54×1.75×10 mm, typical matrix 232 x 182). Breath hold times per slice at a typical heart rate of 60/min were: 16 seconds for T2w, 17 seconds for T2* and 4 seconds for SW data acquisition. For each pulse sequence, images with motion or parallel

imaging artefact were repeated until any artefact was removed or minimised. The highest quality images were used for analysis.

5.4.3. Image analysis

Phase and magnitude data were combined into a SW MRI image using the SWIp algorithm (Susceptibility-Weighted Imaging with Phase enhancement; previously referred to as "PADRE") (Ide et al., 2012; Kakeda et al., 2011). To enable testing of different SWIp parameters, images were processed offline, taking <10 seconds per image (SWIp tool v1.7, Philips Healthcare, The Netherlands). Automated inline processing on the scanner console with fixed parameters is possible with processing time <5 seconds. The SWIp tool calculates a contrast-enhancing mask from the phase images. The phase information can be contaminated by background field effects and so it is initially corrected by applying a homodyne high pass filter to the complex-valued image data (Noll et al., 1991). The SWIp phase (φ) mask is defined by a function, the shape of which is controlled by three adjustable parameters, α, β and σ (Equation 5.1).

$$Mask(x) = \begin{cases} e^{-\alpha\left(|\phi(x)| - \frac{\sigma * \pi}{100}\right)^{\beta}} & if\ |\phi(x)| \geq \frac{\sigma * \pi}{100} \\ 1 & if\ |\phi(x)| < \frac{\sigma * \pi}{100} \end{cases}$$

Equation 5.1. SWIp phase mask function.

Figure 5.1 shows the influence of the parameters on the phase mask. The resulting SWIp image is given by the product of the magnitude image and the SWIp mask.

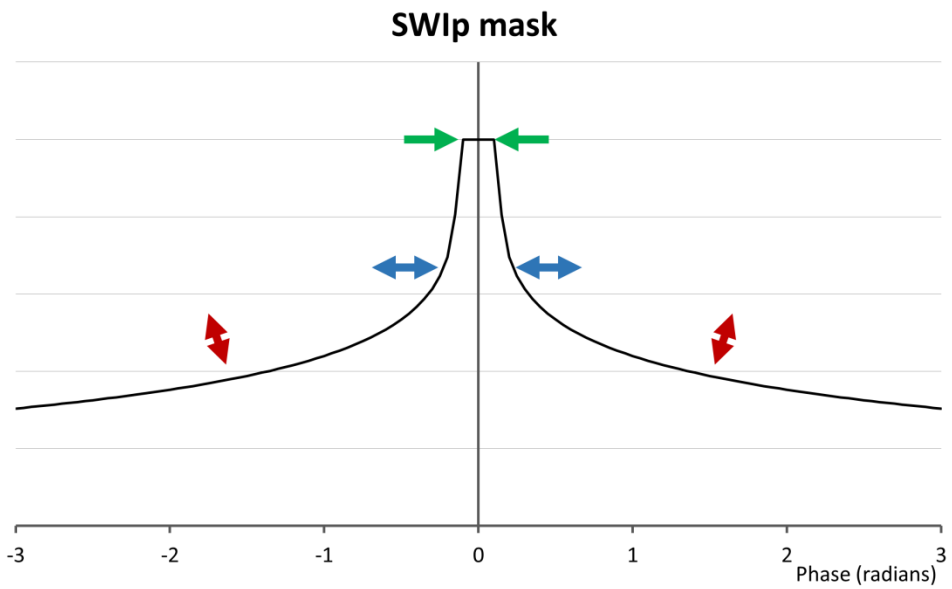

Figure 5.1. Effect of parameters on SWIp phase mask. A plot of mask value (y-axis) vs. phase (x-axis) is shown. α predominantly controls the gradient and height of the mask at higher absolute phase values (red arrows), β predominantly affects the slope of the masking curve at intermediate phase values (blue arrows), and changes in σ predominantly control masking at phase values close to zero (green arrows).

As there are no agreed values for α, β or σ for IMH, the effects of varying these parameters were tested on the first 10 patients with visible IMH on T2w imaging. All possible permutations of the following were tested: filter size: 64 x 64, 128 x 128; α: 0, 0.2, 0.4, 0.6, 0.8, 0.95; β: 0.1, 0.2, 0.3, 0.4, 0.55, 0.6, 0.8, 1.0; σ: 0, 0.5, 1, 2, 3, 5, 7.5, 15, 25, 50, 75. These parameter values were chosen to sample the spread of potential values, and also to focus on specific values previously reported (Kakeda et al., 2011). Filter sizes were chosen to account for the larger comparative size of IMH and higher field strength than previous validation work in neuroimaging (Haacke et al., 2007). Regions of interest were drawn using in-house software written in Matlab (Mathworks, Natick, MA, version R2011b) within areas of IMH as defined on T2w imaging and remote myocardium (in myocardium opposite to the infarct zone as defined on LGE imaging and away from the infarct and peri-infarct zone). Areas of hypointensity were visualised and contoured manually. In order to compare different SWIp parameter values, mean signal intensity (SI) and standard deviation (SD) were measured for each myocardial region. The relative signal to noise (rSNR) for IMH regions was evaluated; tissue contrast was evaluated by calculating rSNR difference (ΔrSNR), using the methods described in Equation 5.2 (Kaufman et al., 1989).

$$rSNR = 0.655 \times \frac{SI}{SD}$$

$$\Delta rSNR = rSNR_{\text{remote}} - rSNR_{\text{IMH}}$$

Equation 5.2. Calculation of rSNR and ΔrSNR.

The SNR calculation is subject to a number of errors including residual B1 inhomogeneity and non-uniform image noise due to parallel image reconstruction (Pruessmann et al., 1999). However, measurement of the absolute SNR was less critical than an accurate estimate of the difference between rSNR measurements. ΔrSNR allows for a quantitative comparison of contrast generation between tissue types in SWIp images using different phase masks, assuming similar coil gain and geometry factor between infarct and IMH ROIs for the acceleration factor used.

The values of filter size, α, β and σ that generated the highest ΔrSNR were derived from the first 10 patients with visible IMH on T2w imaging, and these values then applied to all patients for the main analysis. For analysis, the phase mask was applied once, except where indicated for testing of rSNR and ΔrSNR with multiple applications of the phase mask.

SWIp, T2w and T2* images were independently evaluated for the presence of IMH by two blinded reviewers (AK and DPR, three years of CMR experience). Disagreement between reviewers was resolved by a consensus read. The presented accuracy statistics are based on consensus analysis. A further blinded read was taken (by AK) more than one month after the initial read for intraobserver analysis. The presence of IMH was assessed in conjunction with LGE images, to reflect real-world practice; reviewers were blinded to other imaging sequences, patient and clinical details. IMH was considered to be present when an area of hypointensity was visible within an area corresponding to the infarct zone on LGE imaging. For rSNR analysis, signal intensity and SD were evaluated in IMH and remote myocardial regions based on the consensus read. For T2* images, all echoes were analysed, the single image per slice with the highest ΔrSNR was chosen for statistical analysis. T2w, T2*, cine and LGE images were evaluated offline using commercial software (cvi42 v4.1.5, Circle Cardiovascular Imaging Inc., Calgary, Canada). Image quality was assessed by consensus of 2 observers, and on a slice-by-slice basis according to a 4 point scale: 4= excellent, 3= minor artefact compromising

diagnostic accuracy in myocardium outside of the infarct territory, 2= artefact compromising infarct zone but analysis possible, 1= unusable. Left ventricular volumes and ejection fraction (EF) were analysed from cine images using standard methods (Schulz-Menger et al., 2013). Infarct location was determined by LGE imaging, according to standard guidelines (Cerqueira et al., 2002).

5.4.4. Statistical analysis

Statistical analysis was performed using IBM SPSS® Statistics 21.0. Continuous variables are expressed as mean ± SD. Normality for quantitative data was established using the Kolmogorov-Smirnov test. Demographic comparisons were performed with an independent samples t-test with Bonferroni correction to account for multiple comparisons. Differences in measurements per-slice were evaluated using a multilevel linear mixed-effects model to account for non-independence of slice data. Post-hoc comparisons were made using Tukey's test. Inter and intra-rater reliability were performed using Cohen's Kappa statistic. All statistical tests were 2-tailed; p values <0.05 were considered significant.

5.5. Results

54 patients met the inclusion criteria. In 5 patients the infarct size was too small for accurate analysis as per the criteria above; therefore 49 patients were included in the statistical analysis. Patient characteristics are shown in Table 5.1. Myocardial characteristics are shown in Table 5.2. No gender-based differences in characteristics were present ($p>0.1$ for all).

5.5.1. Choice of image weighting parameters

The first 10 sequential patients with IMH visible on T2w imaging were selected to evaluate the optimal image weighting parameters for the SWIp sequence to detect IMH. $rSNR_{IMH}$ and ΔrSNR (between IMH and remote myocardium) for each combination of parameters were averaged over the 10 patients. These varied substantially depending on parameter values (rSNR: mean 3.55 ± 0.65, range 1.13–4.28; ΔrSNR mean 0.60 ± 0.25, range 0.00–1.33). The highest and lowest ΔrSNR results with corresponding parameter values are shown in Table 5.3. The following parameters produced the highest ΔrSNR (i.e. the greatest relative SNR difference between IMH and remote myocardium) and were hence applied to the SW MRI images used for analysis in the whole population: filter size 128 x 128, $\alpha = 0.95$, $\beta = 0.2$, $\sigma = 3$.

Table 5.1. Patient characteristics

Patient characteristic	
n	49
Age, years	58.0 ± 11.3
Male	42 (86%)
Body mass index, kg/m^2	28.2 ± 3.3
Current smoker	27 (55%)
Hypertension	12 (25%)
Hypercholesterolemia	13 (27%)
Diabetes mellitus	6 (12%)
Pain to balloon time, min (median (IQR*))	219 (275)
MO present	25 (51%)
TIMI flow grade ≥ 2 pre-PCI	4 (8%)
TIMI flow grade 3 post PCI	47 (96%)
Peak troponin I, ng/L (median)	>50000
Peak CK†, iu/L (median (IQR))	601 (1297)
Infarct territory	
Anterior	22 (45%)
Inferior	21 (43%)
Lateral	6 (12%)

Data as mean ± SD or n (%) unless indicated.*_IQR_ interquartile range, †_CK_ creatine kinase.

Table 5.2. Infarct characteristics

Characteristic	**Acute visit**
Ejection fraction,%	49 ± 10
LV EDVi*, ml/m2	82 ± 15
LV ESVi†, ml/m2	42 ± 12
LV mass, g/m2	64 ± 14
LGE infarct volume, ml	48 ± 15
LGE MO volume, ml	3 ± 5

n=49. Data as mean ± SD. **LV EDVi* Left ventricular end diastolic volume, indexed to body surface area, †*LV ESVi* Left ventricular end systolic volume, indexed to body surface area.

Table 5.3. Optimal and worst susceptibility weighting parameters

	Filter	Alpha	Beta	Sigma	ΔrSNR*	rSNR†
1	128	0.95	0.20	3	1.327	2.115
2	64	0.95	0.10	5	1.324	2.025
3	64	0.95	0.20	5	1.321	2.295
4	64	0.80	0.10	5	1.316	2.180
5	128	0.95	0.10	5	1.305	2.702
6	128	0.95	0.30	3	1.304	2.404
7	64	0.95	0.00	7.5	1.301	2.605
8	128	0.80	0.10	3	1.299	1.974
9	64	0.80	0.00	5	1.299	1.904
10	128	0.95	0.10	3	1.297	1.742
1056	128	0.20	0.55	75	0.005	4.019
1055	128	0.80	0.10	0.5	0.008	2.018
1054	64	0.40	0.00	1	0.009	2.528
1053	128	0.95	0.10	0.5	0.028	1.766
1052	64	0.80	0.10	0.5	0.029	2.158
1051	128	0.20	0.55	25	0.033	4.283
1050	64	0.95	0.00	1	0.039	1.270
1049	128	0.20	0.55	7.5	0.043	4.265
1048	128	0.21	0.20	15	0.052	4.255
1047	64	0.80	0.00	1	0.057	1.503

n=10. Top 10 and bottom 10 values of *ΔrSNR difference between remote myocardium and IMH. †rSNR relative signal to noise ratio of IMH. Lower rSNR values indicate more hypointense IMH.

5.5.2. rSNR and ΔrSNR

For SW MRI images, average rSNR was 3.62 ± 2.89 for areas of IMH and 5.61 ± 2.63 for remote myocardium (β=0.47, p<0.001). ΔrSNR between remote myocardium and IMH was 1.7 ± 2.9. ΔrSNR between infarct and IMH was 4.71 ± 4.48, and between infarct and remote was 3.18 ± 3.41 (β =0.87, p<0.001). There were no significant differences in SWIp remote rSNR dependent on ROI location (anterior 5.39 ± 3.28, septal 4.16 ± 3.41, inferior 2.46 ± 0.68, lateral 3.33 ± 2.95, β=0.07, p=0.39). Figure 5.2 and Figure 5.3 show representative images.

For T2w images, average rSNR was 4.23 ± 2.71 for areas of IMH and 4.69 ± 2.04 for remote myocardium (β=0.00, p=0.99). ΔrSNR between remote myocardium and IMH was 1.7 ± 2.9. ΔrSNR between infarct and IMH was 2.20 ± 2.27 and between infarct and remote was 1.50 ± 3.59 (β=0.47, p<0.01). There were no significant differences in remote rSNR dependent on ROI location (anterior 3.32 ± 1.23, septal 4.64 ± 2.06, inferior 4.60 ± 2.03, lateral 5.53 ± 1.99, β=-0.06, p=0.46).

T2* images had average rSNR of 5.74 ± 5.81 for areas of IMH and 8.10 ± 4.43 for remote myocardium (β=0.00, p=0.99). ΔrSNR between remote myocardium and IMH was 5.35 ± 3.55. ΔrSNR between infarct and IMH was 7.29 ± 3.34 and between infarct and remote was 5.81 ± 3.92 (β=0.60, p<0.01). There were no significant differences in remote rSNR dependent on ROI location (anterior 8.50 ± 3.93, septal 9.81 ± 4.68, inferior 8.90 ± 4.45, lateral 7.98 ± 3.58, β=-0.09, p=0.30).

There was no significant difference between SW MRI and T2w imaging for rSNR in areas of IMH (β=-0.27, p=0.5), ΔrSNR between remote and IMH (β=-0.19, p=0.4) and ΔrSNR between infarct and IMH (β=-0.23, p=0.6). rSNR in IMH was significantly higher in T2* images than SW MRI (β=0.56, p<0.01), with no significant difference in ΔrSNR between remote and IMH (β=0.35, p=0.1) or ΔrSNR between infarct and IMH (β=-0.69, p=0.8).

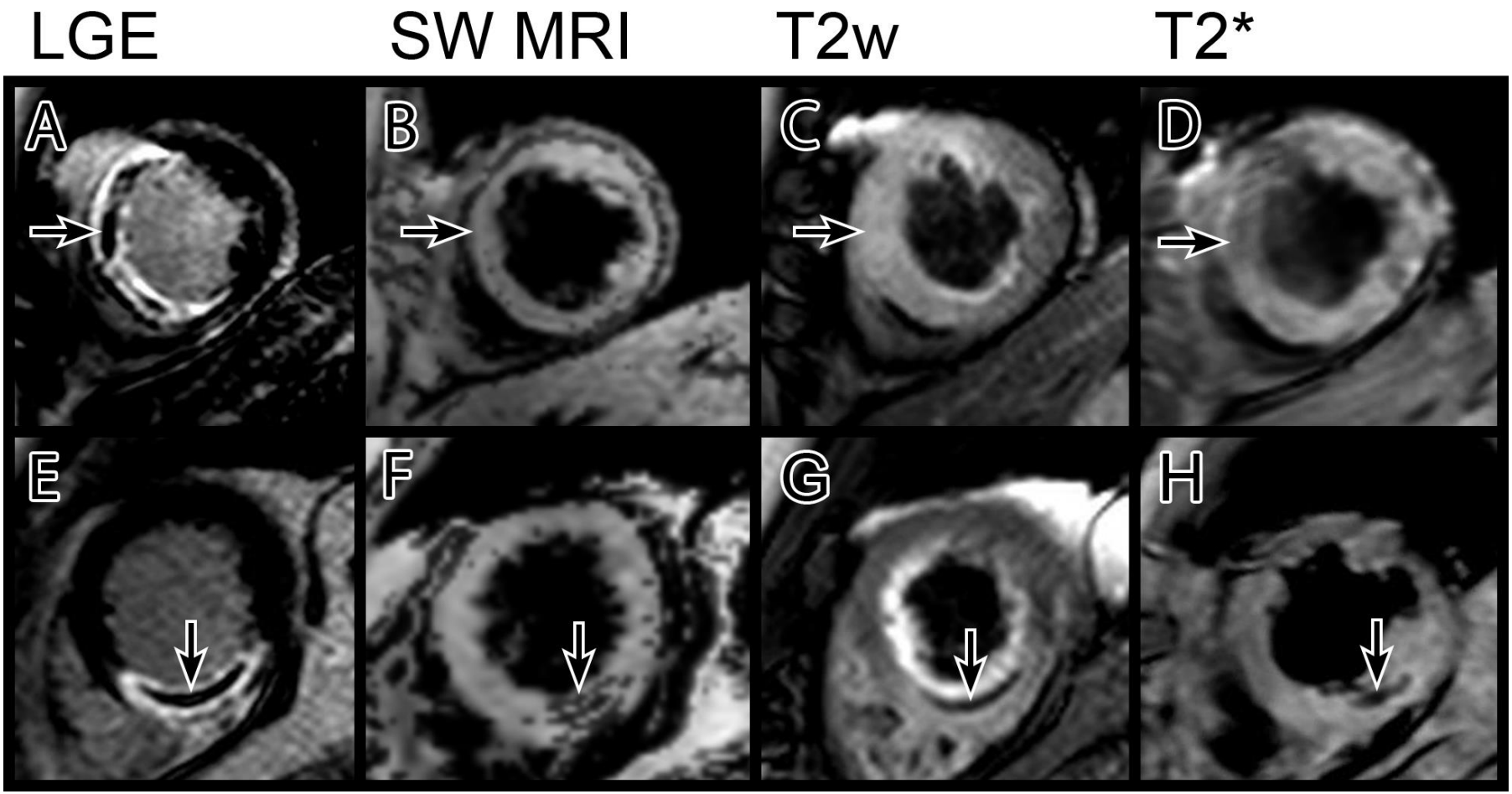

Figure 5.2. SW MRI imaging comparison with T2w and T2*. Top row: MO as shown by LGE imaging (A, arrowed) does not correspond to hypointense myocardium indicating absence of IMH on SW MRI (B), T2w (C) and T2* (D) images. Bottom row: another patient has MO visible on LGE (E, arrowed) corresponding to hypointensity on SW MRI (F, arrowed), T2w (G, arrowed) and T2* (H, arrowed) images indicating presence of IMH.

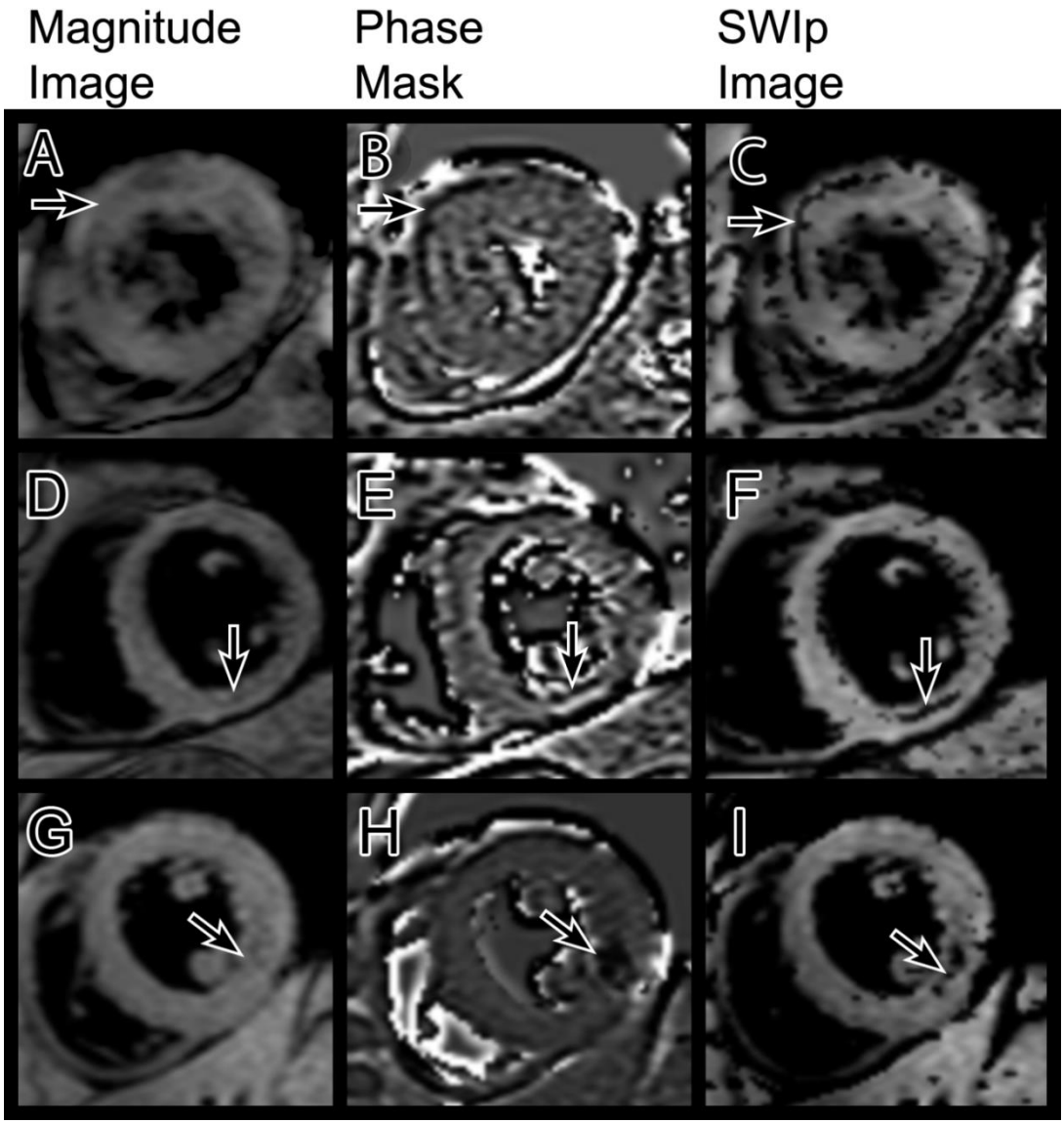

Figure 5.3. Contrast generation by SW MRI in three different patients. Top row: Anterior AMI with IMH (arrowed) is shown in magnitude image without susceptibility weighting (A). A phase mask is generated using the SWIp method (B) and applied to the magnitude image to generate SW images with additional contrast for IMH (C). A similar process is shown for IMH in inferior (D-F) and inferolateral (G-I) territories.

The effect of repeatedly applying the filtered phase mask to the images was evaluated. ΔrSNR and rSNR measurements for each successive iteration of phase mask application are shown in Figure 5.4. Multiple iterations did not significantly alter ΔrSNR between IMH and infarct over and above the first phase mask application (β=-0.06, p=0.2, Figure 5.4a).

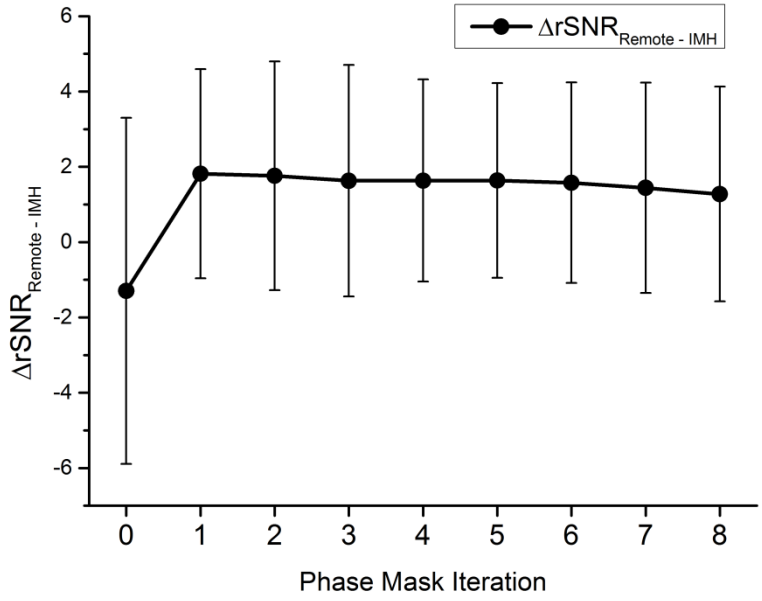

a)

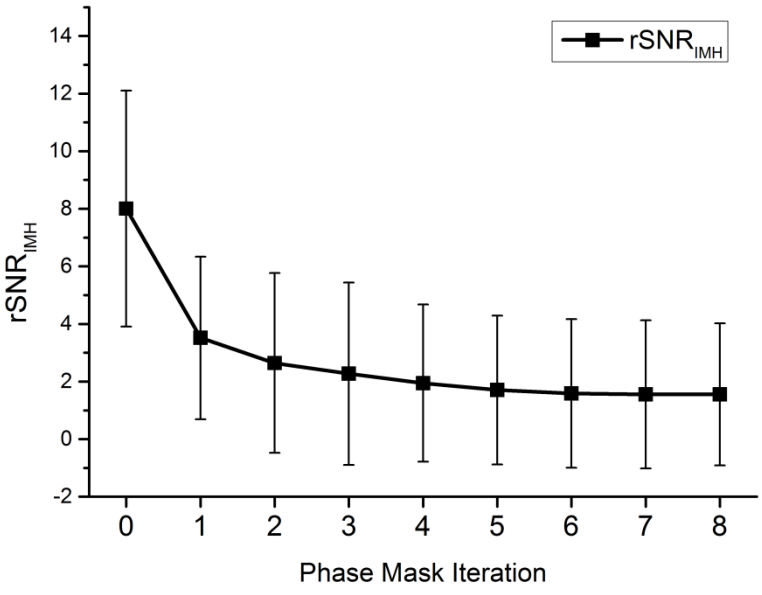

b)

Figure 5.4. Effect of successive filtered phase mask applications. The effect on ΔrSNR (a) and rSNR of IMH (b) is shown. Values are averaged from all patients with IMH visible on SW MRI (n=20). Iteration 0 signifies baseline images with 128x128 homodyne filter applied but no SWIp phase masking. Error bars indicate SD.

5.5.3. Image quality

Mean image quality for SW MRI was 3.8 ± 0.4, for T2w was 3.3 ± 1.0 ($p<0.01$ compared to SW MRI) and for T2* was 2.8 ± 1.1 ($p<0.01$ compared to SW MRI). One (1%) SW MRI slice, 9 (6%) T2w slices and 30 (20%) T2* slices were graded as unusable (Figure 5.5). Of the unusable T2w slices, 6 (67%) had clearly visible motion artefact. Figure 5.6 shows examples of optimal and suboptimal images.

Figure 5.5. Per-slice image quality rating. Images were rated by consensus of two reviewers, blinded to the other sequences, on a scale of 4 (excellent) to 1 (unusable).

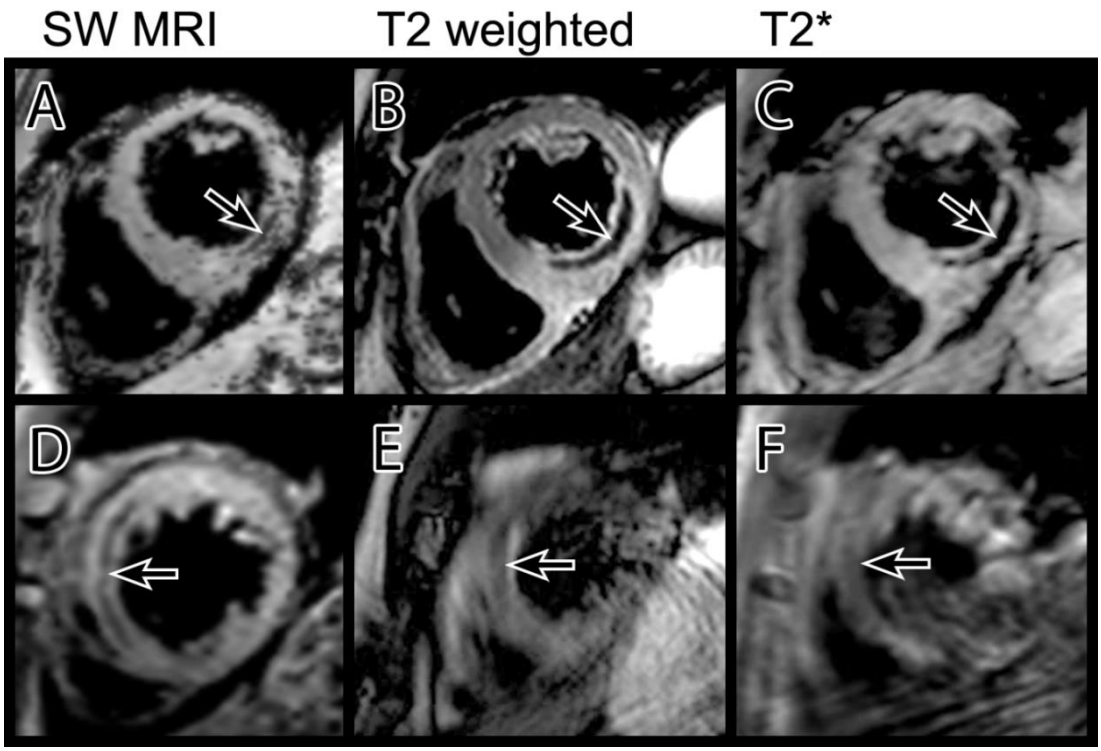

Figure 5.6. Optimal and suboptimal breath holding in SW MRI, T2w and T2* images. Top row: a patient with good breath holding reveals clear inferior IMH on SW MRI (A), T2w (B) and T2* (C) images. Bottom row: a different patient with anteroseptal AMI and reduced ability to breath hold has IMH visible on SW MRI (D), but T2w (E) and T2* (F) images are suboptimal for detection of IMH.

5.5.4. Image interpretation

Per-slice, IMH within the infarct zone was detected on 34 slices (23%) by SW MRI, 38 slices (26%) by T2w imaging (p=0.7 compared to SW MRI) and 31 slices (21%) by T2* imaging (p=0.8 compared to SW MRI). Per-patient detection of IMH was 20 patients (41%) by SW MRI, 21 patients (43%) by T2w (p=1.0 compared to SW MRI) and 17 (34%) patients by T2* (p=0.68 compared to SW MRI). Using T2w imaging as the reference standard, SW MRI images had sensitivity 93% and specificity 86% on a per-patient basis, and 79% and 96% respectively on a per-slice basis. The inter-observer reliability for detection of IMH by SW MRI was κ = 0.82 (95% confidence interval (CI) 0.71 – 0.92), by T2w imaging was κ = 0.78 (0.66 – 0.89) and by T2* imaging was κ = 0.53 (0.36 – 0.69). Intra-observer reliability was κ = 0.79 (0.67 – 0.90), κ = 0.79 (0.68 – 0.90) and κ = 0.74 (0.61 – 0.87) respectively for SW MRI, T2w and T2* imaging.

5.6. Discussion

This study has found that SW MRI at 3T, using the SWIp technique, can accurately and reproducibly identify areas of intramyocardial haemorrhage following acute myocardial infarction, with superior image quality to T2-weighted and T2* imaging and much shorter breath hold time.

Following reperfusion for AMI, the main clinical utility of CMR is to identify complications that affect patient prognosis. IMH is a strong marker of adverse prognosis. However, the most established method of its detection, T2w imaging, is not currently recommended as a routine part of CMR assessment in this context (Kramer et al., 2013). T2, T2* and SW MRI all rely on the paramagnetic effect of deoxygenated haemoglobin products, which in IMH will also be altered by size of haemorrhage and iron content. T2* imaging is specific for detection of IMH (Mather et al., 2011), and has been reported to be more robust than T2 imaging at 1.5T (Kali et al., 2013b). However, at higher field strengths, increased susceptibility effects and greater B_1 magnetic field inhomogeneity substantially degrade diagnostic quality (Guo et al., 2009), whereas these effects, in part, may be utilized to enhance tissue contrast in SW MRI. T2 and T2* imaging are especially difficult post-AMI, as they are sensitive to motion and in general require long breath hold times. Free-breathing T2w and T2* techniques exist (Kellman et al., 2007; Jin et al., 2014), but rely on technically complicated motion correction algorithms and, unlike SWIp, are not yet available for clinical use. Although T2* appears to have higher contrast when IMH is visible, our data show significantly lower overall image quality for T2* imaging at 3T, and numerically lower detection rates for IMH as compared to SW MRI. In comparison, SW MRI magnitude data have relatively low T2-weighting, and we have shown that by integrating phase data, SW MRI provides comparable diagnostic yield to T2w and T2* with much lower breath hold times (in the order of 4 seconds per slice as compared to 16-17 seconds) and superior image quality.

SW MRI offers a novel method of CMR contrast generation in addition to T1 or T2 relaxation. The technique utilises the phase data that is acquired with each k-space dataset, but is discarded when producing the magnitude images that are most often used clinically. By processing filtered phase data and combining it with the magnitude image, an anatomical image can be created in which contrast is enhanced by the phase differences produced by deoxygenated blood

products (Figure 5.3) (Haacke et al., 2009). Phase information can be processed in a number of different ways prior to combining with the magnitude data, and the SWIp technique offers considerable flexibility through the use of multiple parameters, whilst maintaining rapid imaging processing time (<5 seconds for automated inline processing). Neurological applications of SW imaging commonly use TE >10ms to generate strong T2-weighting, but this would result in unacceptably long shot duration and acquisition time (e.g. 200ms and 16s respectively). We have shown that phase data, with appropriate filtering, can be used to help detect haemorrhage in images with relatively short TE and lower T2 weighting, with the benefit of shortened acquisition times and lower image artefacts. In this study we have defined the optimal parameters in this implementation of the SWIp phase mask to enhance IMH.

Susceptibility weighting has been most commonly used in brain imaging, with sparse literature relating to cardiac applications. It is sensitive to early detection of acute haemorrhagic stroke and microbleeds (Hermier and Nighoghossian, 2004), and can also detect intraventricular cerebral haemorrhage in traumatic brain injury and haemorrhagic cerebral tumours (Mittal et al., 2009). Goldfarb et al performed an analysis of 11 patients post-AMI, imaged with T2w and SW MRI, and found that phase differences in areas with IMH were significantly different to normal variations in phase difference (Goldfarb et al., 2013). The Goldfarb study established the feasibility of the technique, and used a pulse sequence with longer TR and TE, resulting in stronger T2* weighting and relatively long breath hold times. The sequence in the current study deliberately uses shorter echo and repetition times to ensure a shorter breath hold time but with comparable clinical utility to T2w and T2* imaging. Image quality was higher for SW MRI, with an increased proportion of studies without artefact (Figure 5.5, Figure 5.6).

The SWIp technique is sensitive to changes in susceptibility, and areas of IMH may appear to have layers rather than a continuous region of reduced signal (Figure 5.2F, Figure 5.6A). It is not clear whether this reflects higher spatial discrimination of SW MRI, or whether it is due to the differences between SW MRI and T2w or T2* imaging. The amount of signal hypointensity within IMH may be related to both iron concentration and oxygenation status of haemoglobin. For these reasons, the size or severity of IMH was not assessed, which additionally have not been shown to have the same diagnostic or prognostic value as detection of its presence. IMH could potentially occur in

small volumes of myocardium, below the detection level of T2w or T2* imaging, or tissue may contain heterogeneous areas of IMH. SW MRI may be sensitive to phase changes between small-volume structures. However, animal studies (such as Fishbein et al. (1980), as discussed in Chapter 1) describe IMH typically as confluent, macroscopic areas. Artefact at the 'heart-lung-liver' interface at the inferolateral wall was typically much less with SW MRI than with T2* imaging (Figure 5.6, top row). The optimal parameters derived in this study did result in some aliased pixels in the phase images being carried into the SWIp images. However, these hypointense pixels are clearly distinguishable from true IMH in their small size and position away from the infarct zone (Figure 5.3).

It has been suggested that multiple phase mask multiplications help to increase the visibility of small areas of haemorrhage in SW brain imaging (Haacke et al., 2004). We evaluated the impact of multiple SWIp phase mask multiplications on ΔrSNR and rSNR for areas of IMH. In contrast to a previous study (Haacke et al., 2004), only a small numerical improvement in ΔrSNR between areas of IMH and infarct between 1 and 2 phase mask applications was found (Figure 5.4); however, multiple iterative phase mask applications did not result in a significant improvement in ΔrSNR over the first application.

5.6.1. Limitations

This study has a number of potential limitations. The AMI population size is small, though larger than studies establishing other CMR techniques such as LGE (Choi et al., 2001) or T2w imaging (Abdel-Aty et al., 2004). Other pulse sequences may detect IMH, such as T1 or T2 mapping (Pedersen et al., 2012; Kali et al., 2013b), and were not tested in this study; however T2w imaging remains the reference standard with established prognostic utility following AMI (Eitel et al., 2011). T2w imaging may provide other insights post-AMI, which SW MRI does not, such as estimation of the area at risk and myocardial salvage (Kidambi et al., 2013b; Eitel et al., 2010). The SNR of SW MRI, with the mask parameters provided, is likely to change at different field strengths, with the potential to alter diagnostic accuracy.

5.7. Conclusions

SW MRI, using the SWIp technique, is an accurate and reproducible way of detecting haemorrhage following AMI. The technique offers considerably shorter breath hold times to T2w and T2* imaging, and does not appear to be as prone to image artefacts.

6. Chapter 6
Myocardial Extracellular Volume and Contractile Recovery

6.1. Abstract

6.1.1. Objectives

To assess if myocardial extracellular volume (ECV) measured by cardiovascular magnetic resonance (CMR) in reperfused acute myocardial infarction (AMI) offers additional predictive value for contractile recovery over late gadolinium enhancement (LGE) extent.

6.1.2. Background

The transmural extent of myocardial infarction as assessed by LGE CMR is an important predictor of functional recovery, but accuracy of the technique may be reduced in AMI. Functional recovery is also determined by the severity of tissue damage within infarcted myocardium, which can be quantified with ECV mapping by CMR.

6.1.3. Methods

26 patients underwent acute (day 2) and convalescent (3 months) CMR scans following AMI. Cine imaging, tissue tagging, modified Look-Locker inversion T1 mapping natively and 15 minutes post gadolinium-contrast administration and LGE imaging were performed. The ability of acute infarct ECV and acute transmural extent of LGE to predict convalescent wall motion, ejection fraction (EF) and strain were compared.

6.1.4. Results

Per-segment, acute ECV and LGE extent were associated with convalescent wall motion score ($p<0.01$; $p<0.01$ respectively) and convalescent EF ($p<0.01$; $p=0.02$). ECV had higher accuracy than LGE extent to predict improved wall motion (area under receiver-operator-characteristics curve 0.80 vs. 0.70, $p=0.04$). Per-patient, ECV and LGE correlated with visual contractile improvement ($r=0.51$, $p<0.01$; $r=0.49$, $p=0.01$ respectively) and convalescent infarct zone strain ($r=0.71$, $p<0.01$; $r=0.41$, $p=0.04$). Acute infarct ECV was independently associated with convalescent infarct strain and EF ($p<0.001$; $p=0.02$) whereas LGE was not ($p=0.7$; $p=0.4$).

6.1.5. Conclusion

Acute infarct ECV in reperfused AMI predicts regional and global LV remodelling, independent of transmural extent of infarction.

6.2. Objectives

To assess if myocardial extracellular volume (ECV) measured by cardiovascular magnetic resonance (CMR) in reperfused acute myocardial infarction (AMI) offers additional predictive value for contractile recovery over late gadolinium enhancement (LGE) extent.

6.3. Background

Following reperfused acute myocardial infarction (AMI), the left ventricle (LV) remodels, with the extent of functional recovery in the infarct zone determined by the proportion of viable, contractile cells present (Pfeffer and Braunwald, 1990). Late gadolinium enhancement (LGE) cardiovascular magnetic resonance (CMR) is the clinical reference standard for imaging of myocardial infarction and allows accurate estimation of the infarct extent *in vivo* (Kim et al., 1999; Wu et al., 2001). In AMI, however, the presence of myocardial oedema and the effects of reperfusion therapy on infarct expansion add complexity to infarct imaging, reducing the accuracy of LGE to predict recovery of regional wall motion (Dall'Armellina et al., 2011; Engblom et al., 2009; Ingkanisorn et al., 2004). Processes within the infarct zone, such as microvascular obstruction (MO) or intramyocardial haemorrhage (IMH), impair functional recovery independent of infarct size (Gerber et al., 2002; Kidambi et al., 2013a), demonstrating that differing degrees of infarct "severity" exist. LGE assesses tissue as dichotomously as "viable" or "non-viable" across the transmural extent of myocardium, but does not consider the severity of tissue damage within the hyperenhanced infarct zone.

Native and post-contrast T1 mapping by CMR allows for quantitative estimation of the myocardial extracellular volume (ECV). ECV estimation provides the potential for quantitative assessment of severity of tissue damage and loss of myocytes within the infarct zone, potentially providing an additional dimension of infarct characterisation to LGE-derived assessment of transmural extent. ECV mapping has been applied to chronic MI with a range of values in the infarct zone reported, suggesting that it can determine the severity of tissue damage in myocardial infarction (Kellman et al., 2012), but the method has not been used in patients with AMI.

We hypothesised that ECV estimation by CMR in reperfused ST-elevation AMI offers additional predictive value for functional contractile recovery as compared to transmural extent of LGE hyperenhancement.

6.4. Methods

Patients with first ST-segment elevation AMI, revascularised by primary percutaneous coronary intervention (PCI) within 12 hours of onset of pain, were prospectively recruited from a single tertiary centre. ST-elevation AMI was defined as per current guidelines (Thygesen et al., 2012). Exclusion criteria were previous AMI or coronary artery bypass grafting (CABG), estimated glomerular filtration rate <30ml/min/1.73m^2, cardiomyopathy, or contraindications to CMR. The study protocol was approved by the institutional research ethics committee; all patients gave written informed consent. Patients with maximal scar extent less than 2 voxels of the in-plane resolution of LGE and T1 mapping were deemed too small for accurate evaluation of the infarct zone and not included in the analysis. Clinical management (including anticoagulation and use of aspiration catheters during primary PCI) was at the discretion of the responsible clinician, reflecting contemporary practice and guidelines, and performed blind to the CMR results. All patients were considered for beta-blockade, angiotensin converting enzyme inhibitors, statins, dual antiplatelet therapy and cardiac rehabilitation. A venous blood sample for haematocrit was obtained at the start of each scan.

6.4.1. Image acquisition

All patients had CMR at 3.0Tesla (Achieva TX, Philips Healthcare, Best, The Netherlands) within 3 days of their index presentation (acute scan) and again 3 months post-AMI (convalescent scan). The same CMR protocol was used for each visit. To ensure consistent slice positioning and analysis of infarct characteristics between time points, T1 mapping, tagging, LGE and wall motion analysis were performed in three identical short-axis positions. These were determined using the '3-of-5' approach by acquiring the central 3 slices of 5 parallel short-axis slices spaced equally from mitral annulus to LV apical cap (Messroghli et al., 2005). In addition, LGE and cine imaging was performed using a contiguous stack of short-axis slices covering the whole LV. The same slice geometry, position and a 10mm slice thickness were used for all sequences. Cine imaging used a balanced steady-state free precession pulse sequence (echo time (TE)/repetition time (TR)/flip angle 1.3ms/2.6ms/40°, spatial resolution 1.6×2.0×10mm, typical temporal resolution 25ms), covering the heart in parallel short-axis slices. Tissue tagging used a spatial modulation of magnetisation (SPAMM) pulse sequence (spatial resolution 1.5×1.5×10mm, tag separation 7 mm, temporal resolution ≤35ms, typical TR/TE/flip angle

5.9/3.5/10°). T1 mapping was performed with a 17-heart beat modified Look-Locker inversion (MOLLI) method to acquire 11 images (3-3-5 acquisition with 3x R-R interval recovery epochs) in a single end-expiratory breath hold (Messroghli et al., 2004; Messroghli et al., 2007b) (balanced steady-state free precession read out in end-diastole, manual RF shim adjustments, 2x sensitivity-encoded (SENSE) acceleration, acquired spatial resolution 1.7×2.1×10mm, typical TE/TR/flip angle 2.7/1.06/35°). 0.1 mmol/kg gadolinium-DTPA (gadopentetate dimeglumine; Magnevist, Bayer, Berlin, Germany) was then administered using a power injector (Spectris, Solaris, PA). Repeat MOLLI T1 mapping was performed at 15 minutes post-contrast, and LGE imaging at 16-20 minutes post contrast (inversion recovery-prepared T1 weighted gradient echo, inversion time according to Look-Locker scout, spatial resolution 1.54×1.75×10mm, TR/TE/flip angle 3.7/2.0/25°). In addition to the three LGE short-axis slices for analysis, a contiguous stack of LGE images was acquired immediately after the three slice LGE acquisition (imaging parameters as above, slice thickness 10mm, no slice gap).

6.4.2. Image analysis

Images were analysed offline using commercial software (cvi42 v4.1.3, Circle Cardiovascular Imaging Inc., Calgary, Canada and inTag v1.0, CREATIS lab, Lyon, France). In addition to alignment of slices during image acquisition, accurate alignment of serial scans was verified by comparing ventricular and papillary muscle morphology. Slices that were not aligned between sequences or time-points were not analysed. Segmental analysis was performed using the three short-axis slices and analysed using the modified 16-segment AHA model (Cerqueira et al., 2002). A per-patient analysis was performed using one region of interest each for infarct and remote zones per patient. One short-axis slice per patient corresponding to the core of the infarct on the acute visit was selected, and the same slice position used in the convalescent scan.

Left ventricular volumes and ejection fraction (EF) were analysed from cine images using standard methods. Infarcted myocardium was denoted by LGE analysis as hyperenhancement ≥5 standard deviations (SD) above remote myocardium (Bondarenko et al., 2005), including any hypointense core. Infarct size and MO were measured from LGE images. Infarct location was determined by CMR, according to standard guidelines (Cerqueira et al., 2002). MO was defined visually as the hypointense core within the infarct zone on LGE imaging. Infarct volumes were calculated across the whole LV stack by the modified Simpson's method. Remote myocardium was selected as a 60° sector

diametrically opposite to the infarct and in an area without LGE. Regional wall motion (RWMA) was graded from cine imaging by an experienced cardiologist (AK, 4 years' CMR experience), blinded to the results of strain and LGE and scored as: 0=normal; 1=mild or moderate hypokinesis; 2=severe hypokinesis; 3=akinesis; 4=dyskinesis (Kim et al., 2000).

Transmural extent of infarction was quantified by dividing each short-axis LGE slice into 100 chords, and measuring the transmural extent of hyperenhanced myocardium to the nearest 5% using a modified centreline method (Schuijf et al., 2004) (Figure 6.1). These data were averaged into either 16-segments for the segmental analysis, or averaged across the infarct zone for the per-patient analysis. Any chords with zero transmural extent within an infarcted segment were not analysed, in order to not underestimate the transmural extent of smaller infarcts.

Myocardial ECV was calculated from native and post-contrast MOLLI images. T1 was calculated for infarcted and remote myocardium using a region of interest within the infarct and remote zone. Care was taken to ensure a conservative region of interest, and to avoid partial-volume effects from neighbouring tissue, MO or blood pool (Figure 6.2). Regions of interest were manually motion corrected as required. ECV was calculated for infarct and remote zones using Equation 1.2 (Miller et al., 2013).

For tagging analysis, short-axis SPAMM images were analysed on a per-patient basis. Strain was measured in the single short-axis slice which demonstrated maximal infarction on LGE imaging. The same position was analysed for the convalescent scan. Mid-myocardial end-systolic circumferential strain was measured through the infarct and remote zones (Figure 6.1).

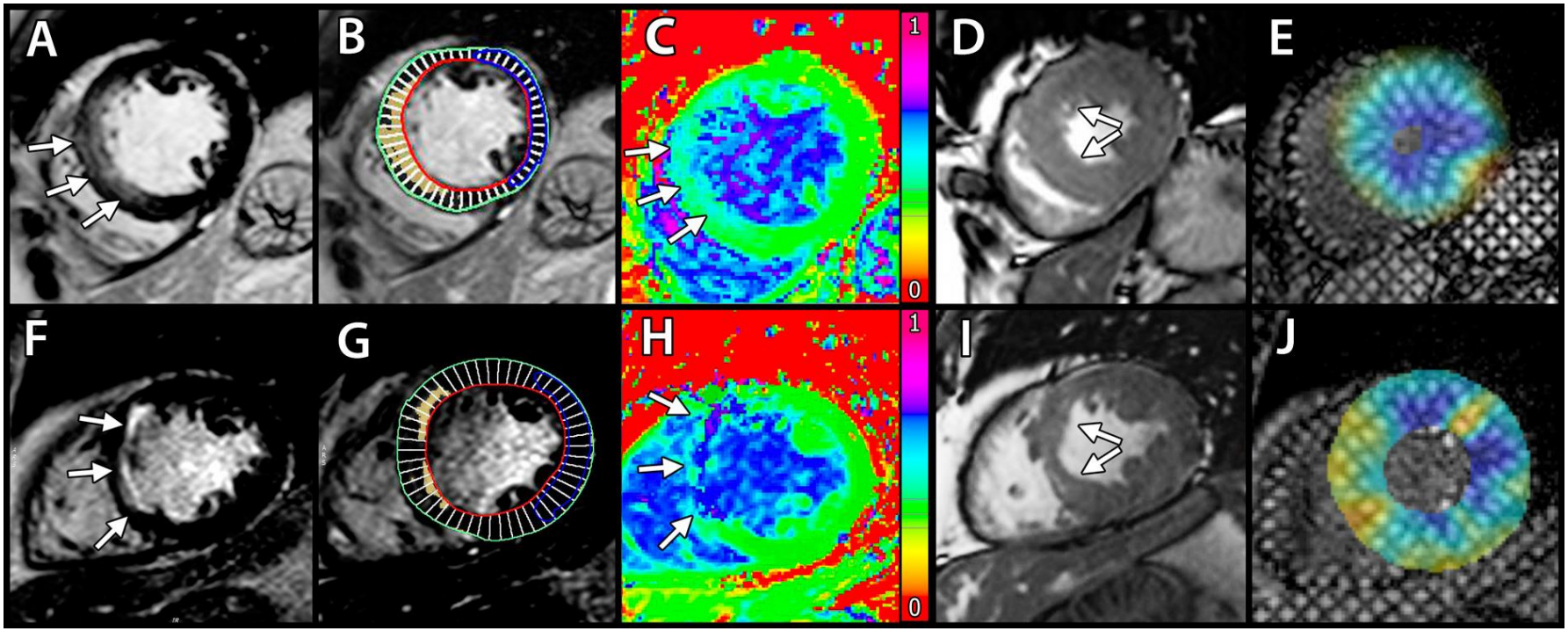

Figure 6.1. Comparison of LGE transmural extent and ECV with regional function and strain. Top row: a patient with high acute infarct transmural extent on LGE (A) and quantified by threshold analysis (B). There is relatively low infarct ECV (0.44), as illustrated here by the modest gradation from normal myocardial ECV (yellow/green) on an ECV map (C). Recovery of function is good at 3 months, as seen on cine imaging (systolic image, D) and normal peak systolic strain (blue myocardium, E). Bottom row: a patient with modest transmural extent of infarction acutely (F and G) has high acute ECV within the infarct zone (0.70, H). A septal regional wall motion abnormality persists at 3 months (systolic cine image, I) with decreased strain septally (yellow myocardium, J).

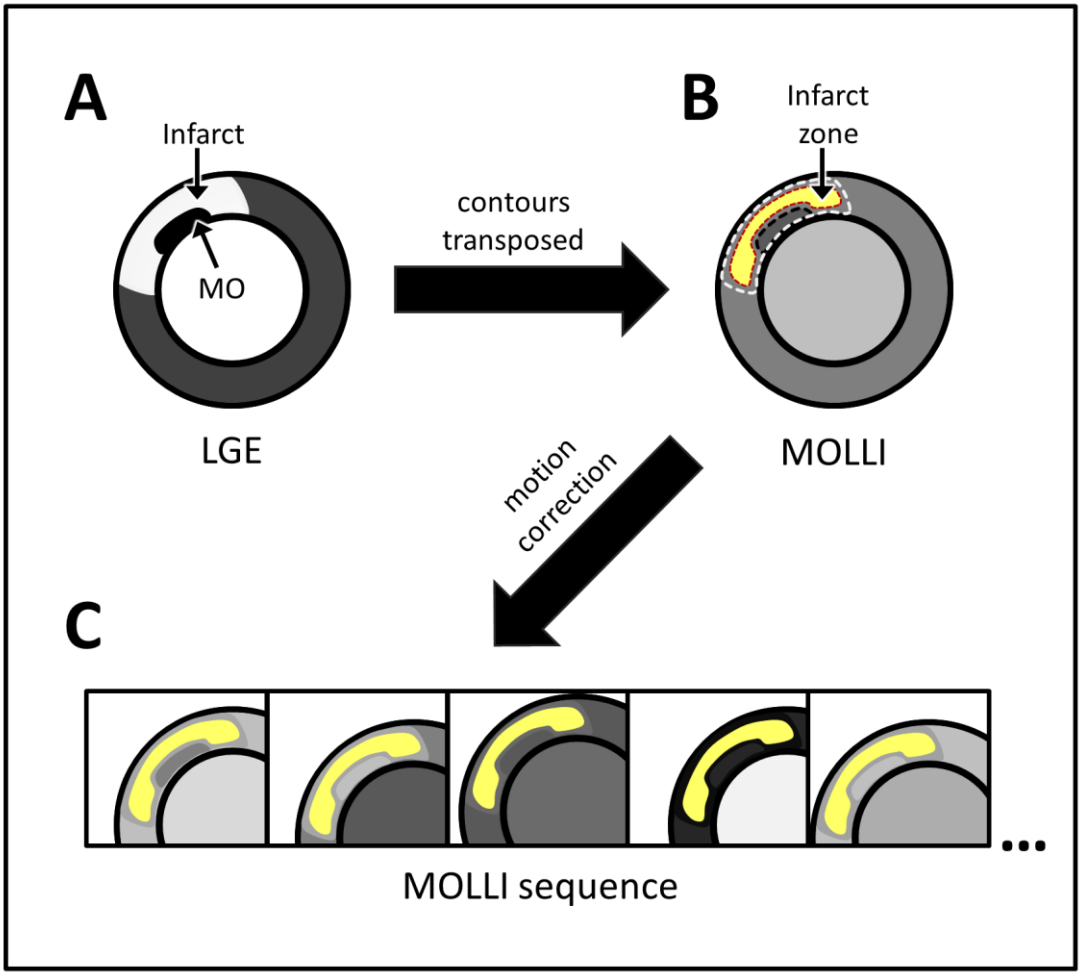

Figure 6.2. Estimation of infarct ECV. Infarct zone as determined by signal intensity analysis on LGE images (A) is transposed to MOLLI images (B). Areas of MO are excluded, as are pixels at a tissue interface that may be susceptible to partial volume effects to highlight the infarct zone (B, yellow contour). This contour is motion corrected for all images in the MOLLI sequence (C) prior to T1 estimation. Pre and post contrast T1 images are used to derive ECV.

6.4.3. Statistical analysis

Statistical analysis was performed using IBM SPSS® Statistics 20.0. Continuous variables are expressed as mean ± SD. All statistical tests were 2-tailed; p values <0.05 were considered significant. Correlation between qualitative measures was derived using Spearman's rank test; quantitative measures were correlated with Pearson's coefficient. Differences in segmental measurements were evaluated using a multilevel linear mixed-effects model to account for non-independence of segmental data, with r denoting partial correlation in this context. A sample size of 24 patients was calculated (Hanley and McNeil, 1983) to detect a 10% difference in accuracy (AUC) with a power of 80% at a significance level of 0.05, assuming rank correlation of 0.6 between ECV and transmural extent of LGE, accuracy of LGE as 0.82, and an average of one third of segments demonstrating infarction (Romero et al., 2013). Normality for quantitative data was established using the Kolmogorov-Smirnov test. Univariable analyses were performed to identify predictors of reduced strain and EF at 90 days. Variables with a probability value <0.1 in the univariable analysis were included in a multivariable linear regression analysis. Receiver operating characteristic (ROC) curves were compared using the method described by DeLong et al (DeLong et al., 1988).

6.5. Results

6.5.1. Patient characteristics

Of 79 eligible patients admitted within the recruitment period, 13 had obesity that precluded CMR, 4 were unable to lie flat, 1 had an MR-incompatible pacemaker, 10 were unable to consent and 5 were due to have CABG prior to the follow-up scan. The remaining 46 patients were approached, of which 9 declined to participate. Therefore 37 patients constituted the study sample. 7 did not attend follow-up and 4 had MI deemed too small for accurate analysis by the criteria detailed above. 26 patients therefore completed baseline and follow up scans and were included in the statistical analysis. Patient demographics are shown in Table 6.1. No gender-based differences were present. 18 slices (23%) did not have good alignment between methods and/or time-points and were excluded from analysis.

Table 6.1. Patient characteristics

Patient characteristic	
N	26
Age, years	59 ± 9
Male	23 (88%)
Body mass index, kg/m^2	28.1 ± 3.0
Current smoker	13 (50%)
Hypertension	6 (23%)
Hypercholesterolemia	6 (23%)
Diabetes mellitus	3 (11%)
Pain to balloon time, min (median (IQR*))	221 (257)
Infarct territory	
Anterior	14
Inferior	9
Lateral	3
Microvascular obstruction	14 (54%)
TIMI flow grade ≥ 2 pre-PCI	1 (4%)
TIMI flow grade 3 post-PCI	26 (100%)
Peak troponin I, ng/L (median)	>50000
Peak CK†, iu/L (median (IQR))	1003 (1598)
Baseline CMR scan, days (median (IQR))	2 (1)
Follow up CMR scan, days (median (IQR))	100 (13)

Data as mean ± SD or n (%) unless indicated.*IQR interquartile range, †CK creatine kinase.

6.5.2. Infarct characteristics

Infarct characteristics are shown in Table 6.2. Infarct native T1 significantly decreased with time (Table 6.2), and was significantly higher in infarct than remote myocardium ($p<0.001$ at day 2 and 3 months). The infarct zone demonstrated a wide range of ECV measurements between patients, both acutely (range 0.33-0.84) and at 3 months (0.26-0.89). Acute infarct ECV in patients with and without MO (ECV measurement excluded any MO zone) was similar (0.58±0.12 vs. 0.51±0.16, $p=0.2$), as was acute LGE transmural extent (74±9% vs. 81±11%, $p=0.14$). Acute infarct ECV and acute transmural extent of LGE did not correlate significantly ($r=0.36$, $p=0.07$). Transmural extent of LGE decreased significantly between acute and convalescent visits (Table 6.2). ECV did not differ significantly between acute and convalescent visits in infarct or in remote zones (Table 6.2). ECV did not differ significantly in segments adjacent to infarction ('peri-infarct' segments) and distant remote segments (0.32 ± 0.11 vs. 0.30 ± 0.09, $p=0.1$).

Table 6.2. Infarct characteristics

Characteristic	**Acute visit**	**Convalescent visit**	**P value**
Ejection fraction,%	48 ± 9	58 ± 8	<0.01
LV EDVi*, ml/m^2	81 ± 17	85 ± 22	ns
LV ESVi†, ml/m^2	42 ± 12	36 ± 15	<0.01
LV mass, g/m^2	66 ± 14	57 ± 12	<0.01
LGE transmural extent, %	77 ± 4	59 ± 15	<0.01
LGE infarct volume, ml	16 ± 11	9 ± 8	<0.01
LGE MO volume, ml	1 ± 2	-	
Infarct native T1	1319 ± 113	1236 ± 128	0.03
Remote native T1	1189 ± 61	1139 ± 72	ns
Infarct ECV	0.54 ± 0.14	0.54 ± 0.18	ns
Remote ECV	0.31 ± 0.07	0.30 ± 0.07	ns

Data as mean ± SD. **LV EDVi* Left ventricular end diastolic volume, indexed to body surface area, †*LV ESVi* Left ventricular end systolic volume, indexed to body surface area.

6.5.3. Per segment

Acute infarct ECV correlated with wall motion score acutely (β=0.46, r=0.46, p<0.01) and at 90 days (β=0.61, r=0.61, p<0.01, Figure 6.3). Improvement in wall motion score decreased with increasing ECV (F=46.5, p<0.01, Figure 6.4). Acute transmural extent of LGE also correlated with wall motion score both acutely (β=0.50, r=0.51, p<0.01) and at 90 days (β=0.45, r=0.45, p<0.01, Figure 6.3). Improvement in wall motion score decreased with increasing acute transmural extent of LGE (F=12.8, p<0.01, Figure 6.4). ROC analysis for the prediction of improvement in wall motion score at 90 days demonstrated a significantly higher area under the curve (AUC) for acute infarct ECV than acute transmural LGE extent (0.80 (95% confidence interval 0.72-0.87) vs. 0.70 (95% confidence interval 0.61-0.78), p=0.04, Figure 6.5). An infarct ECV value of 0.5 or less had sensitivity of 86% and specificity 69% for prediction of improvement in segmental function. Adding acute ECV analysis to a 50% LGE transmural extent cut-off for prediction of wall motion improvement in dysfunctional segments increased sensitivity from 87% to 90% and specificity from 42% to 88%.

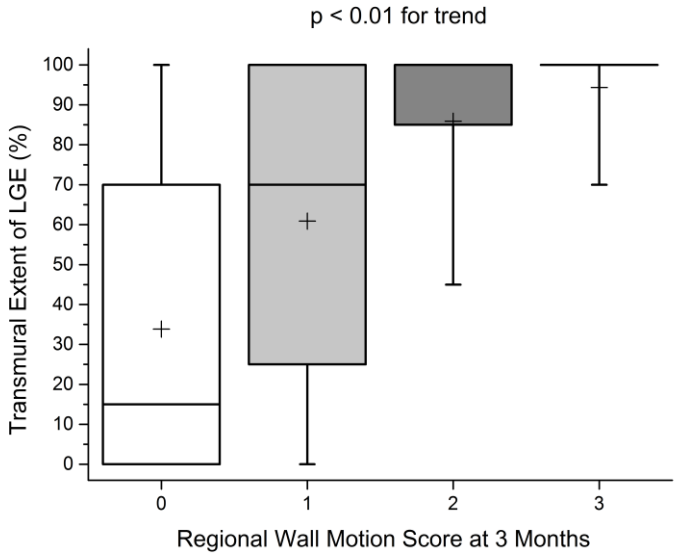

a)

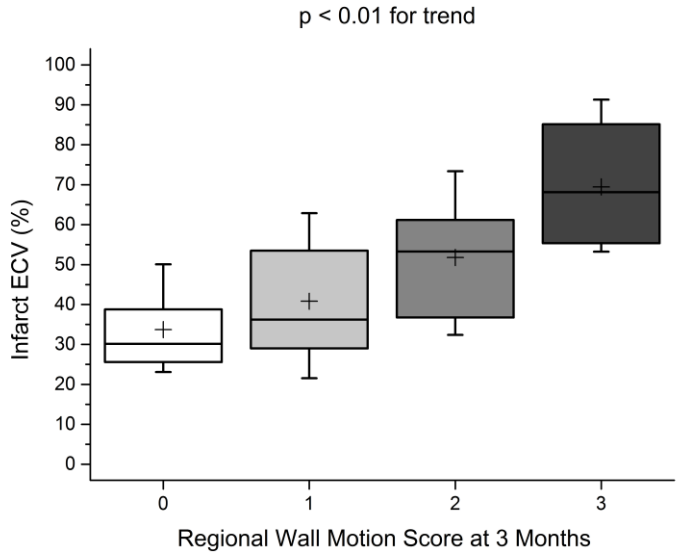

b)

Figure 6.3. Comparison of convalescent regional wall motion score with acute LGE and acute ECV. LGE transmural extent (a) and infarct ECV (b) are shown. Note relatively wide ranges for transmural extent. Box denotes median, 25th and 75th percentiles, mean indicated by + and whiskers at 9th and 91st percentiles.

.

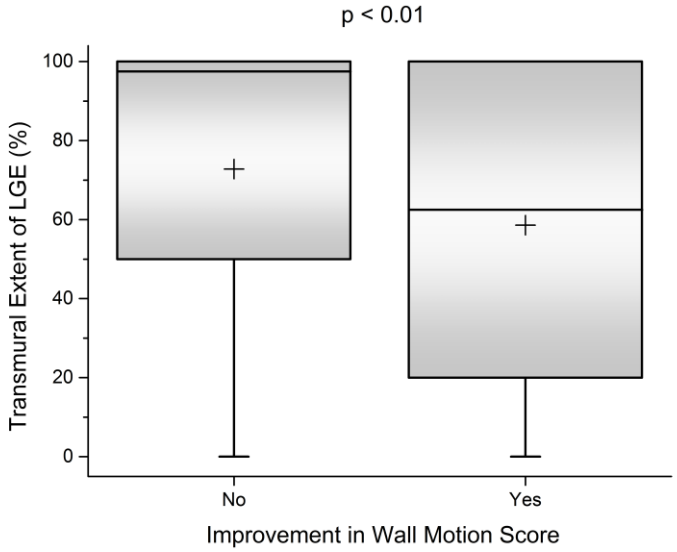

a)

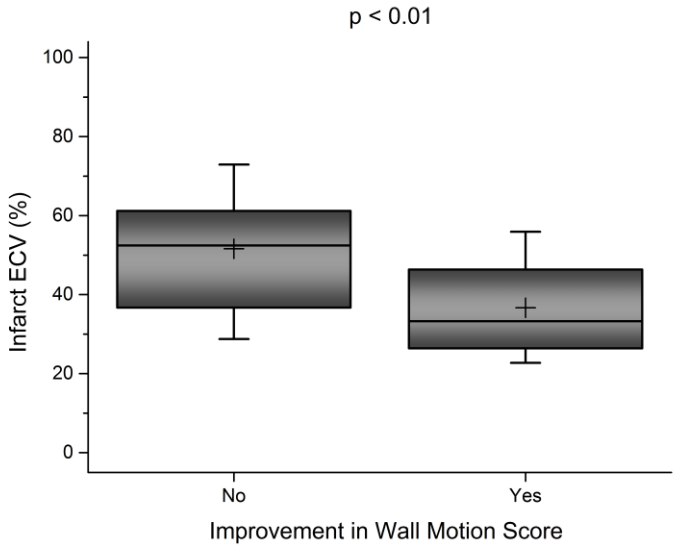

b)

Figure 6.4. Regional wall motion score as predicted by acute LGE and ECV. Acute transmural extent of LGE (a) and acute infarct ECV (b) compared to improvement in wall motion score in dysfunctional segments over 3 months.

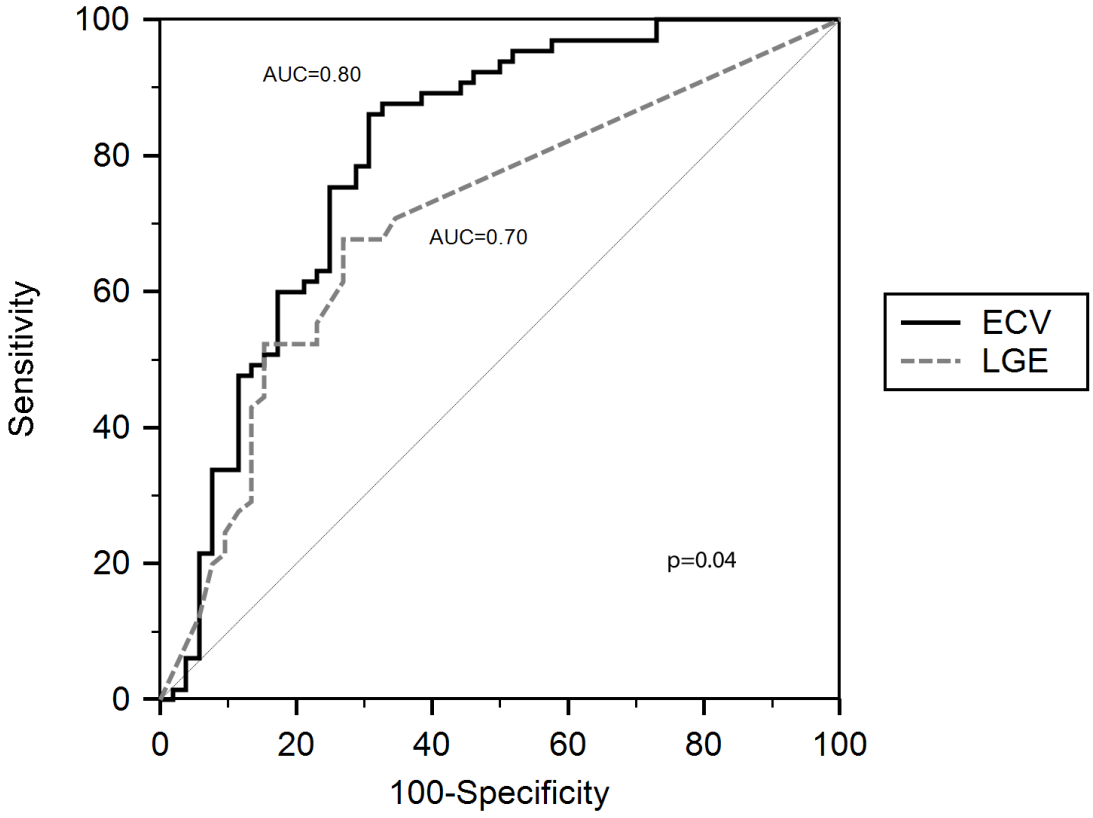

Figure 6.5. ROC curve comparing infarct ECV and LGE. ECV and transmural extent of infarction in dysfunctional segments (n=117) is evaluated against improvement in wall motion score at 90 days. Remote segments not shown.

6.5.4. Per patient

Performance of acute LGE and acute ECV to predict markers of LV function per patient are shown in Table 6.3. ECV had numerically higher correlation than LGE transmural extent for all measured markers of LV function. Figure 6.6 compares the performance of acute LGE and acute ECV to predict convalescent infarct zone strain.

Table 6.3. ECV and LGE vs. LV function.

Marker of LV function	**Acute LGE**		**Acute ECV**	
	Correlation coefficient, r	**p**	**Correlation coefficient, r**	**p**
Acute wall motion score	0.33	0.1	0.26	0.07
Convalescent wall motion score	0.49	0.01	0.51	<0.01
Acute infarct strain	0.41	0.04	0.71	<0.01
Convalescent infarct strain	0.54	<0.01	0.71	<0.01
Convalescent ejection fraction	-0.47	0.02	-0.62	<0.01

Correlation between acute LGE transmural extent and acute ECV per patient with markers of acute and convalescent LV function are shown.

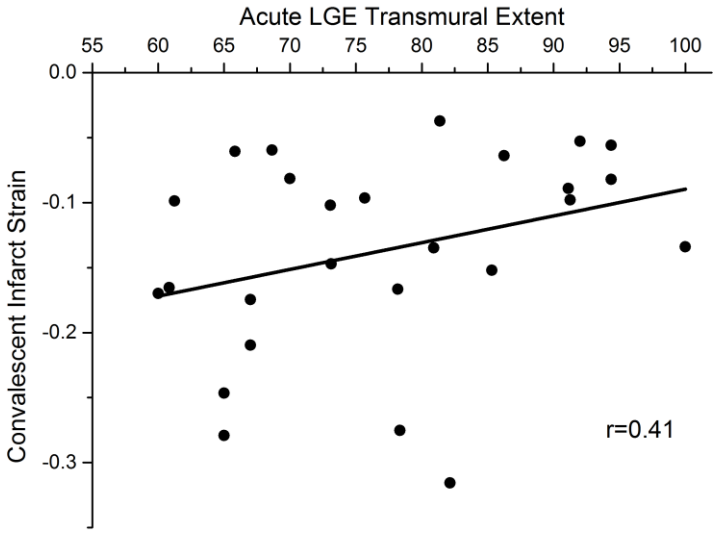

a)

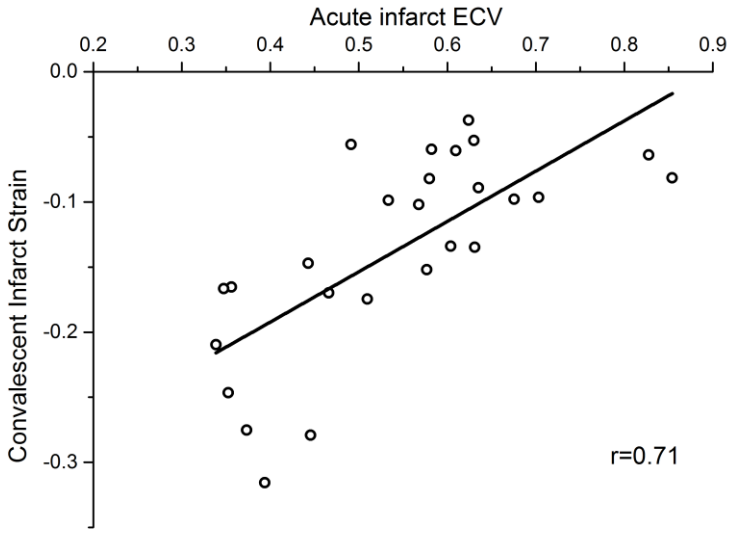

b)

Figure 6.6. Convalescent infarct zone strain. Comparison of strain with acute transmural extent of LGE (a) and acute infarct ECV (b) is shown on a per-patient basis (n=26).

6.5.5. Regression analysis

Univariable linear regression analysis (examining the variables in Table 6.4 per-patient) showed that acute infarct ECV, but not acute LGE transmural extent, was significantly associated with attenuated convalescent infarct zone strain. In multivariable linear regression analysis, acute infarct ECV was significantly associated with convalescent infarct zone strain ($\beta = 0.68$, $p<0.001$) whereas acute transmural extent of LGE was not ($\beta = 0.072$, $p = 0.7$).

Table 6.4. Multivariable regression analysis.

	Strain		**EF at 3 Months**	
	Univariable	**Multivariable**	**Univariable**	**Multivariable**
Variable	p value	p value	p value	p value
Age	0.29	…	0.65	…
Sex	0.09	…	0.03	0.17
Current smoker	0.6	…	0.72	…
Hypertension	0.76	…	0.12	…
Hypercholesterolemia	0.29	…	0.64	…
Diabetes	0.09	…	0.40	…
Heart rate at CMR	0.63	…	0.97	…
Blood pressure, systolic/diastolic	0.9/0.6	…	0.8/0.9	…
Pain onset to balloon time	0.18	…	0.1	…
Anterior AMI	0.46	…	0.66	…
TIMI flow grade before PCI	0.10	…	0.55	…
TIMI flow grade after PCI	1.0	…	1.0	…
LV mass (indexed to BSA)	0.46	…	0.15	…
Remote mid-myocardial circumferential strain	0.64	…	0.65	…
Infarct LGE transmural extent	0.11	0.7	0.03	0.41
Infarct ECV	<0.0001	<0.001	0.003	0.02

Predictors of decreased infarct zone strain and ejection fraction in univariable and standard multivariable regression analysis. Variables are taken from acute visit.

6.6. Discussion

This study has found that the ECV in acute reperfused myocardial infarction is predictive of regional and global LV remodelling, independent of transmural infarct extent. ECV adds quantitative information about severity of myocardial injury within the infarct zone to the assessment of infarct extent by LGE. Acute infarct ECV predicts functional recovery better than transmural infarct extent by LGE, suggesting a potential clinical role for ECV mapping post-AMI.

ECV mapping provides a continuous measure of contrast uptake and thus a potential tool to interrogate the heterogeneous ultrastructural changes in infarcted myocardium. Our data suggest that ECV measurement provides the ability to study severity of cellular damage as evidenced by capacity to recover function. In this study, acute ECV was an incrementally better predictor of ejection fraction and attenuated convalescent strain in the infarct zone than acute LGE transmural extent. ECV demonstrated utility throughout the range of infarct severity observed in reperfused AMI, and notably increased the specificity to predict functional improvement in patients with >50% transmural LGE that was independent of LGE analysis. ECV was a stronger predictor of convalescent function than LGE extent. ECV had a higher accuracy than LGE to predict improvement in regional wall motion score (Figure 6.5), higher degree of correlation with infarct zone strain (Figure 6.6), and reduced spread of values across the range of wall motion abnormalities (Figure 6.3).

LGE is established as a clinical reference standard for viability imaging following AMI, but accuracy may be reduced when using the technique acutely. Several studies have reported on use of LGE in AMI. Choi et al (Choi et al., 2001) compared acute transmural extent of LGE with convalescent function in 24 patients following reperfused STEMI. The observation of decreasing functional recovery with increasing transmural extent was driven largely by segments with either 0% or 100% transmural extent, which made up approximately two thirds of the sample. Ingkanisorn et al (Ingkanisorn et al., 2004) found a significant reduction in wall thickening with increasing transmural extent, but no significant difference in the quartiles between 1-75% transmurality. A comparable analysis in 30 patients demonstrated that 25% of segments with 75-100% acute transmural infarction had functional improvement at 13 weeks (Beek et al., 2003). Gerber et al (Gerber et al., 2002) observed good correlation between infarct transmural extent and segmental strain measurements. Finally, Shapiro et al (Shapiro et al., 2007) found that transmural extent of LGE was predictive of functional outcome in 17 patients, even accounting for presence of MO. Results of the present study were consistent with these previous reports

and showed that higher transmural extent of scar was associated with impaired wall motion both acutely and at 90 days (Figure 6.3) and with lower improvement in wall motion score over time (Figure 6.4).

These previous reports and our data thus indicate that LGE can accurately predict functional outcome in AMI in areas of no LGE or with full transmural infarction, but its accuracy is reduced in intermediate (25-75%) transmural infarct extent. This may be related to a number of factors. Remodelling of the infarct zone over time may lead to comparatively high transmural extent acutely (Anversa et al., 1993). Oedema may also lead to overestimation of transmural extent acutely (Choi et al., 2001; Fishbein et al., 1978), though the role of oedema within the infarct core is questioned (Holmes et al., 2005). The optimal threshold for hyperenhancement is debated (Bondarenko et al., 2005; Beek et al., 2009); in the present study we therefore deliberately chose a conservative method to avoid potential overestimation of infarct size for example due to oedema or noise. We also chose to define infarct size separately for baseline and follow-up visits rather than transposing contours from convalescence to acute studies as has been done in other studies (Kidambi et al., 2013b). This approach allowed us to test the clinically relevant predictive value of acute ECV estimation, which a retrospective transposition would not have allowed. However, because infarcts shrank over time, the amount of tissue for which infarct ECV was estimated differed slightly between the two measurement points ($\sim$0.3cm^2), but this small difference is unlikely to affect the main study results.

LGE is highly accurate in defining the extent of infarction, but cannot differentiate degrees of severity of tissue damage within the hyperenhanced infarct zone. The data from the current study suggest that ECV can provide characterisation in the diagnostic quandary of intermediate LGE extent, and adds an additional dimension to assessment of infarct transmurality by LGE. In histological studies, myocardial infarcts maintain foci of preserved myocytes within areas of necrosis (Fishbein et al., 1978), which raises the potential for functional recovery. Interstitial expansion in infarction is also variable and may depend on the extent of local reperfusion (Anversa et al., 1993). These observations may, in part, explain contractile recovery found within the infarct zone (Gerber et al., 2002; Kidambi et al., 2013a), and the range of infarct ECV values observed in the present study.

Notably, ECV has previously been validated in models of chronic fibrosis rather than acute infarction (White et al., 2013). Studies to date have mainly focused on native T1 in acute infarction, with similar findings to this study

(Dall'Armellina et al., 2012). For both LGE and ECV, the pathophysiological correlates in AMI are less well established, but both methods are likely to detect the expanded interstitial space within the infarct zone arising from cell death with or without oedema or intracellular contrast uptake (Wendland et al., 1999).

Although increased ECV was clearly associated with poorer infarct functional recovery in this study, several confounders should be considered. The presence of oedema within the infarct core is debated (Holmes et al., 2005), but would affect myocardial T1 and hence ECV estimates (Ferreira et al., 2012). Our data however show that native infarct T1 did decrease over time while infarct and remote ECV were stable (Table 6.2). This result is in contrast to animal reperfusion models (Anversa et al., 1985b), though these models do not account for the effects of medical therapies that may influence remote myocardial remodelling.

Infarct ECV is unlikely to be the sole determinant of functional recovery. MO and IMH are independent markers of poor functional outcome (Gerber et al., 2002; Kidambi et al., 2013a; Nijveldt et al., 2008). ECV estimation in these pathologies, which are characterised by poor contrast uptake, has not been established by the bolus-only contrast method. MO may give rise to patchy subendocardial capillary obstruction (Ambrosio et al., 1989), which would not be observed by LGE. The effect of this on overall contrast density and ECV has not been established. In the present study, we chose to exclude areas of visible MO from ECV measurements to avoid confounding by another variable. Care was taken to measure ECV at least one voxel away from peri-infarct myocardium, pericardium or blood pool, to minimise partial volume errors.

6.6.1. Limitations

The sample size in this study is relatively small, but in keeping with similar studies in this demographic (Choi et al., 2001; Gerber et al., 2002; Ingkanisorn et al., 2004) and adequately powered to detect the significant differences observed. Fully adjusting for demographic and other infarct variables would require a larger, likely multicentre study. 4 patients with minimal scar following reperfusion were deemed unsuitable for comparative analysis; all of these patients had normal wall motion in convalescence. Standardisation of T1 mapping and the 'bolus-only' method of ECV estimation is not yet finalised (Moon et al., 2013), however our native T1 values are similar to those reported at 3T with the shortened MOLLI technique (Dall'Armellina et al., 2012).

Absolute ECV values may differ with a different setup, though the trends observed are likely to persist. Areas of MO shrink with time and post-contrast infarct T1 estimation at a single 15 minute time-point may have included areas of early MO.

6.7. Conclusions

This study demonstrates that CMR-derived ECV estimation of the infarct zone after AMI offers increased accuracy to predict functional recovery compared with LGE alone. Acute ECV estimation is feasible in this demographic and can provide clinically relevant information. The potential clinical utility of infarct ECV mapping post-AMI is most pronounced in cases of intermediate LGE transmural extent, and potentially allows for improved early characterisation and prognostication of patients post-AMI.

7. Chapter 7
Conclusions

The thesis has provided an overview of the utility of cardiovascular imaging in making predictions of recovery following ST elevation AMI, and developed CMR-based markers to predict functional recovery. The clinical appeal of using a safe and non-invasive technique to predict outcome is clear, whilst the insights into pathophysiological processes on a tissue level offers novel *in* vivo research information. In Chapters 3 and 4, this thesis has provided original evidence of the functional utility of established imaging sequences for AMI, namely T2-weighted and late gadolinium enhancement imaging. Chapters 5 and 6 evaluate imaging sequences that are novel in this context, namely susceptibility-weighted and ECV imaging. For each of these sequences, this thesis has presented the potential utility, and the limitations, of the techniques. Each imaging sequence discussed has been shown to provide novel ways to predict functional outcome, and has also provided new insights into the pathophysiology of AMI.

7.1. Future directions

Whilst this thesis demonstrates the functional relevance of the imaging techniques that have been studied, the experiments presented form only a part of the development of a clinical imaging sequence. As mentioned in Chapter 1 (Section 1.3), there are a number of further steps to fully validate any imaging technique. Whilst even the most established imaging techniques have not demonstrated all these steps, it is useful to acknowledge that the hypotheses evaluated in this thesis form only a small part of the work required to ensure the safe and effective uptake of an imaging technique into clinical practice. In particular, whilst the link between functional and prognostic outcome following AMI is well established, the prognostic utility of these markers to directly predict hard events has not yet been shown.

The *in vivo* effects observed by CMR also lead to a number of interesting pathophysiological questions. In Chapter 3, the role of oedema in tissue stunning is explored. However, the roles of intracellular and extracellular oedema are not differentiated, and the role of unbound water (which has

approximately 100x greater influence on T2 shortening than protein bound water) remains to be investigated. In Chapters 3, 4 and 6, we see clear and reproduced evidence of contractile recovery in the infarct zone, regardless of transmural extent. The potential reasons for these are discussed at some length, especially in Section 6.6. However, the histological mechanisms that underpin recovery in 'fully infarcted' myocardium have not been established. It is widely assumed that infarcted tissue has minimal contractile cells, but as discussed in Chapter 1, most of these observations are made from animal models, or end-stage heart failure autopsy specimens, which represent a considerable departure from the patients with first-presentation and aggressive treatment that are common in clinical practice and form the substrate for this thesis. Chapter 5 leads to a number of questions about intramyocardial haemorrhage. Is T2w imaging the most sensitive way to detect IMH? Why do some areas of IMH have a 'layered' appearance (e.g. Figure 5.2F)? Does the magnitude of change in susceptibility relate to the amount or density of haemorrhage?

In addition to further validation of established techniques, the versatility of CMR, such as the recent development of parametric techniques and their introduction into clinical practice, gives us an ongoing supply of new ways to image myocardial infarction. The use of CMR to evaluate both functional outcome and infarct pathophysiology is still in its relative infancy. Ongoing developments, including but not limited to those discussed in Section 1.5, may well lead us to further discoveries along this path.

8. References

Abdel-Aty, H. et al. 2004. Delayed enhancement and T2-weighted cardiovascular magnetic resonance imaging differentiate acute from chronic myocardial infarction. *Circulation.* **109**(20), pp.2411-6.

Abdel-Aty, H. et al. 2005. Diagnostic performance of cardiovascular magnetic resonance in patients with suspected acute myocarditis: comparison of different approaches. *J Am Coll Cardiol.* **45**(11), pp.1815-22.

Ahn, K.T. et al. 2013. Impact of transmural necrosis on left ventricular remodeling and clinical outcomes in patients undergoing primary percutaneous coronary intervention for ST-segment elevation myocardial infarction. *Int J Cardiovasc Imaging.* **29**(4), pp.835-42.

Akter, M. et al. 2007. Detection of hemorrhagic hypointense foci in the brain on susceptibility-weighted imaging clinical and phantom studies. *Acad Radiol.* **14**(9), pp.1011-9.

Aletras, A.H. et al. 2006. Retrospective determination of the area at risk for reperfused acute myocardial infarction with T2-weighted cardiac magnetic resonance imaging: histopathological and displacement encoding with stimulated echoes (DENSE) functional validations. *Circulation.* **113**(15), pp.1865-70.

Aletras, A.H. et al. 2008. ACUT2E TSE-SSFP: a hybrid method for T2-weighted imaging of edema in the heart. *Magn Reson Med.* **59**(2), pp.229-35.

Amabile, N. et al. 2012. Incidence, predictors, and prognostic value of intramyocardial hemorrhage lesions in ST elevation myocardial infarction. *Catheter Cardiovasc Interv.* **79**(7), pp.1101-8.

Ambrosio, G. et al. 1989. Progressive impairment of regional myocardial perfusion after initial restoration of postischemic blood flow. *Circulation.* **80**(6), pp.1846-61.

Anversa, P. et al. 1985a. Left ventricular failure induced by myocardial infarction. I. Myocyte hypertrophy. *Am J Physiol-Heart Circulatory Physiol.* **248**(6), pp.H876-H882.

Anversa, P. et al. 1985b. Myocardial response to infarction in the rat. Morphometric measurement of infarct size and myocyte cellular hypertrophy. *Am J Pathol.* **118**(3), pp.484-92.

Anversa, P. et al. 1993. Ischaemic myocardial injury and ventricular remodelling. *Cardiovasc Res.* **27**(2), pp.145-57.

Arai, A.E. 2011a. The cardiac magnetic resonance (CMR) approach to assessing myocardial viability. *J Nucl Cardiol.* **18**(6), pp.1095-102.

Arai, A.E. 2011b. Magnetic resonance imaging for area at risk, myocardial infarction, and myocardial salvage. *J Cardiovasc Pharmacol Ther.* **16**(3-4), pp.313-20.

Arai, M. et al. 1996. An anti-CD18 antibody limits infarct size and preserves left ventricular function in dogs with ischemia and 48-hour reperfusion. *J Am Coll Cardiol.* **27**(5), pp.1278-85.

Atalay, M.K. et al. 1995. Blood oxygenation dependence of T1 and T2 in the isolated, perfused rabbit heart at 4.7T. *Magn Reson Med.* **34**(4), pp.623-7.

Basso, C. and Thiene, G. 2006. The pathophysiology of myocardial reperfusion: a pathologist's perspective. *Heart.* **92**(11), pp.1559-62.

Basso, C. et al. 2007. Morphologic validation of reperfused hemorrhagic myocardial infarction by cardiovascular magnetic resonance. *Am J Cardiol.* **100**(8), pp.1322-7.

Becker, M. et al. 2009. Impact of infarct transmurality on layer-specific impairment of myocardial function: a myocardial deformation imaging study. *Eur Heart J.* **30**(12), pp.1467-76.

Beek, A.M. et al. 2003. Delayed contrast-enhanced magnetic resonance imaging for the prediction of regional functional improvement after acute myocardial infarction. *J Am Coll Cardiol.* **42**(5), pp.895-901.

Beek, A.M. et al. 2009. Quantification of late gadolinium enhanced CMR in viability assessment in chronic ischemic heart disease: a comparison to functional outcome. *J Cardiovasc Magn Reson.* **11**, p6.

Beek, A.M. et al. 2010. Intramyocardial hemorrhage and microvascular obstruction after primary percutaneous coronary intervention. *Int J Cardiovasc Imaging.* **26**(1), pp.49-55.

Bello, D. et al. 2011. Cardiac magnetic resonance imaging: infarct size is an independent predictor of mortality in patients with coronary artery disease. *Magn Reson Imaging.* **29**(1), pp.50-6.

Beyers, R.J. et al. 2012. T(2) -weighted MRI of post-infarct myocardial edema in mice. *Magn Reson Med.* **67**(1), pp.201-9.

Bijnens, B. et al. 2007. Investigating cardiac function using motion and deformation analysis in the setting of coronary artery disease. *Circulation.* **116**(21), pp.2453-2464.

Bodi, V. et al. 1999. Wall motion of noninfarcted myocardium. Relationship to regional and global systolic function and to early and late left ventricular dilation. *Int J Cardiol.* **71**(2), pp.157-65.

Bodi, V. et al. 2009. Prognostic value of a comprehensive cardiac magnetic resonance assessment soon after a first ST-segment elevation myocardial infarction. *JACC Cardiovasc Imaging.* **2**(7), pp.835-42.

Bodi, V. et al. 2010. Contractile reserve and extent of transmural necrosis in the setting of myocardial stunning: comparison at cardiac MR imaging. *Radiology.* **255**(3), pp.755-63.

Bogaert, J. et al. 1999. Functional recovery of subepicardial myocardial tissue in transmural myocardial infarction after successful reperfusion: an important contribution to the improvement of regional and global left ventricular function. *Circulation.* **99**(1), pp.36-43.

Bogaert, J. et al. 2000. Remote myocardial dysfunction after acute anterior myocardial infarction: impact of left ventricular shape on regional function: a magnetic resonance myocardial tagging study. *J Am Coll Cardiol.* **35**(6), pp.1525-34.

Bolli, R. 1990. Mechanism of myocardial "stunning". *Circulation.* **82**(3), pp.723-38.

Bolli, R. 1992. Myocardial 'stunning' in man. *Circulation.* **86**(6), pp.1671-91.

Bolli, R. and Marban, E. 1999. Molecular and cellular mechanisms of myocardial stunning. *Physiol Rev.* **79**(2), pp.609-34.

Bondarenko, O. et al. 2005. Standardizing the definition of hyperenhancement in the quantitative assessment of infarct size and myocardial viability

using delayed contrast-enhanced CMR. *J Cardiovasc Magn Reson.* **7**(2), pp.481-5.

Bottomley, P.A. and Weiss, R.G. 1998. Non-invasive magnetic-resonance detection of creatine depletion in non-viable infarcted myocardium. *Lancet.* **351**(9104), pp.714-8.

Bragadeesh, T. et al. 2008. Post-ischaemic myocardial dysfunction (stunning) results from myofibrillar oedema. *Heart.* **94**(2), pp.166-71.

Braunwald, E. and Kloner, R.A. 1982. The stunned myocardium: prolonged, postischemic ventricular dysfunction. *Circulation.* **66**(6), pp.1146-9.

Braunwald, E. and Kloner, R.A. 1985. Myocardial reperfusion: a double-edged sword? *J Clin Invest.* **76**(5), pp.1713-9.

Broadbent, D.A. et al. 2013. Myocardial blood flow at rest and stress measured with dynamic contrast-enhanced MRI: Comparison of a distributed parameter model with a fermi function model. *Magn Reson Med.*

Brooks, W.W. et al. 1995. Reperfusion induced arrhythmias following ischaemia in intact rat heart: role of intracellular calcium. *Cardiovasc Res.* **29**(4), pp.536-42.

Bruder, O. et al. 2008. Prognostic impact of contrast-enhanced CMR early after acute ST segment elevation myocardial infarction (STEMI) in a regional STEMI network: results of the "Herzinfarktverbund Essen". *Herz.* **33**(2), pp.136-42.

Burns, R.J. et al. 2002. The relationships of left ventricular ejection fraction, end-systolic volume index and infarct size to six-month mortality after hospital discharge following myocardial infarction treated by thrombolysis. *J Am Coll Cardiol.* **39**(1), pp.30-6.

Bush, L.R. et al. 1983. Recovery of left ventricular segmental function after long-term reperfusion following temporary coronary occlusion in conscious dogs. Comparison of 2- and 4-hour occlusions. *Circ Res.* **53**(2), pp.248-63.

Caiati, C. et al. 1999. New noninvasive method for coronary flow reserve assessment: contrast-enhanced transthoracic second harmonic echo Doppler. *Circulation.* **99**(6), pp.771-8.

Capone, R.J. and Most, A.S. 1978. Myocardial hemorrhage after coronary reperfusion in pigs. *Am J Cardiol.* **41**(2), pp.259-66.

Cerqueira, M.D. et al. 2002. Standardized myocardial segmentation and nomenclature for tomographic imaging of the heart. A statement for healthcare professionals from the Cardiac Imaging Committee of the Council on Clinical Cardiology of the American Heart Association. *Circulation.* **105**(4), pp.539-42.

Choi, K.M. et al. 2001. Transmural extent of acute myocardial infarction predicts long-term improvement in contractile function. *Circulation.* **104**(10), pp.1101-7.

Choi, S.I. et al. 2000. Application of breath-hold T2-weighted, first-pass perfusion and gadolinium-enhanced T1-weighted MR imaging for assessment of myocardial viability in a pig model. *J Magn Reson Imaging.* **11**(5), pp.476-80.

Christian, T.F. et al. 1997. Prospective identification of myocardial stunning using technetium-99m sestamibi-based measurements of infarct size. *J Am Coll Cardiol.* **30**(7), pp.1633-40.

Cochet, A. et al. 2010. Prognostic value of microvascular damage determined by cardiac magnetic resonance in non ST-segment elevation myocardial infarction: comparison between first-pass and late gadolinium-enhanced images. *Invest Radiol.* **45**(11), pp.725-32.

Cochet, A.A. et al. 2009. Major prognostic impact of persistent microvascular obstruction as assessed by contrast-enhanced cardiac magnetic resonance in reperfused acute myocardial infarction. *Eur Radiol.* **19**(9), pp.2117-26.

Cohn, J.N. et al. 2000. Cardiac remodeling--concepts and clinical implications: a consensus paper from an international forum on cardiac remodeling. Behalf of an International Forum on Cardiac Remodeling. *J Am Coll Cardiol.* **35**(3), pp.569-82.

Conversano, A. et al. 1996. Delineation of myocardial stunning and hibernation by positron emission tomography in advanced coronary artery disease. *Am Heart J.* **131**(3), pp.440-50.

Croisille, P. et al. 2012. Controversies in cardiovascular MR imaging: T2-weighted imaging should not be used to delineate the area at risk in ischemic myocardial injury. *Radiology.* **265**(1), pp.12-22.

Crossman, D.C. 2004. The pathophysiology of myocardial ischaemia. *Heart.* **90**(5), pp.576-80.

Dall'Armellina, E. et al. 2011. Dynamic changes of edema and late gadolinium enhancement after acute myocardial infarction and their relationship to functional recovery and salvage index. *Circ Cardiovasc Imaging.* **4**(3), pp.228-36.

Dall'Armellina, E. et al. 2012. Cardiovascular magnetic resonance by non contrast T1-mapping allows assessment of severity of injury in acute myocardial infarction. *J Cardiovasc Magn Reson.* **14**, p15.

de Bakker, J.M. et al. 1990. Ventricular tachycardia in the infarcted, Langendorff-perfused human heart: role of the arrangement of surviving cardiac fibers. *J Am Coll Cardiol.* **15**(7), pp.1594-607.

de Simone, G. et al. 1997. Relation of left ventricular longitudinal and circumferential shortening to ejection fraction in the presence or in the absence of mild hypertension. *J Hypertension.* **15**(9), pp.1011-7.

de Waha, S. et al. 2010. Impact of early vs. late microvascular obstruction assessed by magnetic resonance imaging on long-term outcome after ST-elevation myocardial infarction: a comparison with traditional prognostic markers. *Eur Heart J.* **31**(21), pp.2660-8.

de Waha, S. et al. 2012. Relationship and prognostic value of microvascular obstruction and infarct size in ST-elevation myocardial infarction as visualized by magnetic resonance imaging. *Clin Res Cardiol.* **101**(6), pp.487-95.

DeLong, E.R. et al. 1988. Comparing the areas under two or more correlated receiver operating characteristic curves: a nonparametric approach. *Biometrics.* **44**(3), pp.837-45.

Dendale, P. et al. 1998. Contrast enhanced and functional magnetic resonance imaging for the detection of viable myocardium after infarction. *American Heart Journal.* **135**(5), pp.875-880.

DO, H.I. et al. 2012. Cardiovascular magnetic resonance of myocardial edema using a short inversion time inversion recovery (STIR) black-blood technique: Diagnostic accuracy of visual and semi-quantitative assessment. *J Cardiovasc Magn Reson.* **14**, p22.

Dongaonkar, R.M. et al. 2010. Myocardial microvascular permeability, interstitial oedema, and compromised cardiac function. *Cardiovasc Res.* **87**(2), pp.331-9.

Eaton, L.W. et al. 1979. Regional cardiac dilatation after acute myocardial infarction: recognition by two-dimensional echocardiography. *N Engl J Med.* **300**(2), pp.57-62.

Egred, M. et al. 2003. Detection of scarred and viable myocardium using a new magnetic resonance imaging technique: blood oxygen level dependent (BOLD) MRI. *Heart.* **89**(7), pp.738-44.

Eitel, I. et al. 2010. Prognostic significance and determinants of myocardial salvage assessed by cardiovascular magnetic resonance in acute reperfused myocardial infarction. *J Am Coll Cardiol.* **55**(22), pp.2470-9.

Eitel, I. et al. 2011. Prognostic Value and Determinants of a Hypointense Infarct Core in T2-Weighted Cardiac Magnetic Resonance in Acute Reperfused ST-Elevation-Myocardial Infarction. *Circ Cardiovasc Imaging.* **4**(4), pp.354-62.

Eitel, I. and Friedrich, M.G. 2011. T2-weighted cardiovascular magnetic resonance in acute cardiac disease. *J Cardiovasc Magn Reson.* **13**, p13.

El Aidi, H. et al. 2014. Cardiac Magnetic Resonance Imaging findings and the risk of cardiovascular events in patients with recent myocardial infarction or suspected or known coronary artery disease - a systematic review of prognostic studies. *J Am Coll Cardiol.*

Ellis, S.G. et al. 1983. Time course of functional and biochemical recovery of myocardium salvaged by reperfusion. *J Am Coll Cardiol.* **1**(4), pp.1047-55.

Engblom, H. et al. 2009. Rapid initial reduction of hyperenhanced myocardium after reperfused first myocardial infarction suggests recovery of the peri-infarction zone: one-year follow-up by MRI. *Circ Cardiovasc Imaging.* **2**(1), pp.47-55.

Erbel, R. and Heusch, G. 2000. Coronary microembolization. *J Am Coll Cardiol.* **36**(1), pp.22-4.

Ersboll, M. et al. 2013a. Early diastolic strain rate in relation to systolic and diastolic function and prognosis in acute myocardial infarction: a two-dimensional speckle-tracking study. *Eur Heart J.*

Ersboll, M. et al. 2013b. Prediction of all-cause mortality and heart failure admissions from global left ventricular longitudinal strain in patients with acute myocardial infarction and preserved left ventricular ejection fraction. *J Am Coll Cardiol.* **61**(23), pp.2365-73.

Factor, S.M. et al. 1978. The histologic border zone of acute myocardial infarction--islands or peninsulas? *Am J Pathol.* **92**(1), pp.111-24.

Factor, S.M. et al. 1981. The histological lateral border of acute canine myocardial infarction. A function of microcirculation. *Circ Res.* **48**(5), pp.640-49.

Fang, Z.Y. et al. 2004. Relationship between longitudinal and radial contractility in subclinical diabetic heart disease. *Clinical Science.* **106**(1), pp.53-60.

Ferreira, V.M. et al. 2012. Non-contrast T1-mapping detects acute myocardial edema with high diagnostic accuracy: a comparison to T2-weighted cardiovascular magnetic resonance. *J Cardiovasc Magn Reson.* **14**, p42.

Fishbein, M.C. et al. 1978. The histopathologic evolution of myocardial infarction. *Chest.* **73**(6), pp.843-9.

Fishbein, M.C. et al. 1980. The relationship of vascular injury and myocardial hemorrhage to necrosis after reperfusion. *Circulation.* **62**(6), pp.1274-9.

Flett, A.S. et al. 2010. Equilibrium contrast cardiovascular magnetic resonance for the measurement of diffuse myocardial fibrosis: preliminary validation in humans. *Circulation.* **122**(2), pp.138-44.

Friedrich, M.G. et al. 2008. The Salvaged Area at Risk in Reperfused Acute Myocardial Infarction as Visualized by Cardiovascular Magnetic Resonance. *J Am Coll Cardiol.* **51**(16), pp.1581-1587.

Friedrich, M.G. et al. 2011. T2-Weighted Imaging to Assess Post-Infarct Myocardium at Risk. *J Am Coll Cardiol Img.* **4**(9), pp.1014-1021.

Gaasch, W.H. and Bernard, S.A. 1977. The effect of acute changes in coronary blood flow on left ventricular end-diastolic wall thickness. An echocardiographic study. *Circulation.* **56**(4 Pt 1), pp.593-8.

Galiuto, L. et al. 1998. Evaluation of dynamic changes in microvascular flow during ischemia-reperfusion by myocardial contrast echocardiography. *J Am Coll Cardiol.* **32**(4), pp.1096-101.

Galiuto, L. et al. 2003. Temporal evolution and functional outcome of no reflow: sustained and spontaneously reversible patterns following successful coronary recanalisation. *Heart.* **89**(7), pp.731-7.

Ganame, J. et al. 2009. Impact of myocardial haemorrhage on left ventricular function and remodelling in patients with reperfused acute myocardial infarction. *Eur Heart J.* **30**(12), pp.1440-9.

Garcia-Dorado, D. et al. 1990. Determinants of hemorrhagic infarcts. Histologic observations from experiments involving coronary occlusion, coronary reperfusion, and reocclusion. *Am J Pathol.* **137**(2), pp.301-11.

Garcia-Dorado, D. et al. 1992. Favorable effects of hyperosmotic reperfusion on myocardial edema and infarct size. *Am J Physiol.* **262**(1 Pt 2), pp.H17-22.

Garcia-Dorado, D. and Oliveras, J. 1993. Myocardial oedema: a preventable cause of reperfusion injury? *Cardiovasc Res.* **27**(9), pp.1555-63.

Gerber, B.L. et al. 2000. Microvascular obstruction and left ventricular remodeling early after acute myocardial infarction. *Circulation.* **101**(23), pp.2734-41.

Gerber, B.L. et al. 2001. Relation between Gd-DTPA contrast enhancement and regional inotropic response in the periphery and center of myocardial infarction. *Circulation.* **104**(9), pp.998-1004.

Gerber, B.L. et al. 2002. Accuracy of contrast-enhanced magnetic resonance imaging in predicting improvement of regional myocardial function in patients after acute myocardial infarction. *Circulation.* **106**(9), pp.1083-9.

Ghugre, N. et al. 2012. Intramyocardial hemorrhage contributes to microvascular obstruction in acute myocardial infarction. *Journal of Cardiovascular Magnetic Resonance.* **14**(Suppl 1), pP19.

Ghugre, N.R. et al. 2011. Quantitative tracking of edema, hemorrhage, and microvascular obstruction in subacute myocardial infarction in a porcine model by MRI. *Magn Reson Med.* **66**(4), pp.1129-41.

Goldfarb, J.W. et al. 2013. Magnetic resonance susceptibility weighted phase imaging for the assessment of reperfusion intramyocardial hemorrhage. *Magn Reson Med.*

Gorcsan, J., 3rd and Tanaka, H. 2011. Echocardiographic assessment of myocardial strain. *J Am Coll Cardiol.* **58**(14), pp.1401-13.

Gotte, M.J. et al. 2001. Quantification of regional contractile function after infarction: strain analysis superior to wall thickening analysis in discriminating infarct from remote myocardium. *J Am Coll Cardiol.* **37**(3), pp.808-17.

Greenwood, J.P. et al. 2007. Safety and diagnostic accuracy of stress cardiac magnetic resonance imaging vs exercise tolerance testing early after acute ST elevation myocardial infarction. *Heart.* **93**(11), pp.1363-8.

Grines, C.L. et al. 1989. Prognostic implications and predictors of enhanced regional wall motion of the noninfarct zone after thrombolysis and angioplasty therapy of acute myocardial infarction. The TAMI Study Groups. *Circulation.* **80**(2), pp.245-53.

Grothoff, M. et al. 2012. Right ventricular injury in ST-elevation myocardial infarction: risk stratification by visualization of wall motion, edema, and delayed-enhancement cardiac magnetic resonance. *Circ Cardiovasc Imaging.* **5**(1), pp.60-8.

Gunning, M.G. et al. 2002. The histology of viable and hibernating myocardium in relation to imaging characteristics. *J Am Coll Cardiol.* **39**(3), pp.428-35.

Guo, H. et al. 2009. Myocardial T2 quantitation in patients with iron overload at 3 Tesla. *J Magn Reson Imaging.* **30**(2), pp.394-400.

Haacke, E.M. et al. 2004. Susceptibility weighted imaging (SWI). *Magn Reson Med.* **52**(3), pp.612-8.

Haacke, E.M. et al. 2007. Establishing a baseline phase behavior in magnetic resonance imaging to determine normal vs. abnormal iron content in the brain. *J Magn Reson Imaging.* **26**(2), pp.256-64.

Haacke, E.M. et al. 2009. Susceptibility-weighted imaging: technical aspects and clinical applications, part 1. *AJNR Am J Neuroradiol.* **30**(1), pp.19-30.

Hanley, J.A. and McNeil, B.J. 1983. A method of comparing the areas under receiver operating characteristic curves derived from the same cases. *Radiology.* **148**(3), pp.839-43.

Haugaa, K.H. et al. 2013. Strain echocardiography improves risk prediction of ventricular arrhythmias after myocardial infarction. *JACC Cardiovasc Imaging.* **6**(8), pp.841-50.

Hermier, M. and Nighoghossian, N. 2004. Contribution of susceptibility-weighted imaging to acute stroke assessment. *Stroke.* **35**(8), pp.1989-94.

Heusch, G. et al. 2009. Coronary microembolization: from bedside to bench and back to bedside. *Circulation.* **120**(18), pp.1822-36.

Heyndrickx, G.R. et al. 1975. Regional myocardial functional and electrophysiological alterations after brief coronary artery occlusion in conscious dogs. *J Clin Invest.* **56**(4), pp.978-85.

Higginson, L.A. et al. 1982. Determinants of myocardial hemorrhage after coronary reperfusion in the anesthetized dog. *Circulation.* **65**(1), pp.62-9.

Hohnloser, S.H. et al. 2004. Prophylactic use of an implantable cardioverter-defibrillator after acute myocardial infarction. *N Engl J Med.* **351**(24), pp.2481-8.

Holmes, J.W. et al. 2005. Structure and mechanics of healing myocardial infarcts. *Annu Rev Biomed Eng.* **7**, pp.223-53.

Homans, D.C. et al. 1986. Mechanisms of remote myocardial dysfunction during coronary artery occlusion in the presence of multivessel disease. *Circulation.* **74**(3), pp.588-96.

Hombach, V. et al. 2005. Sequelae of acute myocardial infarction regarding cardiac structure and function and their prognostic significance as assessed by magnetic resonance imaging. *Eur Heart J.* **26**(6), pp.549-57.

Hudsmith, L.E. and Neubauer, S. 2009. Magnetic resonance spectroscopy in myocardial disease. *JACC Cardiovasc Imaging.* **2**(1), pp.87-96.

Husser, O. et al. 2010. Head to head comparison of quantitative versus visual analysis of contrast CMR in the setting of myocardial stunning after

STEMI: implications on late systolic function and patient outcome. *Int J Cardiovasc Imaging.* **26**(5), pp.559-69.

Husser, O. et al. 2013. Cardiovascular magnetic resonance-derived intramyocardial hemorrhage after STEMI: Influence on long-term prognosis, adverse left ventricular remodeling and relationship with microvascular obstruction. *Int J Cardiol.* **167**(5), pp.2047-54.

Ibrahim el, S.H. 2011. Myocardial tagging by cardiovascular magnetic resonance: evolution of techniques--pulse sequences, analysis algorithms, and applications. *J Cardiovasc Magn Reson.* **13**, p36.

Ibrahim, T. et al. 2010. Acute myocardial infarction: serial cardiac MR imaging shows a decrease in delayed enhancement of the myocardium during the 1st week after reperfusion. *Radiology.* **254**(1), pp.88-97.

Ide, S. et al. 2012. Delineation of optic radiation and stria of Gennari on high-resolution phase difference enhanced imaging. *Acad Radiol.* **19**(10), pp.1283-9.

Iliceto, S. et al. 1996. Myocardial contrast echocardiography in acute myocardial infarction. Pathophysiological background and clinical applications. *Eur Heart J.* **17**(3), pp.344-53.

Ingkanisorn, W.P. et al. 2004. Gadolinium delayed enhancement cardiovascular magnetic resonance correlates with clinical measures of myocardial infarction. *J Am Coll Cardiol.* **43**(12), pp.2253-9.

Ingul, C.B. et al. 2005. Recovery of stunned myocardium in acute myocardial infarction quantified by strain rate imaging: a clinical study. *J Am Soc Echocardiogr.* **18**(5), pp.401-10.

Inoue, Y. et al. 2010. Peri-infarct dysfunction in post-myocardial infarction: assessment of 3-T tagged and late enhancement MRI. *Eur Radiol.* **20**(5), pp.1139-48.

Ito, H. et al. 1996. Clinical implications of the 'no reflow' phenomenon. A predictor of complications and left ventricular remodeling in reperfused anterior wall myocardial infarction. *Circulation.* **93**(2), pp.223-8.

Iwakura, K. et al. 1996. Alternation in the coronary blood flow velocity pattern in patients with no reflow and reperfused acute myocardial infarction. *Circulation.* **94**(6), pp.1269-75.

Iwakura, K. et al. 2003. Association between hyperglycemia and the no-reflow phenomenon in patients with acute myocardial infarction. *J Am Coll Cardiol.* **41**(1), pp.1-7.

Iwakura, K. et al. 2006. Chronic pre-treatment of statins is associated with the reduction of the no-reflow phenomenon in the patients with reperfused acute myocardial infarction. *Eur Heart J.* **27**(5), pp.534-9.

Izquierdo, M. et al. 2013. Value of early cardiovascular magnetic resonance for the prediction of adverse arrhythmic cardiac events after a first noncomplicated ST-segment-elevation myocardial infarction. *Circ Cardiovasc Imaging.* **6**(5), pp.755-61.

Jaarsma, W. et al. 1986. Prognostic implications of regional hyperkinesia and remote asynergy of noninfarcted myocardium. *Am J Cardiol.* **58**(6), pp.394-8.

Jackowski, C. et al. 2006. Postmortem unenhanced magnetic resonance imaging of myocardial infarction in correlation to histological infarction age characterization. *Eur Heart J.* **27**(20), pp.2459-67.

Jaffe, R. et al. 2008. Microvascular obstruction and the no-reflow phenomenon after percutaneous coronary intervention. *Circulation.* **117**(24), pp.3152-6.

Jennings, R.B. et al. 1960. Myocardial necrosis induced by temporary occlusion of a coronary artery in the dog. *Arch Pathol.* **70**, pp.68-78.

Jennings, R.B. et al. 1985. Effect of reperfusion late in the phase of reversible ischemic injury. Changes in cell volume, electrolytes, metabolites, and ultrastructure. *Circ Res.* **56**(2), pp.262-78.

Jerosch-Herold, M. et al. 2008. Cardiac magnetic resonance imaging of myocardial contrast uptake and blood flow in patients affected with idiopathic or familial dilated cardiomyopathy. *Am J Physiol Heart Circ Physiol.* **295**(3), pp.H1234-H1242.

Jerosch-Herold, M. 2010. Quantification of myocardial perfusion by cardiovascular magnetic resonance. *J Cardiovasc Magn Reson.* **12**, p57.

Jin, N. et al. 2014. Free-breathing myocardial T2* mapping using single-shot GRE-EPI and automatic non-rigid motion correction. *Proc. Intl. Soc. Mag. Reson. Med. [Abstract].* **22**.

Johnston, D.L. et al. 1988. Serial changes in nuclear magnetic resonance relaxation times after myocardial infarction in the rabbit: relationship to water content, severity of ischemia, and histopathology over a six-month period. *Magn Reson Med.* **8**(4), pp.363-79.

Kakeda, S. et al. 2011. A novel tract imaging technique of the brainstem using phase difference enhanced imaging: normal anatomy and initial experience in multiple system atrophy. *Eur Radiol.* **21**(10), pp.2202-10.

Kali, A. et al. 2013a. Chronic manifestation of postreperfusion intramyocardial hemorrhage as regional iron deposition: a cardiovascular magnetic resonance study with ex vivo validation. *Circ Cardiovasc Imaging.* **6**(2), pp.218-28.

Kali, A. et al. 2013b. Detection of acute reperfusion myocardial hemorrhage with cardiac MR imaging: T2 versus T2. *Radiology.* **269**(2), pp.387-95.

Karolle, B.L. et al. 1991. Transmural distribution of myocardial edema by NMR relaxometry following myocardial ischemia and reperfusion. *Am Heart J.* **122**(3 Pt 1), pp.655-64.

Kaufman, L. et al. 1989. Measuring signal-to-noise ratios in MR imaging. *Radiology.* **173**(1), pp.265-7.

Kaufmann, P.A. and Camici, P.G. 2005. Myocardial blood flow measurement by PET: technical aspects and clinical applications. *J Nucl Med.* **46**(1), pp.75-88.

Kawano, H. et al. 2005. Histopathological findings of the no-reflow phenomenon following coronary intervention for acute coronary syndrome. *Int Heart J.* **46**(2), pp.327-32.

Kellman, P. et al. 2007. T2-prepared SSFP improves diagnostic confidence in edema imaging in acute myocardial infarction compared to turbo spin echo. *Magn Reson Med.* **57**(5), pp.891-7.

Kellman, P. et al. 2012. Extracellular volume fraction mapping in the myocardium, part 2: initial clinical experience. *J Cardiovasc Magn Reson.* **14**, p64.

Kidambi, A. et al. 2013a. The effect of microvascular obstruction and intramyocardial hemorrhage on contractile recovery in reperfused

myocardial infarction: insights from cardiovascular magnetic resonance. *J Cardiovasc Magn Reson.* **15**(1), p58.

Kidambi, A. et al. 2013b. Relationship between myocardial edema and regional myocardial function after reperfused acute myocardial infarction: an MR imaging study. *Radiology.* **267**(3), pp.701-8.

Kim, K.B. et al. 1994. Changes in the antioxidative defensive system during open heart operations in humans. *Ann Thorac Surg.* **58**(1), pp.170-5.

Kim, R.J. et al. 1999. Relationship of MRI delayed contrast enhancement to irreversible injury, infarct age, and contractile function. *Circulation.* **100**(19), pp.1992-2002.

Kim, R.J. et al. 2000. The use of contrast-enhanced magnetic resonance imaging to identify reversible myocardial dysfunction. *N Engl J Med.* **343**(20), pp.1445-53.

Kloner, R.A. et al. 1974. The "no-reflow" phenomenon after temporary coronary occlusion in the dog. *J Clin Invest.* **54**(6), pp.1496-508.

Kloner, R.A. et al. 1980. Ultrastructural evidence of microvascular damage and myocardial cell injury after coronary artery occlusion: which comes first? *Circulation.* **62**(5), pp.945-52.

Kloner, R.A. et al. 1983. Studies of experimental coronary artery reperfusion. Effects on infarct size, myocardial function, biochemistry, ultrastructure and microvascular damage. *Circulation.* **68**(2 Pt 2), pp.I8-15.

Kloner, R.A. and Alker, K.J. 1984. The effect of streptokinase on intramyocardial hemorrhage, infarct size, and the no-reflow phenomenon during coronary reperfusion. *Circulation.* **70**(3), pp.513-21.

Kloner, R.A. et al. 1989. Does tissue-type plasminogen activator have direct beneficial effects on the myocardium independent of its ability to lyse intracoronary thrombi? *Circulation.* **79**(5), pp.1125-36.

Klug, G. et al. 2012. Prognostic value at 5 years of microvascular obstruction after acute myocardial infarction assessed by cardiovascular magnetic resonance. *J Cardiovasc Magn Reson.* **14**, p46.

Kraitchman, D.L. et al. 2000. Noninvasive assessment of myocardial stunning from short-term coronary occlusion using tagged magnetic resonance imaging. *J Cardiovasc Magn Reson.* **2**(2), pp.123-36.

Kramer, C.M. et al. 1993. Regional differences in function within noninfarcted myocardium during left ventricular remodeling. *Circulation.* **88**(3), pp.1279-88.

Kramer, C.M. et al. 1996. Remote noninfarcted region dysfunction soon after first anterior myocardial infarction. A magnetic resonance tagging study. *Circulation.* **94**(4), pp.660-6.

Kramer, C.M. et al. 2013. Standardized cardiovascular magnetic resonance (CMR) protocols 2013 update. *J Cardiovasc Magn Reson.* **15**, p91.

Kramer, J.B. et al. 1985. Intramural reentry as a mechanism of ventricular tachycardia during evolving canine myocardial infarction. *Circ Res.* **56**(5), pp.736-54.

Krug, A. et al. 1966. Blood supply of the myocardium after temporary coronary occlusion. *Circ Res.* **19**(1), pp.57-62.

Kukulski, T. et al. 2003. Identification of acutely ischemic myocardium using ultrasonic strain measurements. A clinical study in patients undergoing coronary angioplasty. *J Am Coll Cardiol.* **41**(5), pp.810-9.

Kumar, A. et al. 2011. Detection and quantification of myocardial reperfusion hemorrhage using T2*-weighted CMR. *JACC Cardiovasc Imaging.* **4**(12), pp.1274-83.

Kuntz, I.D., Jr. et al. 1969. Hydration of macromolecules. *Science.* **163**(3873), pp.1329-31.

Larose, E. et al. 2010. Predicting late myocardial recovery and outcomes in the early hours of ST-segment elevation myocardial infarction traditional measures compared with microvascular obstruction, salvaged myocardium, and necrosis characteristics by cardiovascular magnetic resonance. *J Am Coll Cardiol.* **55**(22), pp.2459-69.

Lavallee, M. et al. 1983. Salvage of myocardial function by coronary artery reperfusion 1, 2, and 3 hours after occlusion in conscious dogs. *Circ Res.* **53**(2), pp.235-47.

Lee, W.W. et al. 2012. PET/MRI of inflammation in myocardial infarction. *J Am Coll Cardiol.* **59**(2), pp.153-63.

Leshnower, B.G. et al. 2007. Progression of myocardial injury during coronary occlusion in the collateral-deficient heart: a non-wavefront phenomenon. *Am J Physiol Heart Circ Physiol.* **293**(3), pp.H1799-804.

Lonborg, J.T. et al. 2013. Left atrial volume and function in patients following ST elevation myocardial infarction and the association with clinical outcome: a cardiovascular magnetic resonance study. *Eur Heart J Cardiovasc Imaging.* **14**(2), pp.118-27.

Lotan, C.S. et al. 1992. Assessment of postreperfusion myocardial hemorrhage using proton NMR imaging at 1.5 T. *Circulation.* **86**(3), pp.1018-25.

Mahnken, A.H. et al. 2009. Assessment of myocardial edema by computed tomography in myocardial infarction. *JACC Cardiovasc Imaging.* **2**(10), pp.1167-74.

Manning, A.S. and Hearse, D.J. 1984. Reperfusion-induced arrhythmias: mechanisms and prevention. *J Mol Cell Cardiol.* **16**(6), pp.497-518.

Marcus, J.T. et al. 1997. Myocardial function in infarcted and remote regions early after infarction in man: assessment by magnetic resonance tagging and strain analysis. *Magn Reson Med.* **38**(5), pp.803-10.

Marinho, N.V. et al. 1996. Pathophysiology of chronic left ventricular dysfunction. New insights from the measurement of absolute myocardial blood flow and glucose utilization. *Circulation.* **93**(4), pp.737-44.

Mather, A.N. et al. 2009. Appearance of microvascular obstruction on high resolution first-pass perfusion, early and late gadolinium enhancement CMR in patients with acute myocardial infarction. *J Cardiovasc Magn Reson.* **11**, p33.

Mather, A.N. et al. 2011. Reperfusion haemorrhage as determined by cardiovascular MRI is a predictor of adverse left ventricular remodelling and markers of late arrhythmic risk. *Heart.* **97**(6), pp.453-9.

Matsumura, K. et al. 1998. Progression of myocardial necrosis during reperfusion of ischemic myocardium. *Circulation.* **97**(8), pp.795-804.

Maxwell, M.P. et al. 1987. Species variation in the coronary collateral circulation during regional myocardial ischaemia: a critical determinant of the rate of evolution and extent of myocardial infarction. *Cardiovasc Res.* **21**(10), pp.737-46.

Messroghli, D.R. et al. 2004. Modified Look-Locker inversion recovery (MOLLI) for high-resolution T1 mapping of the heart. *Magn Reson Med.* **52**(1), pp.141-6.

Messroghli, D.R. et al. 2005. Assessment of regional left ventricular function: accuracy and reproducibility of positioning standard short-axis sections in cardiac MR imaging. *Radiology.* **235**(1), pp.229-36.

Messroghli, D.R. et al. 2007a. Myocardial T1 mapping: application to patients with acute and chronic myocardial infarction. *Magn Reson Med.* **58**(1), pp.34-40.

Messroghli, D.R. et al. 2007b. Optimization and validation of a fully-integrated pulse sequence for modified look-locker inversion-recovery (MOLLI) T1 mapping of the heart. *J Magn Reson Imaging.* **26**(4), pp.1081-6.

Mikami, Y. et al. 2009. Relation between signal intensity on T2-weighted MR images and presence of microvascular obstruction in patients with acute myocardial infarction. *AJR Am J Roentgenol.* **193**(4), pp.W321-6.

Miller, C.A. et al. 2013. Comprehensive validation of cardiovascular magnetic resonance techniques for the assessment of myocardial extracellular volume. *Circ Cardiovasc Imaging.* **6**(3), pp.373-83.

Miszalski-Jamka, T. et al. 2010. Extent of RV dysfunction and myocardial infarction assessed by CMR are independent outcome predictors early after STEMI treated with primary angioplasty. *JACC Cardiovasc Imaging.* **3**(12), pp.1237-46.

Mittal, S. et al. 2009. Susceptibility-weighted imaging: technical aspects and clinical applications, part 2. *AJNR Am J Neuroradiol.* **30**(2), pp.232-52.

Moens, A.L. et al. 2005. Myocardial ischemia/reperfusion-injury, a clinical view on a complex pathophysiological process. *International Journal of Cardiology.* **100**(2), pp.179-190.

Monmeneu, J.V. et al. 2009. Cardiac magnetic resonance evaluation of edema after ST-elevation acute myocardial infarction. *Rev Esp Cardiol.* **62**(8), pp.858-66.

Moon, J.C. et al. 2013. Myocardial T1 mapping and extracellular volume quantification: a Society for Cardiovascular Magnetic Resonance (SCMR)

and CMR Working Group of the European Society of Cardiology consensus statement. *J Cardiovasc Magn Reson.* **15**, p92.

Morishima, I. et al. 2000. Angiographic no-reflow phenomenon as a predictor of adverse long-term outcome in patients treated with percutaneous transluminal coronary angioplasty for first acute myocardial infarction. *J Am Coll Cardiol.* **36**(4), pp.1202-9.

Myocardial infarction redefined--a consensus document of The Joint European Society of Cardiology/American College of Cardiology Committee for the redefinition of myocardial infarction. 2000. *Eur Heart J.* **21**(18), pp.1502-13.

Ndrepepa, G. et al. 2010. 5-year prognostic value of no-reflow phenomenon after percutaneous coronary intervention in patients with acute myocardial infarction. *J Am Coll Cardiol.* **55**(21), pp.2383-9.

Nieminen, M. et al. 1982. Serial evaluation of myocardial thickening and thinning in acute experimental infarction: identification and quantification using two-dimensional echocardiography. *Circulation.* **66**(1), pp.174-80.

Nijveldt, R. et al. 2008. Functional recovery after acute myocardial infarction: comparison between angiography, electrocardiography, and cardiovascular magnetic resonance measures of microvascular injury. *J Am Coll Cardiol.* **52**(3), pp.181-9.

Noll, D.C. et al. 1991. Homodyne detection in magnetic resonance imaging. *IEEE Trans Med Imaging.* **10**(2), pp.154-63.

O'Regan, D.P. et al. 2009. Cardiac MRI of myocardial salvage at the peri-infarct border zones after primary coronary intervention. *Am J Physiol Heart Circ Physiol.* **297**(1), pp.H340-6.

O'Regan, D.P. et al. 2010. Assessment of severe reperfusion injury with T2* cardiac MRI in patients with acute myocardial infarction. *Heart.* **96**(23), pp.1885-1891.

Oshinski, J.N. et al. 2001. Imaging time after Gd-DTPA injection is critical in using delayed enhancement to determine infarct size accurately with magnetic resonance imaging. *Circulation.* **104**(23), pp.2838-42.

Osman, N.F. et al. 1999. Cardiac motion tracking using CINE harmonic phase (HARP) magnetic resonance imaging. *Magn Reson Med.* **42**(6), pp.1048-60.

Ozaki, Y. et al. 2011. Thin-cap fibroatheroma as high-risk plaque for microvascular obstruction in patients with acute coronary syndrome. *Circ Cardiovasc Imaging.* **4**(6), pp.620-7.

Payne, A.R. et al. 2011. Bright Blood T2 Weighted MRI Has Higher Diagnostic Accuracy Than Dark Blood STIR MRI for Detection of Acute Myocardial Infarction and for Assessment of the Ischemic Area-at-Risk and Myocardial Salvage. *Circ Cardiovasc Imaging.*

Pedersen, S.F. et al. 2012. Assessment of intramyocardial hemorrhage by T1-weighted cardiovascular magnetic resonance in reperfused acute myocardial infarction. *J Cardiovasc Magn Reson.* **14**, p59.

Pennell, D. 2006. Myocardial salvage: retrospection, resolution, and radio waves. *Circulation.* **113**(15), pp.1821-3.

Pereira, R.S. et al. 1996. The determination of myocardial viability using Gd-DTPA in a canine model of acute myocardial ischemia and reperfusion. *Magn Reson Med.* **36**(5), pp.684-93.

Peshock, R.M. et al. 1989. Assessment of myocardial systolic wall thickening using nuclear magnetic resonance imaging. *J Am Coll Cardiol.* **14**(3), pp.653-9.

Pfeffer, M.A. and Braunwald, E. 1990. Ventricular remodeling after myocardial infarction. Experimental observations and clinical implications. *Circulation.* **81**(4), pp.1161-72.

Pislaru, S.V. et al. 1997. Infarct size, myocardial hemorrhage, and recovery of function after mechanical versus pharmacological reperfusion: effects of lytic state and occlusion time. *Circulation.* **96**(2), pp.659-66.

Pogatsa, G. et al. 1976. The role of myocardial edema in the left ventricular diastolic stiffness. *Basic Res Cardiol.* **71**(3), pp.263-9.

Preuss, K.C. et al. 1987. Time course of recovery of "stunned" myocardium following variable periods of ischemia in conscious and anesthetized dogs. *Am Heart J.* **114**(4 Pt 1), pp.696-703.

Pruessmann, K.P. et al. 1999. SENSE: sensitivity encoding for fast MRI. *Magn Reson Med.* **42**(5), pp.952-62.

Prunier, F. et al. 2008. Three-dimensional MRI assessment of regional wall stress after acute myocardial infarction predicts postdischarge cardiac events. *J Magn Reson Imaging.* **27**(3), pp.516-21.

Rahimtoola, S.H. 1989. The hibernating myocardium. *Am Heart J.* **117**(1), pp.211-21.

Raman, S.V. et al. 2010. Cardiac magnetic resonance with edema imaging identifies myocardium at risk and predicts worse outcome in patients with non-ST-segment elevation acute coronary syndrome. *J Am Coll Cardiol.* **55**(22), pp.2480-8.

Reffelmann, T. and Kloner, R.A. 2002. Microvascular reperfusion injury: rapid expansion of anatomic no reflow during reperfusion in the rabbit. *Am J Physiol Heart Circ Physiol.* **283**(3), pp.H1099-107.

Reimer, K.A. et al. 1977. The wavefront phenomenon of ischemic cell death. 1. Myocardial infarct size vs duration of coronary occlusion in dogs. *Circulation.* **56**(5), pp.786-94.

Reimer, K.A. and Jennings, R.B. 1979a. The changing anatomic reference base of evolving myocardial infarction. Underestimation of myocardial collateral blood flow and overestimation of experimental anatomic infarct size due to tissue edema, hemorrhage and acute inflammation. *Circulation.* **60**(4), pp.866-76.

Reimer, K.A. and Jennings, R.B. 1979b. The "wavefront phenomenon" of myocardial ischemic cell death. II. Transmural progression of necrosis within the framework of ischemic bed size (myocardium at risk) and collateral flow. *Lab Invest.* **40**(6), pp.633-44.

Reimer, K.A. et al. 1981. Total ischemia in dog hearts, in vitro 2. High energy phosphate depletion and associated defects in energy metabolism, cell volume regulation, and sarcolemmal integrity. *Circ Res.* **49**(4), pp.901-11.

Rezkalla, S.H. et al. 2010. No-reflow phenomenon following percutaneous coronary intervention for acute myocardial infarction: incidence,

outcome, and effect of pharmacologic therapy. *J Interv Cardiol.* **23**(5), pp.429-36.

Robbers, L.F. et al. 2013. Myocardial infarct heterogeneity assessment by late gadolinium enhancement cardiovascular magnetic resonance imaging shows predictive value for ventricular arrhythmia development after acute myocardial infarction. *Eur Heart J Cardiovasc Imaging.* **14**(12), pp.1150-8.

Roberts, C.S. et al. 1983. Effect of coronary reperfusion on myocardial hemorrhage and infarct healing. *Am J Cardiol.* **52**(5), pp.610-4.

Rochitte, C.E. et al. 1998. Magnitude and Time Course of Microvascular Obstruction and Tissue Injury After Acute Myocardial Infarction. *Circulation.* **98**(10), pp.1006-1014.

Rogers, W.J. et al. 1999. Early contrast-enhanced MRI predicts late functional recovery after reperfused myocardial infarction. *Circulation.* **99**(6), pp.744-50.

Romero, J. et al. 2013. CMR imaging for the evaluation of myocardial stunning after acute myocardial infarction: a meta-analysis of prospective trials. *Eur Heart J Cardiovasc Imaging.* **14**(11), pp.1080-91.

Ruzsics, B. et al. 2009. Myocardial strain in sub-acute peri-infarct myocardium. *Int J Cardiovasc Imaging.* **25**(2), pp.151-9.

Sado, D.M. et al. 2011. Novel imaging techniques for diffuse myocardial fibrosis. *Future Cardiol.* **7**(5), pp.643-50.

Salustri, A. et al. 1994. Prediction of improvement of ventricular function after first acute myocardial infarction using low-dose dobutamine stress echocardiography. *Am J Cardiol.* **74**(9), pp.853-6.

Santoro, G.M. et al. 1998. Relation between ST-segment changes and myocardial perfusion evaluated by myocardial contrast echocardiography in patients with acute myocardial infarction treated with direct angioplasty. *Am J Cardiol.* **82**(8), pp.932-7.

Schmidt, A. et al. 2007. Infarct tissue heterogeneity by magnetic resonance imaging identifies enhanced cardiac arrhythmia susceptibility in patients with left ventricular dysfunction. *Circulation.* **115**(15), pp.2006-14.

Schroeder, M.A. et al. 2011. Hyperpolarized magnetic resonance: a novel technique for the in vivo assessment of cardiovascular disease. *Circulation.* **124**(14), pp.1580-94.

Schuijf, J.D. et al. 2004. Quantification of myocardial infarct size and transmurality by contrast-enhanced magnetic resonance imaging in men. *Am J Cardiol.* **94**(3), pp.284-8.

Schulz-Menger, J. et al. 2003. Cardiovascular magnetic resonance of acute myocardial infarction at a very early stage. *J Am Coll Cardiol.* **42**(3), pp.513-8.

Schulz-Menger, J. et al. 2013. Standardized image interpretation and post processing in cardiovascular magnetic resonance: Society for Cardiovascular Magnetic Resonance (SCMR) board of trustees task force on standardized post processing. *J Cardiovasc Magn Reson.* **15**, p35.

Schuster, A. et al. 2013. Cardiovascular magnetic resonance myocardial feature tracking for quantitative viability assessment in ischemic cardiomyopathy. *Int J Cardiol.* **166**(2), pp.413-20.

Semelka, R.C. et al. 1990. Interstudy reproducibility of dimensional and functional measurements between cine magnetic resonance studies in the morphologically abnormal left ventricle. *Am Heart J.* **119**(6), pp.1367-73.

Shapiro, M.D. et al. 2007. Utility of cardiovascular magnetic resonance to predict left ventricular recovery after primary percutaneous coronary intervention for patients presenting with acute ST-segment elevation myocardial infarction. *Am J Cardiol.* **100**(2), pp.211-6.

Sharir, T. et al. 2001. Quantitative analysis of regional motion and thickening by gated myocardial perfusion SPECT: normal heterogeneity and criteria for abnormality. *J Nucl Med.* **42**(11), pp.1630-8.

Sinusas, A.J. et al. 1990. Quantification of area at risk during coronary occlusion and degree of myocardial salvage after reperfusion with technetium-99m methoxyisobutyl isonitrile. *Circulation.* **82**(4), pp.1424-37.

Sorajja, P. et al. 2005. Combined prognostic utility of ST-segment recovery and myocardial blush after primary percutaneous coronary intervention in acute myocardial infarction. *Eur Heart J.* **26**(7), pp.667-74.

Stamm, R.B. et al. 1983. Echocardiographic detection of infarct-localized asynergy and remote asynergy during acute myocardial infarction: correlation with the extent of angiographic coronary disease. *Circulation.* **67**(1), pp.233-44.

Steenbergen, C. et al. 1985. Volume regulation and plasma membrane injury in aerobic, anaerobic, and ischemic myocardium in vitro. Effects of osmotic cell swelling on plasma membrane integrity. *Circ Res.* **57**(6), pp.864-75.

Steinbeck, G. et al. 2009. Defibrillator implantation early after myocardial infarction. *N Engl J Med.* **361**(15), pp.1427-36.

Sutherland, G.R. et al. 2004. Strain and strain rate imaging: a new clinical approach to quantifying regional myocardial function. *J Am Soc Echocardiogr.* **17**(7), pp.788-802.

Sutton, M.G. and Sharpe, N. 2000. Left ventricular remodeling after myocardial infarction: pathophysiology and therapy. *Circulation.* **101**(25), pp.2981-8.

Swoboda, P.P. et al. 2014. Reproducibility of myocardial strain and left ventricular twist measured using complementary spatial modulation of magnetization. *J Magn Reson Imaging.* **39**(4), pp.887-94.

Thavendiranathan, P. et al. 2013. Reproducibility of echocardiographic techniques for sequential assessment of left ventricular ejection fraction and volumes: application to patients undergoing cancer chemotherapy. *J Am Coll Cardiol.* **61**(1), pp.77-84.

Theroux, P. et al. 1976. Coronary arterial reperfusion. III. Early and late effects on regional myocardial function and dimensions in conscious dogs. *Am J Cardiol.* **38**(5), pp.599-606.

Thygesen, K. et al. 2007. Universal definition of myocardial infarction. *Circulation.* **116**(22), pp.2634-53.

Thygesen, K. et al. 2012. Third universal definition of myocardial infarction. *J Am Coll Cardiol.* **60**(16), pp.1581-98.

Tranum-Jensen, J. et al. 1981. Tissue osmolality, cell swelling, and reperfusion in acute regional myocardial ischemia in the isolated porcine heart. *Circ Res.* **49**(2), pp.364-81.

Turschner, O. et al. 2004. The sequential changes in myocardial thickness and thickening which occur during acute transmural infarction, infarct reperfusion and the resultant expression of reperfusion injury. *Eur Heart J.* **25**(9), pp.794-803.

Ugander, M. et al. 2012. Myocardial edema as detected by pre-contrast T1 and T2 CMR delineates area at risk associated with acute myocardial infarction. *JACC Cardiovasc Imaging.* **5**(6), pp.596-603.

Underwood, S.R. et al. 2004. Imaging techniques for the assessment of myocardial hibernation. Report of a Study Group of the European Society of Cardiology. *Eur Heart J.* **25**(10), pp.815-36.

Urheim, S. et al. 2000. Myocardial strain by Doppler echocardiography. Validation of a new method to quantify regional myocardial function. *Circulation.* **102**(10), pp.1158-64.

Verani, M.S. et al. 1988. Quantification of myocardial infarction during coronary occlusion and myocardial salvage after reperfusion using cardiac imaging with technetium-99m hexakis 2-methoxyisobutyl isonitrile. *J Am Coll Cardiol.* **12**(6), pp.1573-81.

Verhaert, D. et al. 2011. Direct T2 quantification of myocardial edema in acute ischemic injury. *JACC Cardiovasc Imaging.* **4**(3), pp.269-78.

Verma, A. et al. 2008. Prognostic implications of left ventricular mass and geometry following myocardial infarction: the VALIANT (VALsartan In Acute myocardial iNfarcTion) Echocardiographic Study. *JACC Cardiovasc Imaging.* **1**(5), pp.582-91.

Weisskoff, R.M. and Kiihne, S. 1992. MRI susceptometry: image-based measurement of absolute susceptibility of MR contrast agents and human blood. *Magn Reson Med.* **24**(2), pp.375-83.

Wendland, M.F. et al. 1999. Contrast-enhanced MRI for quantification of myocardial viability. *J Magn Reson Imaging.* **10**(5), pp.694-702.

White, H.D. et al. 1987. Left ventricular end-systolic volume as the major determinant of survival after recovery from myocardial infarction. *Circulation.* **76**(1), pp.44-51.

White, S.K. et al. 2013. T1 mapping for myocardial extracellular volume measurement by CMR: bolus only versus primed infusion technique. *JACC Cardiovasc Imaging.* **6**(9), pp.955-62.

Williams, F.H. 1896. A Method for More Fully Determining the Outline of the Heart by Means of the Fluoroscope Together with Other Uses of This Instrument in Medicine. *The Boston Medical and Surgical Journal.* **135**(14), pp.335-337.

Wu, E. et al. 2001. Visualisation of presence, location, and transmural extent of healed Q-wave and non-Q-wave myocardial infarction. *Lancet.* **357**(9249), pp.21-8.

Wu, E. et al. 2008. Infarct size by contrast enhanced cardiac magnetic resonance is a stronger predictor of outcomes than left ventricular ejection fraction or end-systolic volume index: prospective cohort study. *Heart.* **94**(6), pp.730-6.

Wu, K.C. et al. 1998a. Prognostic significance of microvascular obstruction by magnetic resonance imaging in patients with acute myocardial infarction. *Circulation.* **97**(8), pp.765-72.

Wu, K.C. et al. 1998b. Quantification and time course of microvascular obstruction by contrast-enhanced echocardiography and magnetic resonance imaging following acute myocardial infarction and reperfusion. *J Am Coll Cardiol.* **32**(6), pp.1756-64.

Yan, A.T. et al. 2006. Characterization of the peri-infarct zone by contrast-enhanced cardiac magnetic resonance imaging is a powerful predictor of post-myocardial infarction mortality. *Circulation.* **114**(1), pp.32-9.

Ye, Y.X. et al. 2013. Monitoring of monocyte recruitment in reperfused myocardial infarction with intramyocardial hemorrhage and microvascular obstruction by combined fluorine 19 and proton cardiac magnetic resonance imaging. *Circulation.* **128**(17), pp.1878-88.

Yeatman, M. et al. 1988. Mannitol and reperfusion-induced arrhythmias: possible mechanisms of action in the isolated rat heart. *Can J Cardiol.* **4**(6), pp.287-94.

Yoshino, H. et al. 1998. Asynergy of the noninfarcted left ventricular inferior wall in anterior wall acute myocardial infarction secondary to isolated

occlusion of the left anterior descending artery. *Am J Cardiol.* **81**(7), pp.828-33.

Zaman, A. et al. 2014. Robust myocardial T and T * mapping at 3T using image-based shimming. *J Magn Reson Imaging.*

Zweier, J.L. 1988. Measurement of superoxide-derived free radicals in the reperfused heart. Evidence for a free radical mechanism of reperfusion injury. *J Biol Chem.* **263**(3), pp.1353-7.

9. Appendix

9.1. Ethics committee approval

24 APR 2012

NHS
Health Research Authority

NRES Committee Yorkshire & The Humber - Leeds West
First Floor
Millside
Mill Pond Lane
Leeds
LS6 4RA

Telephone: 0113 3050122
Facsimile: 0113 8556191

18 April 2012

Dr Sven Plein
Consultant Cardiologist, British Heart Foundation Senior Clinical Research Fellow
University of Leeds
Academic Unit of Cardiovascular Medicine
G floor, Jubilee Wing
Leeds General Infirmary
LS1 3EX

Dear Dr Plein

Study title: **QUANTITATIVE EVALUATION OF MYOCARDIAL CHARACTERISTICS IN REPERFUSED ST-ELEVATION MYOCARDIAL INFARCTION – A 3 TESLA CARDIOVASCULAR MAGNETIC RESONANCE STUDY**

REC reference: **12/YH/0169**

The Research Ethics Committee reviewed the above application at the meeting held on 13 April 2012. The Committee would like to thank Dr Kidambi for attending the meeting.

Ethical opinion

The procedure for dealing with identification of an unexpected condition was queried; Dr Kidambi explained that if the participant is still an inpatient their cardiologist would be informed; if they have been discharged their GP and cardiologist would be notified. Members asked that this is included in the participant information sheet and GP letter.

The members of the Committee present gave a favourable ethical opinion of the above research on the basis described in the application form, protocol and supporting documentation, subject to the conditions specified below.

Ethical review of research sites

NHS Sites

The favourable opinion applies to all NHS sites taking part in the study, subject to management permission being obtained from the NHS/HSC R&D office prior to the start of the study (see "Conditions of the favourable opinion" below).

Conditions of the favourable opinion

The favourable opinion is subject to the following conditions being met prior to the start of the study.

Management permission or approval must be obtained from each host organisation prior to

the start of the study at the site concerned.

Management permission ("R&D approval") should be sought from all NHS organisations involved in the study in accordance with NHS research governance arrangements.

Guidance on applying for NHS permission for research is available in the Integrated Research Application System or at http://www.rdforum.nhs.uk.

Where a NHS organisation's role in the study is limited to identifying and referring potential participants to research sites ("participant identification centre"), guidance should be sought from the R&D office on the information it requires to give permission for this activity.

For non-NHS sites, site management permission should be obtained in accordance with the procedures of the relevant host organisation.

Sponsors are not required to notify the Committee of approvals from host organisations

1 The GP letter should make it clear that if an unexpected condition is identified they will be informed.

2 The participant information sheet should make it clear that the GP and cardiologist will be informed if any unexpected condition is identified.

It is responsibility of the sponsor to ensure that all the conditions are complied with before the start of the study or its initiation at a particular site (as applicable).

You should notify the REC in writing once all conditions have been met (except for site approvals from host organisations) and provide copies of any revised documentation with updated version numbers. Confirmation should also be provided to host organisations together with relevant documentation

Approved documents

The documents reviewed and approved at the meeting were:

	Document	*Version*	*Date*
✓	Evidence of insurance or indemnity		28 September 2011
✓	GP/Consultant Information Sheets	1	01 March 2012
	Investigator CV		
✓	Participant Consent Form	1	01 March 2012
✓	Participant Information Sheet	1	01 March 2012
✓	Protocol	1	01 March 2012
	REC application		12 March 2012

Membership of the Committee

The members of the Ethics Committee who were present at the meeting are listed on the attached sheet.

Statement of compliance

The Committee is constituted in accordance with the Governance Arrangements for Research Ethics Committees and complies fully with the Standard Operating Procedures for Research Ethics Committees in the UK.

After ethical review

Reporting requirements

The attached document "After ethical review – guidance for researchers" gives detailed guidance on reporting requirements for studies with a favourable opinion, including:

- Notifying substantial amendments
- Adding new sites and investigators
- Notification of serious breaches of the protocol
- Progress and safety reports
- Notifying the end of the study

The NRES website also provides guidance on these topics, which is updated in the light of changes in reporting requirements or procedures.

Feedback

You are invited to give your view of the service that you have received from the National Research Ethics Service and the application procedure. If you wish to make your views known please use the feedback form available on the website.

Further information is available at National Research Ethics Service website > After Review

12/YH/0169	**Please quote this number on all correspondence**

With the Committee's best wishes for the success of this project

Yours sincerely

Dr Rhona Bratt
Chair

Email: Elaine.hazell@nhs.net

Enclosures: *List of names and professions of members who were present at the meeting and those who submitted written comments*
"After ethical review – guidance for researchers"

Copy to: *Mrs Rachel E De Souza*

Mrs Anne Gowing, Leeds Teaching Hospitals NHS Trust

NRES Committee Yorkshire & The Humber - Leeds West

Attendance at Committee meeting on 13 April 2012

Committee Members:

Name	*Profession*	*Present*	*Notes*
Miss Brygitta Atraszkiewicz	Information Analyst	Yes	
Professor Howard Bird	Consultant Rheumatologist	Yes	
Dr Rhona Bratt	Retired Multimedia Project Manager	Yes	
Mr David Bryant	Pharmacist	No	
Dr Martin Elliott	Consultant Paediatric Oncologist	No	
Dr Sheila E. Fisher	NCRI Associate Director for PPI	Yes	
Mr Peter Margerison	Retired Solicitor	Yes	
Mr Jerry Masterson	Practice Learning Facilitator	Yes	
Dr Wendy Neil	Consultant Psychiatrist	No	
Dr Vera Neumann	Consultant in Rehabilitation Medicine	No	
Dr Jane Orton	Consultant Oncologist	Yes	
Dr Reema Sirriyeh	Research Fellow	No	
Professor Anne Topping	Director, Centre for Health and Social Care Research	Yes	

Also in attendance:

Name	*Position (or reason for attending)*
Mrs Elaine Hazell	REC Co-ordinator
Ms Ariana Mihoc	Observer
Mrs Shobhana Ningoo	Assistant Co-ordinator

NHS
Health Research Authority

NRES Committee Yorkshire & The Humber - Leeds West
First Floor
Millside
Mill Pond Lane
Leeds
LS6 4RA

Telephone: 0113 3050122
Facsimile: 0113 8556191

25 April 2012

Dr Sven Plein
Consultant Cardiologist, British Heart Foundation Senior Clinical Research Fellow
University of Leeds
Academic Unit of Cardiovascular Medicine
G floor, Jubilee Wing
Leeds General Infirmary
LS1 3EX

Dear Dr Plein

Full title of study: **QUANTITATIVE EVALUATION OF MYOCARDIAL CHARACTERISTICS IN REPERFUSED ST-ELEVATION MYOCARDIAL INFARCTION – A 3 TESLA CARDIOVASCULAR MAGNETIC RESONANCE STUDY**

REC reference number: **12/YH/0169**

Thank you for your letter of 24 April 2012. I can confirm the REC has received the documents listed below as evidence of compliance with the approval conditions detailed in our letter dated 13 April 2012. Please note these documents are for information only and have not been reviewed by the committee.

Documents received

The documents received were as follows:

Document	*Version*	*Date*
GP/Consultant Information Sheets	1	01 April 2012
Participant Consent Form	1	01 April 2012
Participant Information Sheet	1	01 April 2012

You should ensure that the sponsor has a copy of the final documentation for the study. It is the sponsor's responsibility to ensure that the documentation is made available to R&D offices at all participating sites.

12/YH/0169 **Please quote this number on all correspondence**

Yours sincerely

Mrs Elaine Hazell
Committee Co-ordinator

9.2. Patient information sheet

Study code 3T-STEMI

Quantitative evaluation of myocardial characteristics in reperfused ST-elevation myocardial infarction – a 3 Tesla cardiovascular magnetic resonance study

PATIENT INFORMATION SHEET Version 1.1; April 2012

Chief Investigator: Dr S Plein

Dear Patient,

You are being invited to take part in a research study. Before you decide it is important for you to understand why the research is being done and what it will involve. Please take time to read the following information carefully and discuss it with friends, relatives and your GP if you wish. Ask us if there is anything that is not clear or if you would like more information. Take time to decide whether or not you wish to take part.

Purpose of the study

Magnetic Resonance Imaging (MRI) is a test, which produces detailed pictures of your internal organs by putting you within a strong magnetic field. With Cardiac MRI we are able to detect several important abnormalities that are caused by heart disease, for example the scarring of the heart from heart attacks and the restrictions of blood flow to the heart muscle that lead to angina. Also, MRI produces pictures of the heart with much greater detail than with other types of heart scans. Importantly, MRI is also a safer test than most other heart scans, because it does not expose patients to any harmful radiation and pictures of the heart can be taken “from the outside”. Because of all of these qualities, MRI may become one of the most important tests in patients who suffer with different types of heart disease.

We have been doing MRI scans of the heart in Leeds since 1995. We are continuously carrying out research into improving the images and thereby improving patient care.

During a heart attack the heart muscle cells are damaged. Some heart muscle will not return to normal and will be replaced by a scar. Other parts of the heart muscle are less severely affected by the heart attack and can recover to normal over time.

With MRI the consequences of a heart attack can be shown in much greater detail than with other tests.

In this research we aim to find out how heart attacks affect the heart early on and in the recovery phase that follows. We would therefore like to scan patients like you twice or three times over a 3 month period.

Why have I been chosen?

This study is looking at people like you, who have recently had a heart attack and had the blocked blood vessel reopened. We are hoping to recruit 150 patients like you into this study.

Do I have to take part?

It is up to you to decide whether or not to take part. If you do decide to take part you will be given this information sheet to keep and be asked to sign a consent form. If you decide to take part you are still free to withdraw at any time and without giving a reason. This will not affect the standard of care that you receive from the NHS. If there is a possibility that you might be pregnant, you should not take part in the study. Our research team will be happy to discuss any other questions that you may have concerning your suitability for the study, before you decide whether to take part.

What will happen to me if I take part?

All patients in this study will have two or three MRI scans. We would aim to scan you twice within the first ten days after your heart attack, which is important to find out how changes in the heart evolve, though circumstances (including how you are feeling) may limit us to just one scan during this period. The final scan will take place 3 months later.

The MRI scans will be performed at the Leeds General Infirmary and will each take approximately 60 minutes to complete. You lie in a short 'tunnel', which holds a large magnet. Short bursts of magnetic fields and radio waves from the MRI scanner allow images to be created. You will hear periodical loud “banging” noises while we are acquiring the images of your heart, though we do protect your ears with headphones. You can listen to the radio, or to one of your own CDs. We will remain in communication with you throughout the scan. During the scan, we will inject an MRI contrast medication into a vein in your arm. For this we will insert a small tube (cannula) in a vein in your arm. If you come down from the ward with a cannula (whilst you are staying in hospital) we would use the one that is already there. Usually people are not aware of the actual contrast dye injection.

Whilst you are an in-patient on the ward you will have a blood sample taken every day. This would happen regardless of whether you are in the study or not. We will use some of the results for the research study. We will also take a blood sample (at most 15 mls = 3 teaspoons) from you at every scan visit. We will take this from the cannula we have to insert to inject the contrast dye so there are no extra needles involved. With your permission we will store these samples and analyse them at the end of the study for markers of heart function. Any use of your samples after this study could only happen if an ethics committee approved it.

As part of the study we would like to make a follow-up telephone call to you after one year and at 3 years to ask you some simple questions about your health. With your permission we may also look at your hospital records, request access to your GP records, central NHS records and/or use information from the NHS Information Centre.

After you leave hospital it is very helpful if we can continue to track your health condition over a long term period. The Medical Research Information Service (MRIS) allows us to access health information about you with your permission. In order to this we are seeking your permission to provide MRIS with some of your personal details (including your name, date of birth, address and NHS number) and with this information MRIS will be able to provide us with simple health information about you beyond the 3 year follow up period of this study. It is very important to understand the long term health condition of patients after a heart attack to find out if the treatments we are giving are effective. Information will be provided to MRIS in strict confidence and will be kept securely by them and will not be released to a third party.

Risks and discomforts

Magnetic Resonance Imaging (MRI) at 3 Tesla is safe and no x-rays or radiation are used for this scan. There are no known risks from this technique. Some people may experience claustrophobia. Our MRI staff will do all that they can to make you feel comfortable during the scan, and will be monitoring you via a video camera and an audio link. If we are unable to make you feel comfortable in the scanner, we will not go ahead with scanning. The contrast medication we use during the scan is very safe but, as with any injection, reactions may occur. These include a warm sensation at the injection site, nausea or vomiting and transient skin rash. These effects usually only last for a few minutes. People with a history of allergy are more likely to suffer a more severe reaction, but this is rare (less than 1 in 3000). The department is equipped to cope with allergic reactions if they happen.

Benefits to you

This study does not form part of your normal clinical care and is done solely for research purposes.

Expenses

We will provide reasonable travel expenses should this be necessary for you to attend the MRI scan. We are also happy to arrange transport to the hospital and return you home if needs be.

Will my taking part be kept confidential?

All information collected about you during the course of the study will be kept strictly confidential. This information will be securely stored, electronically on the Leeds General Infirmary secure server, and on paper, under the provisions of the 1998 Data Protection Act. The data collected will be coded and your personal details will be kept separately. You will not be identified in any publication that may result from this research.

With your permission we will inform your GP of your participation in the study. If any unexpected abnormality or condition were found we would inform your GP and your cardiologist.

We may contact the NHS Information Service at a later stage for information, which they hold on your health status. This means some of your personal data will be shared with the NHS Information Service. Any information exchanged between us and the NHS Information Service will be subject to strict data protection regulations.

With your permission, your data may also provide a resource for future studies. If any information from this study is used to develop new research, data protection regulations will be observed and strict confidentiality maintained. Any information about you which leaves the hospital will have your name and address removed so that you cannot be identified. Your data and or images may be sent to institutions in the UK, the European Economic Area or outside the EEA. Ethical approval will be obtained for any future studies involving your data.

If you withdraw consent from further study follow-up, or if you were to become incapacitated, any data collected about you up to that point will remain on file and will be included in the final study analysis.

What will happen to the results of the research study?

When the study is complete the results will be published in a medical journal, but no individual patients will be identified. If you would like a copy of the published results, please ask your doctor.

Indemnity/Compensation

If you are harmed as a direct result of taking part in this study, there are no special compensation arrangements. If you are harmed due to someone's negligence, then you may have grounds to a legal action. Regardless of this, if you have any cause to complain about any aspect of the way you have been approached or treated during the course of this study, the normal National Health Service complaints mechanisms are available to you.

The research organisation

This is a research project of the Cardiac MRI department of the Leeds General Infirmary and the University of Leeds.

Who has reviewed the study?

The study has been reviewed and approved both by a nationally approved Research Ethics Committee and your hospital Research and Development Office. More details can be provided, on request, by your study doctor.

For further information please contact:

Dr Ananth Kidambi
Research Fellow in Cardiac MRI
British Heart Foundation Cardiac MRI Department
B Floor, Clarendon Wing
Leeds General Infirmary
Leeds
LS1 3EX
T 0113 392 [XXXX]

Or

Petra Bijsterveld
Research Nurse
Academic Unit of Cardiovascular Medicine
G Floor Jubilee Wing
Leeds General Infirmary
Leeds
LS1 3EX
T 0113 392 [XXXX]

Thank you.

9.3. Consent form

CONSENT FORM v 1.1; April 2012

Quantitative evaluation of myocardial characteristics in reperfused ST- elevation myocardial infarction – a 3 Tesla cardiovascular magnetic resonance study.
CI: Dr S Plein

Patient Study Number: …….. Date of Birth: ……

Please initial boxes

1. I have read the Patient Information Sheet dated April 2012 (Version 1.1) for the above study and I have had the opportunity to ask questions and discuss the research study and I am satisfied with the answers to my questions. ☐

2. I understand that my participation is voluntary and that I am free to withdraw from the study at any time without giving a reason. ☐

3 I give my consent for my General Practitioner to be informed, and I understand that my cardiologist will be informed only if we find any abnormality over and above which is already known. ☐

4. I understand that data and images collected will be stored on a computer system, and, after my personal details have been removed, may be available to researchers at other institutions in the UK, the EEA, and countries outside the EEA. ☐

5. I understand that some of the blood samples taken from me will be stored and may be analysed in the future for markers of a heart attack. ☐

6. I understand that relevant sections of my medical notes and data collected during the study may be looked at by individuals from the University of Leeds, from regulatory authorities, or from the Leeds Teaching Hospitals NHS Trust, where it is relevant to my taking part in this research. I give permission for these individuals to have access to my records. ☐

7. I understand that information held by the NHS and records maintained by the NHS Information Centre, the NHS Central Register and by my General Practitioner may be used to contact me and provide information about my health status. I give permission for this information to be obtained from the NHS Information Centre, the NHS Central Register and/or my GP if necessary. ☐

8. If I were to lose capacity or withdraw consent for further follow-up I understand that data already collected will be kept and used for the purposes of the study. ☐

9. I agree to take part in this research study and that the general results of the study will be made available to the medical community most likely through publication in a reputable medical journal. ☐

Signature.....

Name (block capitals)..... Date.....

Signature of witness.....

Name (block capitals).....Date……

9.4. GP letter

Study code 3T-STEMI

Quantitative evaluation of myocardial characteristics in reperfused ST-elevation myocardial infarction – a 3 Tesla cardiovascular magnetic resonance study

GP INFORMATION SHEET

Version 1.1; April 2012

Chief Investigator: Dr S Plein

[Date]

[Dr .....]

[Surgery Name]

[Address]

[Town]

[Postcode]

[Re: Patient name]

[Patient address]

[Patient d.o.b.]

Dear Colleague,

Your patient has agreed to take part in a research study called 'Quantitative evaluation of myocardial characteristics in reperfused ST- elevation myocardial infarction – a 3 Tesla cardiovascular magnetic resonance study'.

We would like to give you some relevant information about this study.

What is the purpose of the study?

The aim of this study is to characterise the time course of MVO, haemorrhage, peri-infarct oedema and stunning following reperfused acute myocardial infarction using cardiovascular magnetic resonance imaging (MRI). We also aim

to develop models that predict recovery of left ventricular function as a surrogate for clinical outcome, and determine the value of standard biomarkers in predicting MRI findings and clinical outcome.

Why has this patient been chosen?

Your patient has had a myocardial infarction which has been reperfused by primary PCI. He/she has provided consent to the study, with both verbal and written patient information.

What will happen to the patient?

The patient will undergo 1 or 2 CMR imaging studies on a 3 Tesla MRI scanner during the first 10 days of presentation. The number of scans undertaken will depend on the patient's willingness and on logistical considerations. He / she will have a further scan at 3 months.

Each scan will take approximately one hour and will involve the injection of a conventional Gadolinium-based MRI contrast agent.

Blood samples will be taken from the patient to measure cardiac biomarkers whilst the patient is in hospital and at follow up.

Following the MRI scan, the patient will be offered a guided review of the images with one of the doctors in the department. Because many of the methods used in this study are in the research phase, the results of the scan are not routinely available for clinical use.

If as a result of the scan an unexpected abnormality or condition were found you will be informed.

Risks and discomforts

MRI has no known risks or side-effects. Side-effects of Gadolinium-based contrast agents can include a warm sensation at the injection site, nausea or vomiting and transient skin rash. These effects usually last only a few minutes. Patients with a history of allergy are more likely to suffer a more severe reaction, but this is rare (less than 1 in 3000).

What if there is a problem?

If you or the patient have a concern about any aspect of this study, you should ask to speak with the Principal Investigator who will do his best to answer your questions (contact number at the end of this information sheet). The study has undergone review by the local ethics committee.

Who is organising and funding the research?

The research is being organised by researchers at the University of Leeds and the Leeds Teaching Hospitals NHS Trust.

If you require any further information, please do not hesitate to contact:

Dr. Sven Plein, Consultant Cardiologist
British Heart Foundation Cardiac MRI Department,
B Floor, Clarendon Wing,
Leeds General Infirmary.
Tel: 0113 392 [XXXX].